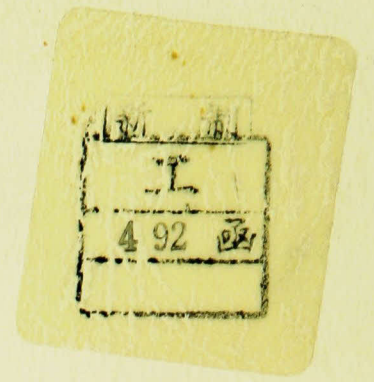


COMPUTER EXPERIMENTS ON THE ENERGY
CONVERSION BY MAGNETIC
FIELD RECONNECTION



by
Masayuki UGAI

April 1980

Department of Electrical Engineering
Ehime University, Matsuyama, Japan

Handwritten text, possibly a signature or initials, located in the top left corner of the page.

**COMPUTER EXPERIMENTS ON THE ENERGY
CONVERSION BY MAGNETIC
FIELD RECONNECTION**

by

Masayuki UGAI

April 1980

Department of Electrical Engineering
Ehime University, Matsuyama, Japan

ACKNOWLEDGMENTS

The author wishes to express his sincere appreciation to Professor Takao Tsuda, Kyoto University, for his continual guidance throughout the present work and his careful reading of the manuscript.

The author is deeply indebted to Professors Toshinobu Takagi, Iwane Kimura and Ryohei Itatani, Kyoto University, for their useful and critical discussions.

The author wishes to express his hearty appreciation to Dr. Atsuhiro Nishida, University of Tokyo, for useful comments and suggestions and to Professor Tatsuzo Obayashi, University of Tokyo, for his encouragement and interest in this work. Useful discussions with Drs. Tetsuya Sato, University of Tokyo, and Shoichiro Fukao, Kyoto University, are also acknowledged.

The author is grateful to Professors Hiromu Ariyoshi, Nisaku Matsuda, Shigehiro Isomura and Hitoshi Abe, Ehime University, for their encouragement and interest in this work.

The author also thanks Mr. Masaharu Aono, Ehime University, for his support of this work. Thanks are due to colleagues in the Department of Electrical Engineering of Ehime University.

The computation was performed at the Data Processing Centers, Ehime, Kyushu and Kyoto Universities.

PREFACE

It has widely been recognized that some new available energy should be developed so as to take the place of petroleum in the near future. In this respect, the device to realize nuclear fusion in laboratory plasmas must be one of the greatest projects in this century. Besides nuclear fusion research, plasma that does not naturally exist on the earth is now thought to be quite important for many technological purposes.

In actual systems, there are a wide variety of plasmas from laboratory plasmas to space plasmas. Various phenomena are accordingly caused by various plasmas, and they are frequently too complicated to be easily understood. In researching plasmas, there are now well established the following three methods, namely, theoretical study on the basis of analytical calculations, laboratory experiment or observation by rockets and artificial satellites, and computer experiment by computer machines. In recent days, we are recognizing that computer experiment becomes more and more important since mathematical treatments are very complicated and laboratory experiments are usually not easily performed; also, observations of phenomena occurring in space reveal many important features of plasma.

In understanding complicated plasma processes, one of the key mechanisms is plasma acceleration mechanism. In fact,

mechanisms causing increase in plasma energies are essential in many plasma devices, for instance, in yielding high-energy ion beams and in heating plasma in order to realize nuclear fusion, as well as in many distinct phenomena occurring in space. In a very simple case, an externally applied electric field can readily cause plasma acceleration. On the other hand, there may be another important situation where plasma gains energy without externally applied electric field. In this case energy conversion should occur self-consistently because of remarkable properties inherent to plasma itself. In such a plasma process magnetic field may play a crucial role since it can largely control plasma behaviors.

The present thesis studies by computer experiments large-scale conversion of magnetic energy into plasma energies. We are interested in only macroscopic properties of plasma. We note that magnetically stored energy should be released in a large scale region when a magnetic field configuration of high potential energy topologically relax into another one of lower potential energy. It should be kept in mind that "magnetic field line reconnection" involves topological translation of magnetic field configuration and may hence be essential in large-scale energy conversion process.

In chapter 1, the background of the present problem is generally described. The concept of magnetic field line reconnection is introduced in a rather intuitive manner. It should

be recognized that the basic mechanism of the energy conversion by field line reconnection is, at least in principle, the same as the well-known energy conversion mechanism involved in electric machines such as generator and motor. Also, recent laboratory reconnection experiments are referred to, and major observations concerning large dissipative events in space, such as solar flares and magnetospheric substorms, are shortly mentioned.

Chapter 2 systematically examines theoretical models on the fast reconnection process that have been proposed during the last two decades. Most analytical studies have concentrated on steady-state reconnection processes in incompressible fluids. They succeeded in showing some essential physical mechanisms required for the rapid energy conversion by field line reconnection but not in a convincing manner. In fact, many fundamental reconnection processes remain masked because of mathematical difficulties. We discuss limitation of analytical calculations and refer to important problems concerning the fast reconnection that should be solved.

Chapters 3-6 show and discuss our computer experiments. We investigate the temporal dynamics of reconnection, which is of high current interest in actual systems. In chapters 3 and 4, a development of fast reconnection from a neutral current sheet is demonstrated. The condition for occurrence of the fast reconnection process can be clarified. It is found that remarkable conversion of magnetic energy into plasma energies in fact results without specially imposed external condition. In the quasi-steady

configuration a finite electric field is spontaneously set up almost uniformly in space. Chapter 5, on the other hand, examines influences of an externally imposed electric field on the reconnection process. It is shown that the fundamental structure of the steady reconnection can scarcely be influenced by the imposed electric field. Chapter 6 again examines the spontaneously developing reconnection process and shows that the finally set-up electric field has a weak (logarithmic) dependence on the magnitude of electrical resistivity. Note that this consequence assures that the energy conversion process can effectively proceed even in highly conducting fluids.

In chapter 7, important consequences derived from the computer experiments are summarized and extensively discussed. It is suggested that the fast reconnection process should basically be regarded as a gross instability inherent to the current sheet system itself. We then apply the numerical results to flare phenomena and show that they are in fact in good agreement with observations. We also suggest that the effective magnetic energy conversion by field line reconnection should be available for many plasma devices.

CONTENTS

ACKNOWLEDGMENTS

PREFACE

Chapter 1. GENERAL INTRODUCTION	1
§1. Introduction	1
§2. Basic Concept of Magnetic Field Line Reconnection	2
§3. Basic Mechanism of the Energy Conversion by Magnetic Field Line Reconnection	4
§4. Laboratory Experiments and Observations	8
4.1 General remarks	8
4.2 Laboratory experiments	8
4.3 Observations of phenomena in space	12
4.3.1 Remarks	12
4.3.2 Solar flares	13
4.3.3 Magnetospheric substorms	15
Chapter 2. SURVEY OF THEORETICAL RECONNECTION MODELS	19
§1. Introduction	19
§2. Sweet-Parker Model	21
§3. Petschek's Model	24
§4. Similarity Models	27
§5. Discussion	29

Chapter 3. MAGNETIC FIELD LINE RECONNECTION BY
LOCALIZED ENHANCEMENT OF RESISTIVITY;
EVOLUTIONARY PROCESS

- §1. Introduction
- §2. Governing Equations
- §3. Numerical Experiment
 - 3.1 Assumptions of our model
 - 3.2 Initial-boundary conditions
 - 3.3 Numerical scheme
- §4. Evolutionary Process of Field Line Reconnection
 - 4.1 Diffusive stage
 - 4.2 Hydromagnetic stage
 - 4.3 Further remarks
- §5. Magnetic Energy Conversion
- §6. Concluding Remarks

Chapter 4. QUASI-STEADY PROCESS

- §1. Introduction
- §2. Numerical Experiment
- §3. General Remarks
- §4. Quasi-Steady Process of Reconnection
 - 4.1 The diffusion region
 - 4.2 The field reversal region
 - 4.3 The external region
- §5. Concluding Remarks

Chapter 5.	CONTROLLING FACTORS OF FAST RECONNECTION	100
§1.	Introduction	100
§2.	Numerical Experiment	102
§3.	Some Remarks on the Present Model	104
§4.	Results	107
§5.	Concluding Remarks	121
Chapter 6.	DEPENDENCE OF FAST RECONNECTION ON THE MAGNITUDE OF RESISTIVITY	124
§1.	Introduction	124
§2.	Results	127
§3.	Discussion	137
§4.	Summary	143
Chapter 7.	SUMMARY AND DISCUSSION	147
§1.	Summary of the Computer Experiments	147
§2.	Comparison with Fast-Reconnection Theories	149
§3.	Applications to Phenomena in Actual Plasmas	151
§4.	Conclusion	155
REFERENCES		157

GENERAL INTRODUCTION

§1. Introduction

In the real physical world, there are various forms of energy, and energy conversion is essential in many technological devices. Simple forms of energy can easily be provided by natural resources such as petroleum and coal, which are converted into other forms of energy according to practical purposes.

In plasma devices plasma acceleration or heating is quite essential as well known. In this respect, it should be noted that magnetic field may have a crucial role in determining macroscopic plasma processes. The present chapter thus gives general remarks on the basic mechanism of plasma acceleration that results from interaction with large-scale magnetic field.

In §2 we describe the basic concept of "magnetic field line reconnection". We note that by field line reconnection magnetic field may modify its configuration in a large-scale region. One may thus expect that field line reconnection would be essential in large-scale conversion of magnetic energy into plasma energies.

§3 refers to the principle of conversion between electrical and mechanical energies. We then consider the energy conversion by field line reconnection on the basis of the general principle of energy conversion.

In §4 we mention recent laboratory experiments of reconnection and observations of phenomena in space that have been considered to be associated with field line reconnection. In fact, to show evidence of reconnection in actual plasmas will lead to a deeper understanding of the present problem. Some observational data will be employed to compare with our numerical results in the last of the present thesis.

§2. Basic Concept of Magnetic Field Line Reconnection

In order to visualize field line reconnection, we should identify individual field lines of force and their motion (Stern, 1966). Newcomb(1958) showed that any velocity \underline{v} given by

$$\frac{\partial \underline{B}}{\partial t} - \nabla \times (\underline{v} \times \underline{B}) = \underline{0} \quad (1.1)$$

satisfies conditions associated with the concept of the motion of lines of force, such as line preservation and flux preservation.

As a matter of fact, it seems more instructive to describe field line reconnection in an intuitive manner. Generally, any magnetic field lines should be closed and a loop must be formed

since magnetic field \underline{B} satisfies the solenoidal condition ($\nabla \cdot \underline{B} = 0$). However, it should be noted that a magnetic field line loop may be broken at a magnetic neutral point where field strength vanishes. This could readily be recognized if one considers that magnetic field has no definite direction where $\underline{B} = 0$. With this in mind, consider a pair of magnetic field line loops which approach each other. If they meet and touch each other at a neutral point, they will be broken and then "reconnect" with each other at the neutral point, which should result in formation of a new field line loop. The implication is certainly that magnetic flux transfers with the overall field configuration being modified topologically.

In actual physical systems such a magnetic flux transfer is not surprising but rather popular. Suppose, for instance, that bar magnets are placed in vacuum. Since there is no electrical current in vacuum, the problem is trivial. Magnetic field configuration produced by the magnets can easily be modified by varying the disposition of the magnets or by reversing their polarities. The magnetic field reconfiguration should obviously result from magnetic flux transfer due to "field line reconnection". In plasmas, on the other hand, the problem becomes extremely complicated since electric currents can now easily flow. Changes in magnetic field configuration may directly influence plasma behaviors, so that field line reconnection should be accompanied with some drastic plasma processes. To study such plasma processes is the main theme of the present thesis.

It should be noted that the presence of magnetic neutral point is essential in the proceeding of field line reconnection. It is well known that there exist two types of neutral points, namely X-type and O-type neutral points (Dungey, 1953). Fukao et al. (1975) further showed that in the general three-dimensional case there can exist other types of neutral points such as spiral-type and node-type neutral points. In the three dimensional system magnetic field configuration, and hence the reconnection process, may become much complicated. The present thesis will study, for simplicity, two-dimensional aspects of plasma processes, and only X- and O-type neutral points will be considered.

§3. Basic Mechanism of the Energy Conversion by Magnetic Field Line Reconnection

As seen from the foregoing discussion, magnetic field line reconnection allows a magnetic field configuration of high potential energy to topologically relax into another one of lower potential energy. In view of the remarkable magnetic energy conversion involved, this problem must be one of the most fundamental subjects in plasma physics. As will be shown in detail in the next chapter several theoretical models of fast reconnection have been proposed during the last two decades, but there remains considerable confusion concerning the basic concept on the physical mechanism.

The detailed features of the fast reconnection are generally too complicated to be easily understood since the process involves strong nonlinear effects. In what follows, let us systematically examine the fundamental problem on the basis of the general principle of energy conversion.

The simple version of the Ohm's law is given by $\underline{E} + \underline{u} \times \underline{B} = \eta \underline{J}$, where η is the electrical resistivity, which can usually be written as $\underline{E} + \underline{u} \times \underline{B} \simeq 0$ in cosmic plasmas. The energy conversion rate per unit volume is in general given by $\underline{E} \cdot \underline{J}$, which becomes $\underline{E} \cdot \underline{J} = \underline{u} \cdot (\underline{J} \times \underline{B}) + \eta \underline{J}^2 \simeq \underline{u} \cdot (\underline{J} \times \underline{B})$ by using the Ohm's law. As well known, if $\underline{E} \cdot \underline{J} > 0$, a motor effect is represented by which electrical energy is converted into mechanical energy; on the other hand, if $\underline{E} \cdot \underline{J} < 0$, a generator effect is described such that mechanical energy is utilized so as to generate an electric field \underline{E} . In considering the physical mechanism releasing the magnetic potential energy stored in the current sheet system, a most fundamental problem apparently lies in how a large-scale electric field can ultimately be established in the system.

Consider an X-type field configuration, which is thought to have developed from an initially antiparallel field, where a steady fast reconnection (for instance, see Petschek (1964)) is proceeding, as schematically shown in Fig. 1. The region is of scale dimension $2L_x \times 2L_y$, and the problem is assumed to be two-dimensional as usual. The origin 0 is the position of both the magnetic neutral point and the plasma stagnation point. Note

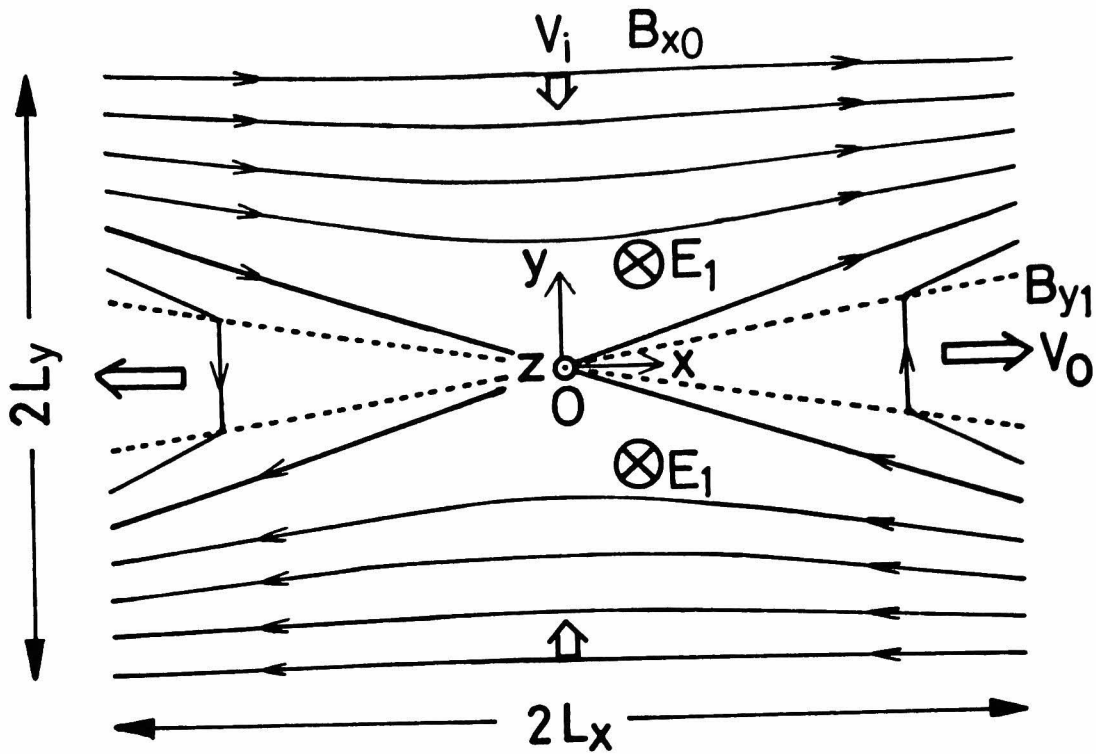


Fig. 1. Schematic illustration of magnetic-field (solid lines and plasma-flow (broad arrow) configuration where steady-state fast reconnection is proceeding.

that magnetic diffusion is important only in a small region near the neutral point. There must now be global plasma flows: at $(x, y) = (L_x, 0)$ the field component $B_y = B_{y1}$ and the outflow velocity $u_x = V_o$; at $(x, y) = (0, L_y)$ the field component $B_x = B_{x0}$ and the inflow velocity $u_y = -V_i$. Also, there is a constant electric field $E_z = -E_1$ where $E_1 \simeq V_i B_{x0} \simeq V_o B_{y1}$. Integrating $\underline{E} \cdot \underline{J}$ over the region in the first quadrant only, we may describe the energy conversion rate as $E_1 I = W_0 + W_1$, where

$$W_0 = E_1 I_0 ; I_0 = \frac{1}{\mathcal{M}_0} \int_0^{L_x} B_x(x, y=L_y) dx \simeq \frac{B_{x0}}{\mathcal{M}_0} L_x , \quad (1.2)$$

where we consider $B_x \simeq B_{x0}$ at $y=L_y$, and

$$W_1 = -E_1 I_1 ; I_1 = \frac{1}{\mathcal{M}_0} \int_0^{L_y} B_y(x=L_x, y) dy. \quad (1.3)$$

Here we take it into account that the total current I in the region can be written as $I = -I_0 + I_1$ (usually $I_0 \gg I_1$) where $-I_0$ is the current associated with the initial antiparallel field B_{x0} and I_1 is the one associated with the B_y field resulting from the reconnection. Obviously, W_0 is positive and corresponds to the annihilation rate of the antiparallel field; on the other hand, W_1 is negative and hence indicates a generator effect such that part of the resultant plasma energy is utilized so as to generate the electric field E_1 . As can be seen from Eq. (1.3), the generator mechanism is effective in the inner region (near the x-axis) since as will be shown later the B_y field decreases with increasing y ; hence, this mechanism can be considered to come from the intrinsic properties involved in the current sheet system itself. In fact, in order to produce the B_y field in the system, there should be some active mechanism yielding localized enhancement of magnetic diffusion near the neutral point.

§4. Laboratory Experiments and Observations

4.1 General remarks

We note that there is a large difference between laboratory plasmas and space plasmas in the scale of space where plasmas exist. Laboratory plasmas are confined by rather small apparatus; on the other hand, space plasmas exist in the enormous cosmic space and interact with planetaries. There are in fact a much wide variety of plasma phenomena in space, and simulating space plasmas by laboratory plasmas usually involves many technological difficulties. Recently, much effort has been given by many experimenters and notable progress has been made. The problem of magnetic field line reconnection which originated from flare phenomena in space, has increasingly attracted much interest with respect to laboratory experiments too. Let us show below important consequences, associated with magnetic reconnection, that have been obtained from laboratory experiments as well as from observations of phenomena in space.

4.2 Laboratory experiments

Important reconnection experiments that have been reported are mostly associated with tearing modes and Petschek modes. These experiments were extensively discussed and reviewed by Baum & Bratenahl(1977). Tearing modes have been considered of great importance in researching pinch, stellarator and tokamak

where instability of magnetic field configurations has been observed (Colgate & Furth 1960; Stodiek et al. 1962).

Theoretical studies on tearing modes have been presented by many workers (Furth et al. 1963; Gross & Van Hoven 1971; Dobrott et al. 1977). In tearing modes a neutral current sheet develops into many X- and O-type neutral points, and in the classical theory the sheet is infinitely long and is perturbed by random wavelength disturbances.

In a tubular pinch, Anderson & Kunkel(1969) showed that circular field lines, oppositely directed on the inner and outer sides of the pinch, are broken and that alternating X-, and O- type neutral points are formed. An experiment by Alideeres et al. (1968) showed evidence of reconnection in a hard core theta pinch, but no classical tearing mode was observed. Also, an experiment by Ohyaabu et al. (1974) which treated a neutral current sheet, is taken as evidence for the tearing mode (Ohyaabu & Kawashima 1972). However, we may note that it would not present the classical tearing mode since the classical tearing mode does not evaluate the influence of finite boundaries (Baum & Bratenahl 1977).

In fact, theoretical study on the nonlinear development of tearing modes is quite essential in understanding the experiments, but it has not convincingly be shown yet. Van Hoven (1976) hypothesized that the classical Petschek mode may approximate the nonlinear tearing mode since both the tearing mode and the Petschek mode develop from a neutral current sheet. However,

it may be noted that there is an apparent discrepancy between the classical tearing mode and the classical Petschek mode in how the associated electric field exists. In the Petschek-mode geometry there should be a large-scale electric field in the whole region as shown in Fig.1, while it is apparent that such a large-scale uniform electric field cannot exist in the tearing-mode geometry. We may hence consider that nonlinear tearing modes would not be so effective in large-scale conversion of magnetic energy stored in the current-sheet system.

An experiment by Baum, Bratenahl and others has researched a reconnection process in the Petschek-mode geometry (Bratenahl & Yeates 1970; Baum et al. 1973 a, b, c, d; Baum & Bratenahl 1974 a, b, 1975). The device is called the double inverse pinch device (DIPD). It should be noted that the experiment is different from the usual turbulence experiments (cf. Hamberger & Jancarik 1972) in that electric field which leads to turbulence develops from the plasma flow rather than from the application of an external electric field (Baum et al. 1973 c).

The DIPD is shown in Fig. 2. Fig. 2(b) shows the initial formation of cylindrical return current sheets around the rods which propagate radially outward. Fig. 2(c) illustrates a potential field produced by the two rods which define three flux cells. As the rod current changes, flux is transferred from cells 1 and 2 into cell 3 or vice versa. Every flux transfer is accompanied by field line reconnection. The rod currents

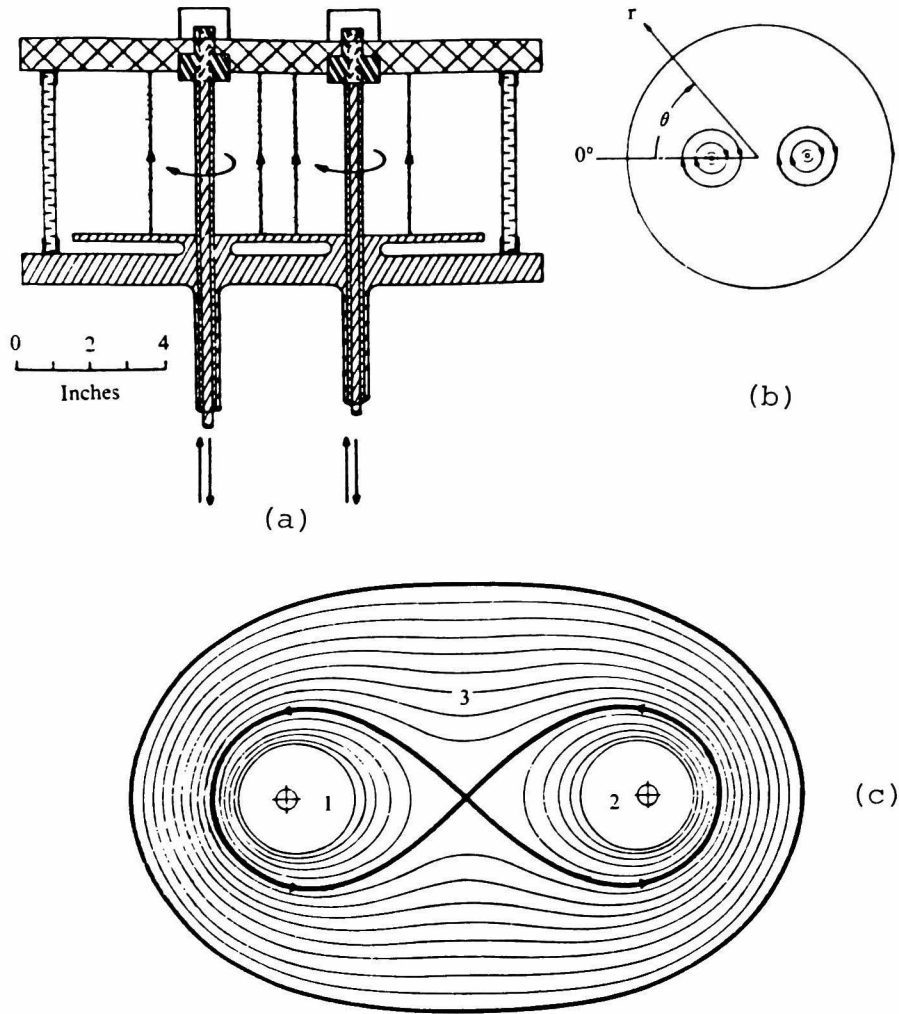


Fig. 2. The double inverse pinch device (DIPD). (a) Device side view. (b) Top view of two cylindrical inverse pinches. (c) Potential field from two rods defining three flux cells.

are directly driven by capacitor banks but that the neutral point current system is inductively driven (Baum & Bratenahl 1977)

They argued by measuring current density contours that slow shocks similar to Petschek's form are set up. As a matter for regret, however, the shock structure does not sufficiently develop and is not so definite, since the plasma is confined in rather a small region. One may in fact note that it is impossible to

achieve a steady state reconnection process in the geometry shown in Fig. 2(c) under any conceivable set of boundary conditions (Baum et al. 1973 d). But certainly the experiment must be quite important in understanding the Petschek-type reconnection in actual plasmas.

One of the most important consequences obtained from the DIPD may be that an anomalously high electrical resistivity is caused in the vicinity of the neutral point due to plasma turbulence. This may indicate that the effective resistivity near the neutral point is closely related to the proceeding of field line reconnection. Baum & Bratenahl(1974 b) in fact concluded that the impulsive reconnection event observed in the experiment is caused by an abrupt resistivity increase. One will see later in this thesis that the experimental result is, at least in essence, in good agreement with our computer experiments.

4.3 Observations of phenomena in space

4.3.1 Remarks

Historically, the study of magnetic field line reconnection grew out of suggestions by Giovanelli (1947, 1948) that charged particles responsible for solar flares and the aurora, respectively, could be accelerated at X-type neutral points. Recently, remarkable progress of observational means such as rockets and

artificial satellites has enabled us to gain much more information as to phenomena occurring in space, and reconnection process has now been recognized to be essential in various astrophysical systems, for instance in the formation of chromospheric spicules (Uchida, 1969), in the detachment of the magnetic field of an interstellar cloud from the surrounding field (Mestel & Strittmatter 1967) and in galactic flares (Sturrock & Barnes 1972).

Special concern has been paid to explosive plasma phenomena occurring in the solar and the terrestrial atmospheres. Solar flares are now well understood to be caused by some mechanism of releasing the energy stored in sunspot magnetic fields. In magnetospheric substorms, the magnetic energy stored in the geomagnetic tail is suddenly released into plasma energies. In what follows, let us briefly summarize observations concerning solar flares and magnetospheric substorms and show their possible interpretations in terms of magnetic field line reconnection.

4.3.2 Solar flares

In recent years, cinematographic and magnetographic studies have enabled complex structures of the solar atmosphere to be observed (Cheng & Widing 1975; Kabler et al. 1975). The energy of solar flares originates in complex rotational and convective motions in the photosphere, being stored temporarily as an excess magnetic stress in sunspot fields. Sunspot fields may thus be largely twisted and be likely to be sheared before

the onset of solar flare (Tanaka & Nakagawa 1973). However, as a matter for regret, the detailed internal structures of sunspot fields are not well identified yet.

A variety of theoretical models have been suggested with respect to the remarkable magnetic energy conversion occurring in the solar flare phenomenon (cf. Gold & Hoyle 1960; Sturrock 1966); Gold(1961, 1962) suggested a topological transfer of solar fields due to reconnection. But most theoretical models that have been proposed are rather qualitative, and it may be said that the basic physical mechanism causing solar flares is not well understood.

At present, theoretical models, not to mention detailed observations, should be needed that can systematically explain the major processes associated with the solar flare phenomenon. The following two plasma processes seem especially noteworthy, namely the abrupt plasma heating and the subsequent ejection of plasma clouds. The plasma heating may well be caused by some abrupt onset of anomalous electrical resistivity due to microinstabilities; on the other hand, the plasma ejection should result from some large-scale plasma instability. It should hence be kept in mind that any theory applicable to the solar flare phenomenon may be desired to provide some physical connection between anomalous resistivity and large-scale plasma instability.

It seems instructive to show some major observational evidences concerning the solar flare phenomenon in order to have

Item	Sun	Earth
Energy source	Photospheric motions (Rotation)	Solar wind ($\mathbf{E} = -\mathbf{V} \times \mathbf{B}$)
Energy storage	Sunspot field	Magnetotail
Growth phase	Coronal condensation plage-filaments twist and winding $\tau = ?$	Tail field Plasma sheet Plasma convection $\tau = 1 \sim 2$ h
Explosive phase	H α flash Ribbon flare ? $\tau \sim 10^3$ s	Aurora break-up Auroral surges Electrojet $\tau \sim 10^3$ s
Flare ejecta	Radio bursts Solar cosmic rays Shock wave Plasma cloud	ULF-VLF emissions Energetic particles ? Plasma cloud
Energy release	$10^{30} \sim 10^{32}$ erg	$10^{20} \sim 10^{22}$ erg

Table 1. Characteristics of solar and auroral flares.

an overall picture of it. Obayashi(1975) recognized that flare phenomena in the solar atmosphere and in the terrestrial magnetosphere exhibit many similarities. According to him, important characteristics of solar and auroral flares may be shown in table 1.

4.3.3 Magnetospheric substorms

It is now convinced that field line reconnection plays a crucial role in plasma processes occurring in the terrestrial magnetosphere. Especially, distinct plasma behaviors in the dayside magnetosphere and in the geomagnetic tail have attracted

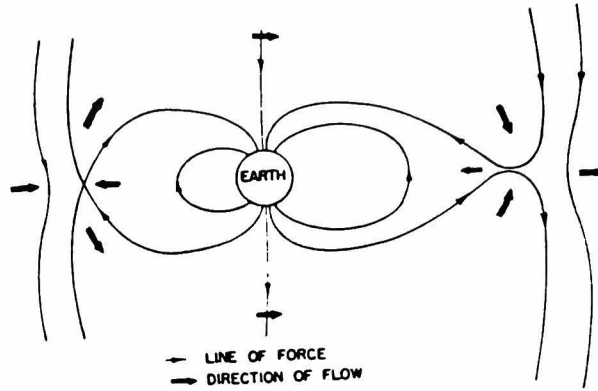


Fig. 3. Interplanetary plasma flow in a plane containing neutral point.

much interest with respect to the reconnection process. In this respect, it is noteworthy to show Dungey's reconnection model of the magnetosphere (Dungey 1961), which is shown in Fig.3. In this model the interplanetary magnetic field (IMF) is convected towards the geomagnetic tail due to reconnection when its field component is directed southward.

Dungey's suggestion has been observationally supported by the dependence of the magnetic activity in the auroral zone on the southward component of the IMF (e.g., Fairfield & Cahill 1966; Rostoker & Fälthammar 1967; Arnoldy 1971). Also, decrease in the total magnetic flux, as revealed by the dayside magnetopause observations (Aubry et al. 1970; Maezawa 1974) as well as low-altitude polar cusp observations (Burch 1972, 1973), occurs only when the IMF is directed southward. This is of course in agreement with the Dungey's reconnection model. For more detailed observational evidences of reconnection in the dayside magnetosphere the readers are referred to Maezawa(1975).

In the magnetotail the energy obtained from the solar wind is stored, and the stored magnetic field energy is converted explosively into the kinetic energy of charged particles, which leads to a magnetospheric substorm (Nishida 1978). It is widely believed that the onset of a substorm is a consequence of, and is closely associated in time with, the onset of rapid magnetic reconnection in the tail (Hones, 1977).

One of the basic signatures of the magnetotail substorm is rapid decrease in the field magnitude in the tail lobe (Aubry & McPherron 1971). The start of this decrease is coincident, within a range of several minutes, with the appearance of an expansion-phase signature on the ground, namely with the earliest onset of a low-latitude positive bay (Nishida & Nagayama 1973; Caan et al. 1973). At the corresponding moment the tail diameter starts to decrease (Maezawa 1975), and hence the flux content of the magnetotail is indeed reduced by the occurrence of a substorm. This certainly supports that some field line reconnection process builds up in the tail. In this respect, one may note that there should be formed an X-type magnetic neutral line. The neutral line model has been developed by several groups by putting various pieces of evidences together (e.g., Russell & McPherron 1973; Hoffman & Burch 1973; Hones et al. 1973; Terasawa & Nishida 1976; Hones 1976), although the precise position of the neutral line is not identified because of technical difficulties.

Table 1 summarizes major characteristics of magnetospheric

substorms. In addition, the following may be kept in mind. In the near-earth polar region, energetic particles are precipitated from the magnetosphere to the ionosphere. In the polar ionosphere, there is the formation of an intense westward electrojet. Field-aligned currents as well as field-aligned electric fields are observed, which, together with the electrojet in the ionosphere, form a closed current loop in the ionosphere-magnetosphere system. These plasma processes seem to suggest an existence of some "battery" in the tail that drives the current systems: this battery would have a voltage of several tens of kV according to the observations. For the plasma processes during a substorm near the ionosphere see, for instance, a review paper by Fälthammar (1977).

SURVEY OF THEORETICAL RECONNECTION MODELS


§1. Introduction

The present chapter examines the theoretical reconnection models that have been proposed during these two decades. Major points to be discussed are the following. Firstly, we are interested in what field geometry is suitable for the one where magnetic energy is critically stored. Secondly, important consequences derived from the analytical studies, as well as significant ideas introduced in the models, are shown, and also some limitations involved in the analytical treatments are pointed out. Finally, we raise a question what physical mechanism the reconnection process should be regarded as.

Historically, the dynamical behavior of a highly conducting plasma in the vicinity of the X-type neutral point was first studied by Dungey(1953). He found that the two branches of the separatrix, which initially intersect almost at right angles (i.e., there is approximately no net electric current), approach each other with the current being concentrated near the neutral point. Simultaneously, of course, the magnetic field lines as well as the plasma quantities are accumulated in the vicinity of

the sheet-like geometry. However, it may perhaps be noted that for attaining a deeper understanding of such a plasma process the problem should not be restricted to a local region near the neutral point; the associated overall process of the whole system should be taken into account. Dungey's mechanism might then suggest that if some external mechanical forces work on a system containing a magnetic neutral point the associated energy would be stored in the current-sheet geometry finally formed within the system, although this suggestion is different from Dungey's original idea that regarded the process as a local electrical discharge near the neutral point. Dungey's mechanism has extensively been studied and discussed (cf. Uberoi 1963; Imshennik & Syrovatskii 1967; Forbes & Speiser 1978), but the overall process describing the whole system has scarcely been investigated.

The next step was the model proposed by Sweet (1958) and further developed by Parker (1957, 1963). This model was the first to treat quantitatively the reconnection process in relation to large-scale conversion of magnetic energy into plasma kinetic energy. They considered as a possible cause of releasing magnetic energy only the magnetic diffusion due to finite electrical resistivity, and found the reconnection rate too small to account for the solar flare phenomenon. Petschek (1964) first recognized for the fast-reconnection problem the importance of MHD slow waves that can give, independently of magnetic-field diffusion, another way of reducing the magnetic field and increasing the plasma



energy. His basic idea was incorporated by Sonnerup(1970) and Yeh & Axford(1970) who independently proposed exact similarity solutions.

In what follows, let us examine these theoretical studies that concentrated on seeking possible solutions of the MHD equations that describe steady-state fast-reconnection processes. It should be kept in mind that the analytical models mostly assume the phenomena to be two-dimensional; namely, every quantity depends only on x and y coordinates and not on z , and there is no magnetic field nor fluid velocity in the z direction. Also, plasma is usually assumed to be incompressible. For the detailed mathematical treatments involved in the models see an excellent review paper by Vasylunas(1975).

§2. Sweet-Parker Model

Fig. 4 shows the sketch of Sweet-Parker model. Elementary considerations predict that, when two oppositely directed magnetic fields are pressed together, the plasma is squeezed out from between the fields, permitting the fields to approach each other. In the region $|y| < 2\delta$ where magnetic field notably changes its polarity the electric current flows in the z -direction (perpendicular to the paper). This region is called the field reversal region. Parker(1963) considered that in the field reversal region

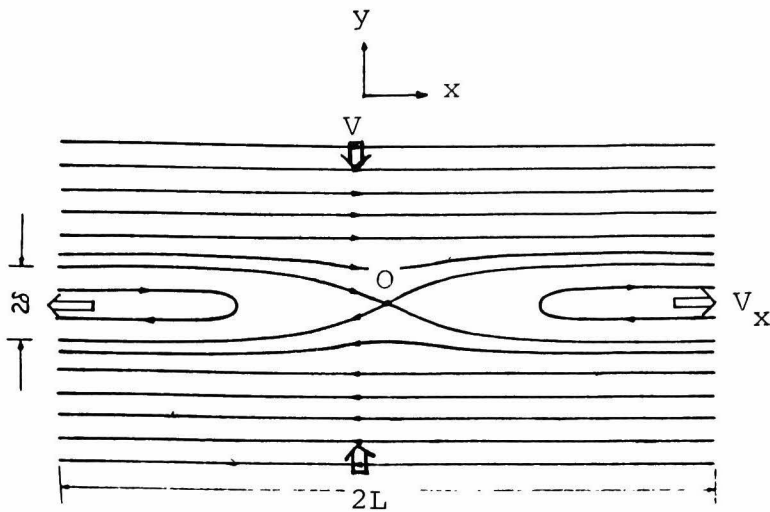


Fig. 4. Sweet-Parker reconnection model. The electric current flows only in the thin region $|y| < 2S$. Plasma flows into the region with speed V and is ejected with speed V_x .

only the magnetic field diffusion due to finite resistivity is dominant, so that in this model the field reversal region is entirely identified with the so-called diffusion region.

In this simple field geometry the plasma inflow velocity V and the plasma outflow velocity V_x can readily be estimated as follows. If the magnetic force ($\underline{j} \times \underline{B}$) is assumed negligible in the field reversal region we obtain the outflow velocity V_x from Bernoulli's law: $\rho V_x^2/2 = P_0 - P_b$, where ρ is the mass density, P_0 is the gas pressure at the origin and P_b is the gas pressure at large distances from the origin. The pressure balance across the field reversal region gives $P_0 - P_b \simeq B_{x0}^2/2 \mu_0$ if V is very small, where B_{x0} is the field strength outside the field reversal region. These equations lead to $V_x \simeq V_A$ where $V_A = B_{x0}/(\rho \mu_0)^{1/2}$ is the Alfvén speed. Also in a steady state the magnetic field must continuously be carried in

by the plasma inflow of velocity V at the same rate as that at which the field lines diffuse away due to finite resistivity η in the diffusion region. This means from the x -component of the diffusion equation

$$v = \eta / (\mu_0 \delta) \quad (2.1)$$

where δ is the half-width of the diffusion region. Considering the mass conservation law of an incompressible plasma gives $V_L = v_x \delta$, we finally obtain

$$M_0 = V/V_A \simeq R_m^{-1/2} \quad (2.2)$$

where $R_m = \mu_0 L V_A / \eta$ is the magnetic Reynolds number.

Eqn. (2.2) gives the dimensionless Alfvén Mach number which is defined as the plasma inflow velocity divided by the Alfvén speed. This is conventionally regarded as the reconnection rate. We can readily see that the reconnection rate is strongly dependent on the magnitude of resistivity. Considering that the magnetic Reynolds number is usually extremely large in cosmic systems, we may recognize that the reconnection rate given by Eqn. (2.2) is too small to account for the solar flare phenomenon. Note that this result comes from the basic assumption that magnetic energy is decreased by the finite resistivity only.

§3. Petschek's Model

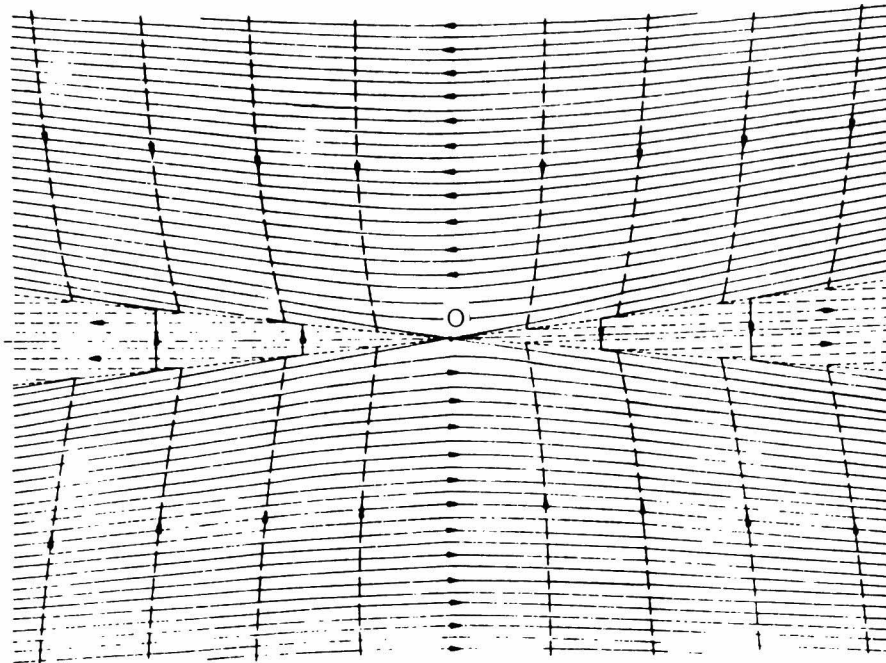


Fig. 5. The Petschek mode calculated by Vasyliunas. The solution is shown only for the convection region.

Petschek(1964) first recognized that MHD waves would realize a much faster reconnection rate than that predicted by the Sweet-Parker model. Fig. 5 shows the Petschek-type configuration that was accurately calculated by Vasyliunas(1975). There are four standing slow shocks (shown in dotted lines in the figure) attached to the diffusion region which is now restricted to a small region in the vicinity of the neutral point.

According to Vasyliunas, the existence of the slow shocks can be expected from the following consideration. Consider a problem in ordinary fluid dynamics: collisions of two oppositely directed jets. If the two jets approach each other at supersonic speed, no deflection can take place until the flow has been made subsonic by a shock transition; thus a pair of shocks must exist



in the flow field. In the reconnection problem the relevant waves are not sound waves (or fast waves) but slow mode waves: they are the ones that carry the information about the presence of the field reversal region. Since the slow wave speed approaches zero as the propagation direction becomes perpendicular to the magnetic field, the plasma flow is supersonic with respect to the slow wave in any region where $\underline{V} \cdot \underline{B}$ approaches zero, including in particular the vicinity of the y axis in the present problem. Thus magnetic reconnection can be regarded as the collision of two jets of plasma carrying oppositely directed magnetic fields; in the vicinity of the neutral point they approach each other at a speed that, no matter how small, is always supersonic with respect to the MHD slow wave, and hence their collision is expected to give rise to slow shocks. Since slow shocks cannot propagate perpendicular to \underline{B} either, they must remain attached to the diffusion region.

Vasyliunas precisely computed the steady-state Petschek mode in an incompressible fluid by a perturbation expansion for small reconnection rates. He gave analytical solutions in the limit of $R_m \rightarrow \infty$ for the convection region that corresponds to the large-scale region surrounding the diffusion region. In the diffusion region, on the other hand, the results shown in the previous section are simply assumed to be directly applied. In order to obtain the entire solution, he postulated that the size of the diffusion region would adapt to any imposed external flow and then matched the solution for the convection region to

the solution for the diffusion region.

Recently, Soward & Priest(1977) independently presented mathematical solutions for the steady Petschek mode. Fig.6 shows the reconnection rates for the Petschek mode shown by Priest & Soward(1976). In obtaining the results the same postulate as above is also introduced. This figure shows the relations between the Alfvén Mach number at the distance L_e , the characteristic scale length of the whole region to be considered, (denoted by M_e which may be identified with the reconnection rate) and the same quantity just outside the diffusion region (denoted by M_i) on the y axes. In the figure the relation between M_i and M_e is shown using $R_{me} (= \mu_0 L_e V_A / \eta)$, as a parameter. It should be noted that for a given R_{me} any

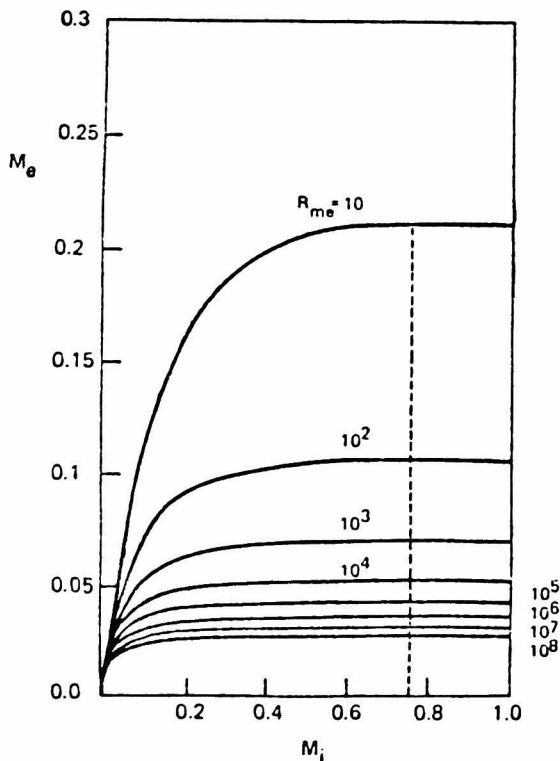


Fig. 6. Relation between the Alfvén Mach number M_e at the distance L_e and the same quantity M_i just outside the diffusion region, calculated by Soward and Priest.

reconnection rate is considered to be possible from zero to an upper limit. This conclusion certainly comes from the basic postulate prescribed in order to match the convection region to the diffusion region.

§4. Similarity Models

Sonnerup (1970) and Yeh & Axford (1970) incorporated Petschek's basic idea and developed the similarity models. These authors approximate for simplicity that the solutions should have a property of similarity and obtained exact solutions for incompressible fluids with zero resistivity. Yeh & Axford obtained an entire family of solutions of MHD equations for the reconnection problem, and Sonnerup independently obtained one solution that is the sole nonsingular member of the family. But, the singular similarity models must be discarded as extraneous solutions of the mathematical equations that cannot be realized in the physical world (Vasyliunas 1975).

Fig. 7 shows the nonsingular similarity model proposed by Sonnerup. As seen in the figure, there appear four outer discontinuities outside the slow shocks. These outer discontinuities in fact appear to be physically unrealistic. Sonnerup (1973) concluded that "one would not expect the outer discontinuities actually to be present. Rather the outer discontinuities should be viewed as a mathematical model, lumping all of the

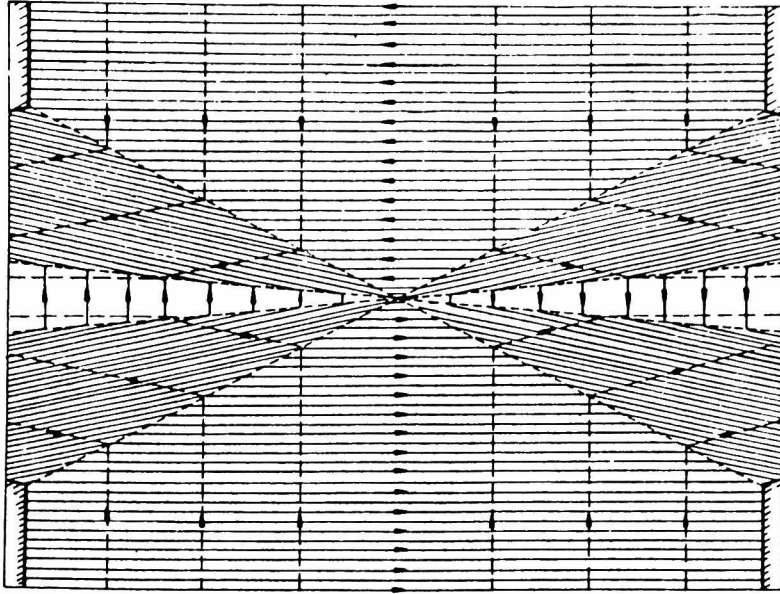


Fig. 7. Nonsingular similarity model proposed by Sonnerup. The suggested corners of Sonnerup at the edges of the system are also shown.

MHD interactions in front of the Petschek waves into one line."

Also noted is the special boundary condition imposed at the edges of the system: the suggested corners of Sonnerup, shown in Fig. 7 , is considered as bounding the system with impermeable walls on the sides. It seems doubtful whether such a boundary condition can be provided in actual physical systems, but Sonnerup's model may be an illustrative solution of the governing equations that serves to demonstrate another possible configuration of fast reconnection different from the Petschek mode.

§5. Discussion

The theoretical studies have taken many serious assumptions in order to make the problem analytically tractable but have revealed several fundamental physical mechanisms that would be crucial in realizing rapid large-scale conversion of magnetic energy into plasma energy due to field line reconnection. Especially, Petschek's basic idea that standing slow shocks should be important for the present problem may resolve the question raised by Parker. It is now well recognized that the Petschek mode is the only workable model for the fast reconnection process (Priest & Soward 1976).

It seems instructive to show some major limitations involved in the analytical treatments for the present two-dimensional model. These may be summarized as follows.

(1) Fluid compressibility

Most analytical treatments assume that the plasma is incompressible. However, it should be noted that the whole region under consideration consists of the two characteristic regions, namely the field reversal region and the external flow region. Since magnetic field is rather weak in the field reversal region but, on the other hand, sufficiently strong in the external region, the plasmas existing in the system must range from low- β to high- β plasmas. Hence, the above assumption is questionable in the real physical system. It is quite important in understanding the fast-reconnection process to study a compressible

plasma, especially so in analyzing the shock structure.

(2) Matching between the convection region and the diffusion region

The analytical studies mostly concentrated on seeking the fast-reconnection solutions in the convection region where the resistivity effect was assumed to be negligible. In order to construct the entire solution, they intended to match the obtained convection region to the diffusion region. However, the detailed structure of the diffusion region which should be matched to the external flow has not as yet been shown in a convincing manner (Vasyliunas 1975).

(3) Temporal dynamics of fast reconnection

The suggested models of fast reconnection were concerned with steady-state configurations. There may hence arise a most fundamental question whether or not the Petschek mode can eventually be established in actual plasma systems. If possible, one may then ask what is the ultimate cause of realizing the Petschek mode and what physical factors control the reconnection rate. These essential questions could not be answered in any convincing manner without examining the temporal dynamics of fast reconnection by solving the governing equations as an initial-boundary problem.

There remain many fundamental problems still unsolved because of mathematical difficulties, since the reconnection process involves strong nonlinear hydromagnetic effects. Without doubt, computer experiment may provide a useful means for such a problem.

The following chapters show our recent computer experiments that deal with the temporal dynamics of fast reconnection in order to elucidate fundamental problems of the Petschek mode.

MAGNETIC FIELD-LINE RECONNECTION BY LOCALIZED
ENHANCEMENT OF RESISTIVITY;
EVOLUTION IN A COMPRESSIBLE MHD FLUID*

§1. Introduction

The present chapter studies by computer experiment the temporal dynamics of field-line reconnection in a conducting fluid. As an initial static equilibrium we consider a compressible plasma permeated by an antiparallel magnetic field. Suppose a situation such that the effective resistivity is somehow suddenly enhanced locally in the current sheet because of some micro-instabilities. The only and the most fundamental assumption is, as will be discussed later, that such an indentation of anomalous resistivity is maintained with the growth of merging process, and then the full set of MHD (magnetohydrodynamic) equations is numerically solved by computer. Both the time and spatial domains for computation are taken so large that the hydromagnetic nonlinear effects are fully taken into account. Field-line reconnection begins in the above situation in the initial stage, and then the plasma

* See Ugai and Tsuda (1977)

bulk flow grows as a result of the reconnection. The strong hydromagnetic nonlinear effects of the system can bring about the build-up of the X-type field configuration occupying an extended region, as well as the global flow pattern with sufficiently large outflow and inflow velocities. The rapid release of magnetic energy into kinetic and thermal energies occurs and then the remarkable ejection of enhanced plasma energy through the field reversal region follows. The required configuration can spontaneously be set up without any specially imposed boundary condition, so that the progress of reconnection is strongly influenced by the local condition near a magnetic neutral point. This is quite different from the analytical results for the steady state process which state that the boundary conditions are the major influence (e.g., Vasylunas 1975)

§2. Governing Equations

The MHD equations are written in the form

$$\begin{aligned}
 D \xi / Dt &= - \int \nabla \cdot \underline{u} \\
 \int D \underline{u} / Dt &= - \nabla P + \underline{J} \times \underline{B}, \\
 \partial \underline{B} / \partial t - \nabla \times (\underline{u} \times \underline{B}) &= - \nabla \times (\eta \underline{J}),
 \end{aligned}
 \tag{3.1}$$

$$\rho \, D e / D t = -P \nabla \cdot \underline{u} + \eta \underline{J}^2,$$

$$\nabla \cdot \underline{B} = 0,$$

$$\underline{J} = \mu_0^{-1} \nabla \times \underline{B},$$

where we have employed the usual convention, $D/Dt \equiv \partial/\partial t + \underline{u} \cdot \nabla$, and assumed the Ohm's law, $\underline{E} + (\underline{u} \times \underline{B}) = \eta \underline{J}$. Here e is the internal energy per unit mass and η is the electrical resistivity. We assume the gas law

$$P = (\gamma - 1) \rho e,$$

where γ is the specific heat ratio. Since, from (3.1), $\partial(\nabla \cdot \underline{B})/\partial t = 0$, the solenoidal condition is necessary only at the start of computation.

Next, we perform scaling on the variables. In selecting the characteristic quantities for scaling, we employ those based on the initial data that will be given in §3. Distances x , etc., are normalized by L , the perpendicular half-width of the current sheet; magnetic field \underline{B} , mass density ρ and fluid velocity \underline{u} by B_0 , ρ_0 and $V_A (= B_0/(\mu_0 \rho_0)^{1/2})$; the Alfvén speed), respectively, each pertaining to the respective quantity outside the current sheet. Time t is thus normalized by L/V_A , the time required for an Alfvén wave to cross the half-width of the current sheet. Accordingly, energy density

is normalized by $B_0^2/(2\mu_0)$, electric field by $B_0 V_A$, current density by $B_0/(\mu_0 L)$, and so forth. Hereafter, unless otherwise specified, all the variables that appear are understood to have been normalized in this way. Also, the electrical resistivity η that depends on space variables in our model is normalized by η_0 , the ambient resistivity at distances from the co-ordinate origin that will be the neutral point of magnetic field.

In the present experiment, we assume that the phenomenon we study is two-dimensional; namely, there is no magnetic field nor fluid velocity in the z direction and every quantity depends on x and y co-ordinates and not on z . Electric current flows in the z direction only. The numerical scheme adopted here requires a further transformation of (3.1) to a conservation form. After some manipulation, the set of equations to be solved can be written as

$$\partial \underline{U} / \partial t + \partial \underline{\tilde{F}}(\underline{U}) / \partial x + \partial \underline{\tilde{G}}(\underline{U}) / \partial y = 0. \quad (3.2)$$

Here

$$\underline{U} = \begin{pmatrix} \rho \\ \rho u_x \\ \rho u_y \\ B_x \end{pmatrix}, \quad \underline{\tilde{F}} = \begin{pmatrix} \rho u_x \\ \rho u_x^2 + (P + B_y^2 - B_x^2)/2 \\ \rho u_x u_y - B_x B_y \\ 0 \end{pmatrix}, \quad \underline{\tilde{G}} = \begin{pmatrix} \rho u_y \\ \rho u_x u_y - B_x B_y \\ \rho u_y^2 + (P + B_x^2 - B_y^2)/2 \\ u_y B_x - u_x B_y + R_m^{-1} \eta J \end{pmatrix},$$

$$\begin{pmatrix} B_Y \\ E_T \end{pmatrix} = \begin{pmatrix} u_x B_Y - u_Y B_x - R_m^{-1} \eta J \\ F \end{pmatrix} = \begin{pmatrix} 0 \\ G \end{pmatrix}$$

where

$$\left. \begin{aligned} E_T &= P/(\gamma-1) + \rho(u_x^2 + u_y^2) + (B_x^2 + B_y^2), \\ F &= \gamma P u_x / (\gamma-1) + \rho u_x (u_x^2 + u_y^2) + 2(u_x B_Y^2 - u_Y B_x B_Y - R_m^{-1} \eta J B_Y), \\ G &= \gamma P u_y / (\gamma-1) + \rho u_y (u_x^2 + u_y^2) + 2(u_y B_x^2 - u_x B_x B_Y + R_m^{-1} \eta J B_x) \end{aligned} \right\} (3.2')$$

$$\text{and} \quad J = \partial B_Y / \partial x - \partial B_x / \partial y. \quad (3.3)$$

Also, R_m is the magnetic Reynolds number defined as

$$R_m = \mathcal{M}_0 V_A L / \eta_0.$$

The sixth component of (3.2) corresponds to the energy conservation equation. We may note there that E_T is the total energy (normalized by $B_0^2/2\mathcal{M}_0$) and that F and G are the total energy-flux densities (normalized by $V_A B_0^2/2\mathcal{M}_0$). The Ohm's law we have employed gives the electric field

$$E = E_z = -(u_x B_Y - u_Y B_x) + R_m^{-1} \eta J. \quad (3.4)$$

§3. Numerical Experiment

We first recapitulate the fundamental assumptions of our model, and then describe our somewhat simplified initial-boundary conditions, together with the numerical scheme adopted.

3.1. Assumptions of our model

An antiparallel magnetic field, or a current sheet, is supposed to exist in an initial equilibrium. If the conditions are favourable, a number of micro-instabilities can eventually grow in the current sheet, giving rise to a considerable increase of resistivity due to their turbulent effects (Coppi and Friedland 1971). The time scales of micro-instabilities are in general much shorter than macroscopic times, and thus an anomalous resistivity would be established almost instantaneously. In addition, the actual magnetic field configuration in an equilibrium state would not be strictly one-dimensional, so that a resistivity increase would, in actual systems, be confined to the region where the conditions are most satisfactory. We hence suppose a situation such that the resistivity is suddenly enhanced locally in the current sheet.

Let some point in the middle of the current sheet be the origin O ; this will be the magnetic neutral point (see Fig. 8). We then assume the enhanced resistivity η in the simple dimensionless form given by

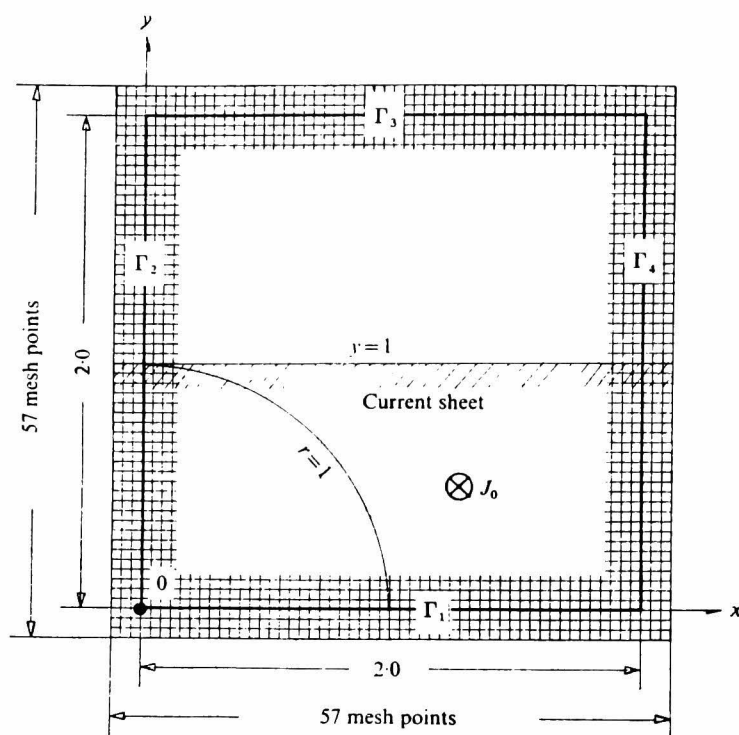


Fig. 8. Actual region for computation with 57×57 mesh points. Numerical solutions are required for the domain of size 2.0×2.0 , enclosed by thick lines. Origin O is the magnetic neutral point at which there is an enhancement of anomalous resistivity over the circular region $r \leq 1$. The electric current J_0 that forms the antiparallel magnetic field B_0 points vertically into the plane of the figure. At boundaries Γ_1 (midplane of the current sheet with null magnetic field) and Γ_2 , symmetry conditions hold. Boundaries Γ_3 and Γ_4 are free boundaries.

$$\left. \begin{aligned} \eta &= \frac{S-1}{k^3} (2r^3 - 3kr^2) + S && \text{for } r < k, \\ &= 1 && \text{for } r \geq k, \end{aligned} \right\} \quad (3.5)$$

where $r = (x^2 + y^2)^{1/2}$ is the distance from the origin. This means that η smoothly increases with decreasing r and becomes S times larger at the origin than in the background. The half-width of this enhanced resistivity is $r = 0.5$ for $k = 1$ and $S \gg 1$. It is assumed in our model that throughout our computation the resistivity η is maintained in the form of (3.5).

3.2. Initial-boundary conditions

The antiparallel magnetic field $\underline{B}_0 = (B_{x0}, B_{y0})$ is initially assumed as

$$\left. \begin{aligned} B_{x0}(x, y) &= y && \text{for } |y| \leq 1; \quad B_{x0} = \pm 1 && \text{for } y \gtrless \pm 1; \\ B_{y0}(x, y) &= 0. \end{aligned} \right\} \quad (3.6)$$

Therefore, the current density $J_0 = J_{z0} = -1$ for $|y| < 1$ and $J_0 = 0$ for $|y| > 1$ initially. The equilibrium state requires that the initial gas pressure P_0 be consistent with the balance condition

$$P_0(x, y) = 1 + \beta_0 - B_{x0}^2, \quad (3.7)$$

where β_0 is, in our dimensionless form, the initial gas pressure (i.e., the ratio of the kinetic pressure to the magnetic pressure) outside the current sheet. The mass density ρ_0 and the flow velocity $\underline{w}_0 = (u_{x0}, u_{y0})$ are initially assumed to be such that

$$\rho_0(x, y) = 1, \quad u_{x0}(x, y) = 0, \quad u_{y0}(x, y) = 0. \quad (3.8)$$

The symmetry of our present problem allows us to restrict the solution to the first quadrant only. In Fig. 8 the boundaries are labelled by T_i ($i=1,2,3,4$). On T_1 and T_2 the symmetry condition is imposed, but T_3 and T_4 are free boundaries: the values on T_3 and T_4 are simply extrapolated from the values at the nearest points immediately inside. More exactly, we assume

$$\partial \rho / \partial x = \partial u_x / \partial x = \partial u_y / \partial x = \partial B_y / \partial x = \partial P / \partial x = 0$$

on T_4 , and

$$\partial \rho / \partial y = \partial u_x / \partial y = \partial u_y / \partial y = \partial B_x / \partial y = \partial P / \partial y = 0$$

on T_3 ; B_x on T_3 and B_y on T_4 are given by the solenoidal condition. This means that the plasma can flow

freely across Γ_3 and Γ_4 in accordance with the states of the inner region.

3.3. Numerical scheme

The conservation form of the MHD equations, for the case of two Cartesian variables x and y , is given in (3.2). Let Δx and Δy denote the mesh sizes in the x and y directions respectively and Δt denote the time step. The two-step Lax-Wendroff scheme, which is adopted in our computation, first provides the auxiliary variables at time $t = (2m + 1)\Delta t$ with the equation

$$\begin{aligned} \underline{U}_{j,l}^{2m+1} = & \frac{1}{4} (\underline{U}_{j+1,l}^{2m} + \underline{U}_{j-1,l}^{2m} + \underline{U}_{j,l+1}^{2m} + \underline{U}_{j,l-1}^{2m}) \\ & - \frac{\Delta t}{2\Delta x} (\tilde{F}_{j+1,l}^{2m} - \tilde{F}_{j-1,l}^{2m}) - \frac{\Delta t}{2\Delta y} (\tilde{G}_{j,l+1}^{2m} - \tilde{G}_{j,l-1}^{2m}), \end{aligned}$$

(where the first subscript is for space variable x and the second for y), and then gives the physical variables at time $t = (2m + 2)\Delta t$ by the equation

$$\underline{U}_{j,l}^{2m+2} = \underline{U}_{j,l}^{2m} - \frac{\Delta t}{\Delta x} (\tilde{F}_{j+1,l}^{2m+1} - \tilde{F}_{j-1,l}^{2m+1}) - \frac{\Delta t}{\Delta y} (\tilde{G}_{j,l+1}^{2m+1} - \tilde{G}_{j,l-1}^{2m+1})$$

However, in the present case the fourth and the fifth components of (3.2) contain diffusion terms due to $R_m^{-1}\eta J$. A natural arrangement is to ignore these diffusion terms in constructing the auxiliary variables at time t^{2m+1} , and only

bring them in at the second step using $(R_m^{-1} \eta_j)^{2m}$ when the physical variables are recomputed at time t^{2m+2} . This rule is not observed in computing (3.2') where terms with η are retained throughout the first and second steps.

The above scheme will be numerically stable if it satisfies

$$(|u| + c) \Delta t / \Delta < 1/2^{1/2}$$

for the hyperbolic terms (here $\Delta = \Delta x = \Delta y$, and c and u are, respectively, the local wave speed and the fluid velocity), and

$$R_m^{-1} S(2\Delta t) / (2\Delta)^2 < 1/4 \quad (\text{cf. } \max_{j,l} (R_m^{-1} \eta_j) = R_m^{-1} S)$$

for the parabolic terms (where the resistivity η is given by (3.5)). The numerical errors were checked by calculations with two different time steps, $\Delta t = 0.003$ and $\Delta t = 0.0045$. We then found that the results of the two agreed at all times to within a small fraction of 0.1 % even after several hundred time steps. In addition, we may use the energy conservation law for checking errors. The details will be argued in §5; here we simply note that the energy conservation was correct to within 2-3 % after a few thousand time steps.

§4. Evolutionary Process of Field-Line Reconnection

In analytical studies of the steady states of reconnection, the domain of interest is divided into the diffusion region where lines of force decouple from the flow and the convection region where the flow is frozen in the magnetic field. This concept is also valid in the present time-dependent process. The present experiment, as mentioned above, initially supposes a localized enhancement of resistivity and no plasma flow, so that the start of the evolutionary process is triggered by field-line reconnection due to diffusion in the neighborhood of the magnetic neutral point. The plasma bulk flow will then arise in accordance with the change of the field configuration and a global flow pattern will be set up. The evolutionary process now at issue may thus be characterized by two stages: the initial diffusive stage and the subsequent hydromagnetic stage. The most significant features of the hydromagnetic stage are the strong nonlinear interactions between the diffusing field-lines near the neutral point and the convection of them in the adjacent region. With this in mind, the numerical results will be shown and discussed.

All the numerical results shown below are for the typical case $\Delta t = 0.0045$, $\gamma = 2$, $\beta_0 = 0.1$, $R_m = 1000$, $S = 100$ and $k = 1.0$. By varying the values of S and k , we see that the results do not change qualitatively. Note that be-

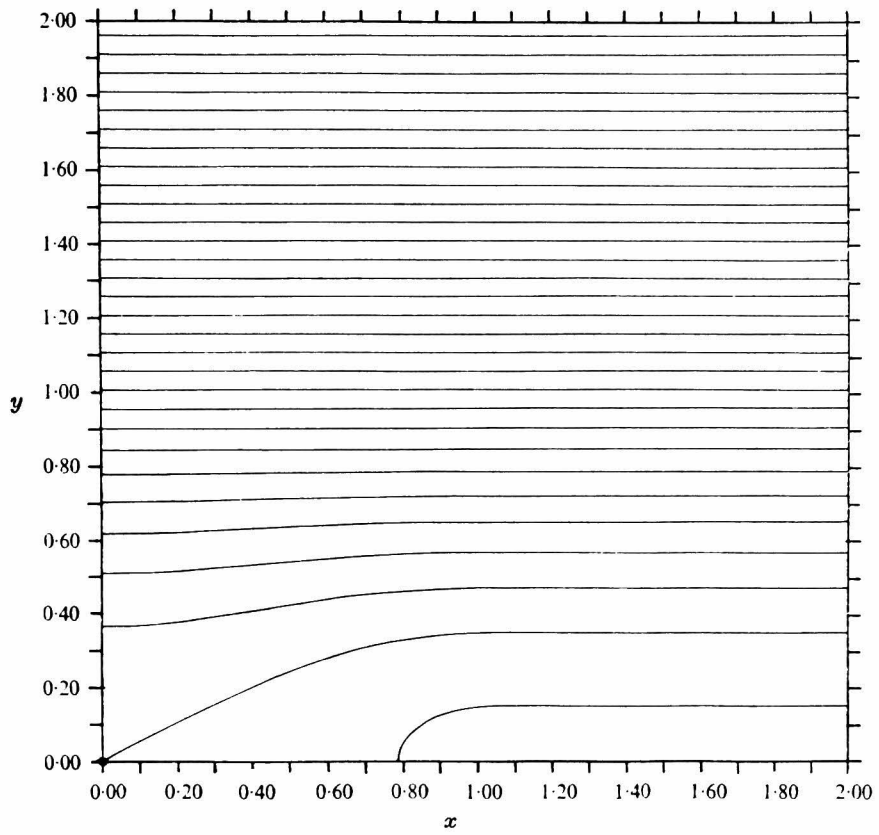
cause of the axisymmetry of the present problem the co-ordinate origin remains a magnetic neutral point and a stagnation point of the flow in the course of the evolutionary process.

4.1. Diffusive stage

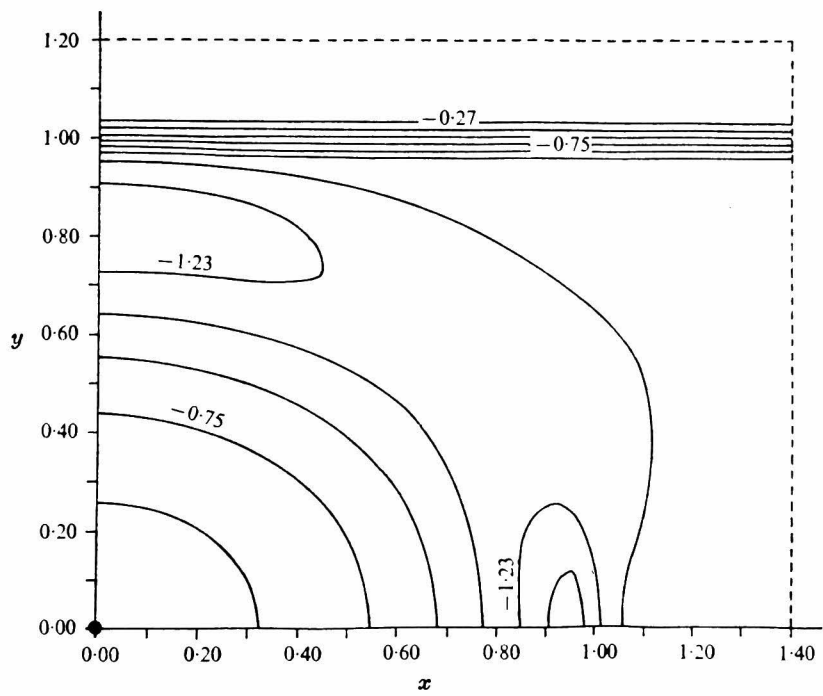
Prior to the very complex nonlinear effects in the hydromagnetic stage, we have the mechanism of initiating field-line reconnection by the localized enhancement of resistivity. We expect, from the consideration of magnetic-field diffusion, that the slippage velocity of the lines of force will be faster where the resistivity is larger (Stern 1966), so that

LEGEND TO Fig. 9

Fig. 9. Configurations in the diffusive stage at $t=0.9$ when the hydromagnetic effects remain negligibly small. (a) Computer-drawn magnetic field configuration. Lines are contour $A = \text{constant}$ (for graphical purpose only, the vector potential $\underline{A} = (0, 0, A)$ is obtained by numerically integrating $\underline{B} = \nabla \times \underline{A}$) and shown with contour interval of 0.05. (b) Current density distribution. Lines are contour $J = \text{constant}$ and shown with contour interval of 0.16 (this figure is shown only for the narrow region enclosed by dotted lines since in the remaining region the quantity of interest changes very little; similar remarks apply to Figs. 12, 13(a) and 13(b) also). The dot at the left bottom corner is the position of both the magnetic neutral point and the stagnation point of the fluid. Hereafter unless otherwise specified, all the similar figures that will appear are shown in the same way.



(a)



(b)

Fig. 9. For legend see page 44.

the localized enhancement of resistivity given by (3.5) will produce an apex in the lines of force in the region of enhanced resistivity and thus immediately initiate the field-line reconnection. Certainly, a rippling mode due to resistive instability may simultaneously be involved.

Figs. 9(a) and (b) show the field configuration and the contour lines of current density, respectively, at time $t = 0.9$ when the plasma flow velocity is still negligibly small; hence this time corresponds to the diffusive stage. We can see that the reconnection in fact builds up, although the resulting formation of an X-type field configuration at this stage is rather local in the region of enhanced resistivity. Also, we can see from Fig. 9(b) that the current density grows along the region where the resistivity increases. This is obviously owing to the field-line kink resulting from the bending of field lines in the local region of enhanced resistivity. No significant conversion mechanism of magnetic energy beyond the Joule dissipation is involved at this stage in the absence of plasma bulk flow.

4.2. Hydromagnetic stage

The hydromagnetic stage arises when the plasma flow has grown sufficiently large and strongly modifies the field configuration. On the basis of the complex numerical results, we show below the temporal dynamics of field-line reconnection

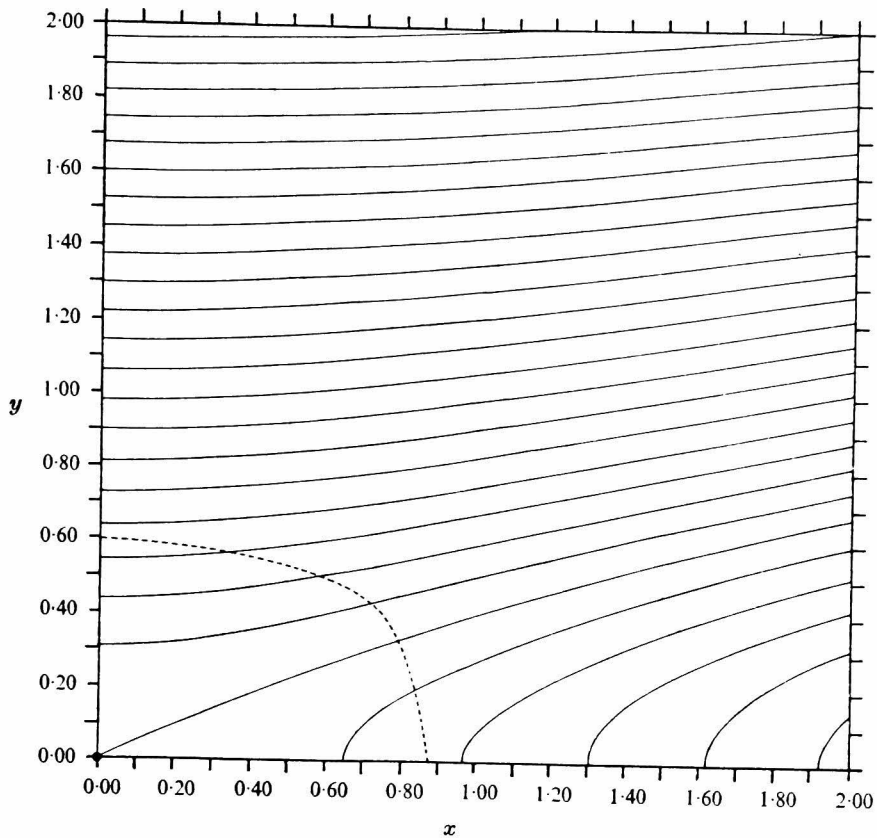


Fig. 10. Magnetic field configuration at $t = 14.4$.
 indicates the boundary of the diffusion region given
 by $D (\equiv |\underline{u} \times \underline{B} / (R_m^{-1} \eta | \underline{J} |) = 10$.

in this stage.

Fig . 10 is the computer-drawn configuration of magnetic field at time $t = 14.4$. Note that there are two different classes of field lines bounded by the separatrix; namely, the field lines prior to reconnection and those post reconnection. The X-type field configuration, which formed rather locally near the neutral point in the initial time range, grows spatially because of the strong hydromagnetic effects. It should be

remarked that the separatrix stretches out almost straight.

Figs. 11(a) and (b) show the temporal behaviour of flow vectors. We can first confirm from (a) that the fluid is in fact accelerated in bulk because of the initial field-line reconnection. In this figure a vortex of fluid is formed near the neutral point where the magnetic field is very weak. This seems to be a reaction to the initial abrupt reconnection by the indentation of resistivity, which disappears with time, as shown by Fig. 11(b). For a possible interpretation of this phenomenon, see §6. Fig. 11(b) shows that, if the anomalous resistivity is sustained, then the plasma bulk flow further grows because of the hydromagnetic effects, and we can see that the global flow pattern is set up over the whole region. We may remark that the plasma flow out of the region rather than into the region grows in the initial time range, and that the incoming flow is eventually induced to a high

LEGEND TO Fig. 11

Fig. 11. Temporal variations of flow pattern. (a) $t=3.6$; (b) $t=14.4$. The magnitude of the velocity at each rear end of arrows is measured by the distance from there to the center of the associated triangle. Length of 0.07 by the scale of the coordinate axes corresponds to 0.1 in the magnitude of normalized velocity.

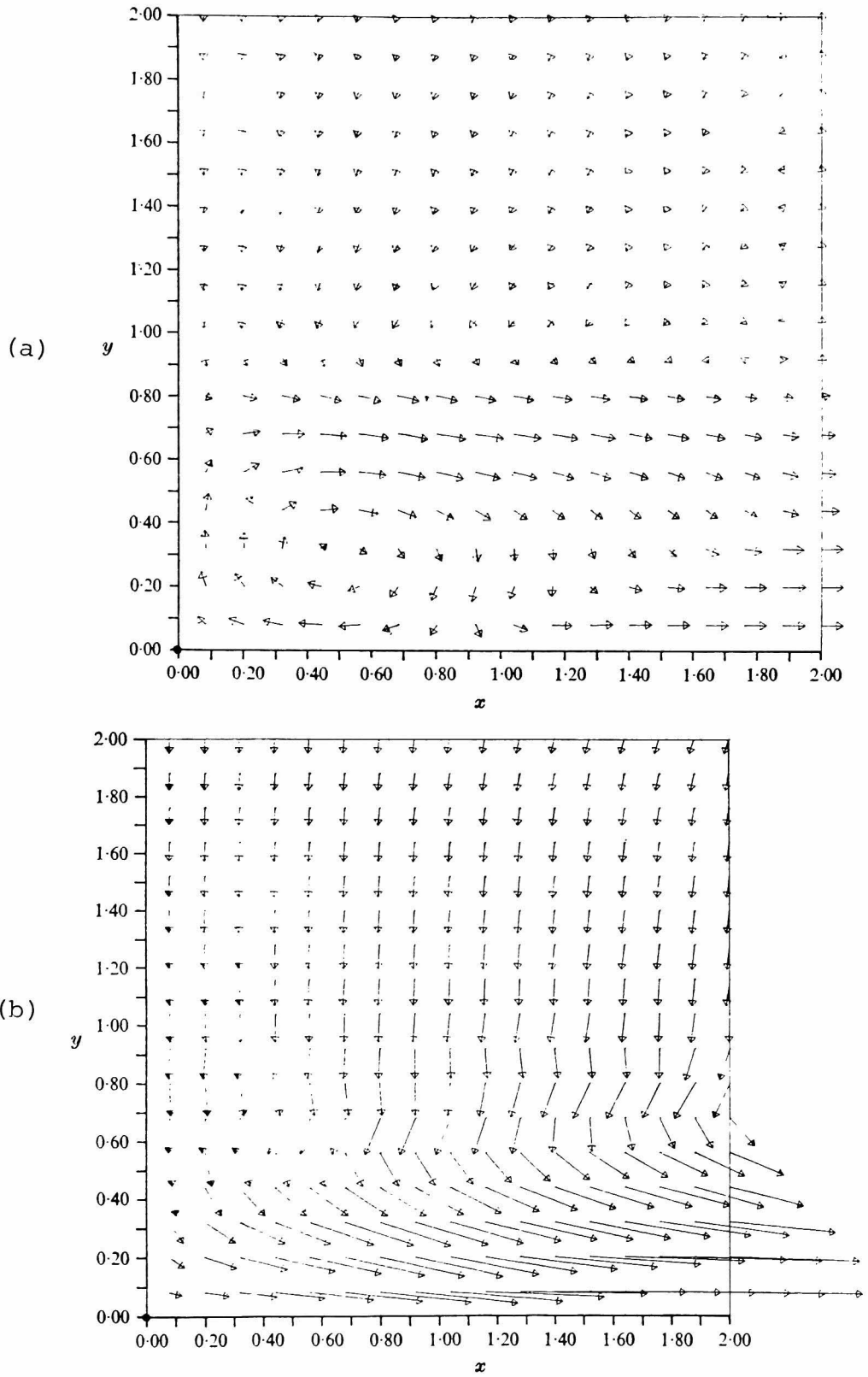


Fig. 11. For legend see page 48.

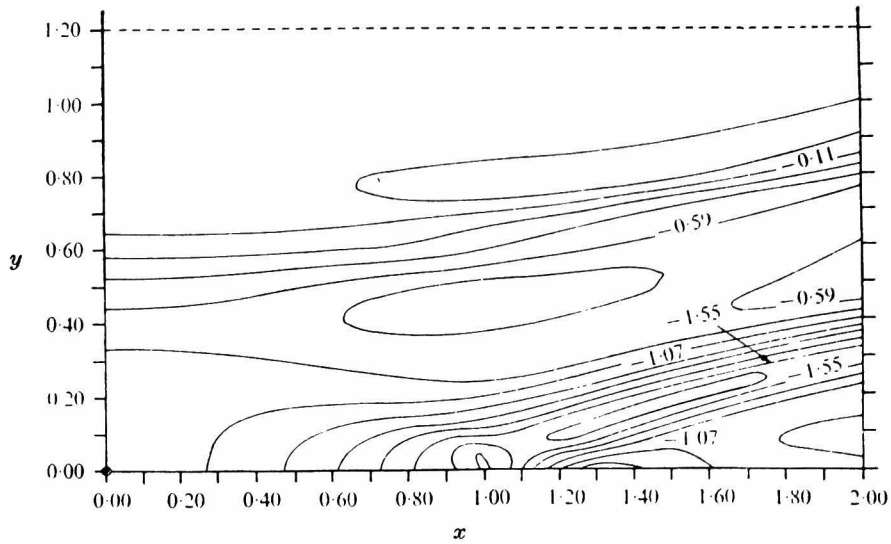


Fig. 12. Contour lines showing the current density distribution at $t = 14.4$.

speed to compensate for the rapidly growing outflow.

Fig. 12 shows the contour lines of current density at time $t = 14.4$. At $t = 0$, the current density $J = -1$ in $|y| < 1$ and $= 0$ in $|y| \geq 1$. The figure clearly shows how the initial current sheet collapses as the reconnection proceeds. At early times, such as $t = 3.6$, we see that there exist two regions of enhanced currents below and above the separatrix. One near $(x, y) = (1.0, 0)$ is obviously due to the accumulation of the reconnected field lines, since up to that time diffusion from within rather than outward convection of field lines has been the dominant process there. Such an accumulation will be shown more quantitatively shortly (see Fig. 14). The other region of enhanced current density extends along the field lines from the vicinity of $(x, y) =$

(0, 0.8). This seems due to the fast wave that can be excited by the bending of field lines owing to the enhanced resistivity and which propagates along the magnetic field, since there exists a sufficiently strong zero-order magnetic field to allow for the growth of MHD waves. From Fig. 12, however, it can be seen that the nearly current-free region has broadened with time in the shape of a down-coming wedge in accordance with the build-up of the X-type field configuration and the growth of the inflow. Note that the uppermost contour line corresponds to a positive value of 0.05, which means the current flows in the inverse direction there.

Figs. 13(a) and (b) show the temporal behaviour of mass density distribution. At $t = 0$ the distribution of mass density is set to $\rho = 1$ over the whole region. From 13(a), we can observe that a thin transition region gradually appears, within which the mass density considerably changes, and extends with time along the field lines from the vicinity of $(x, y) = (0, 0.8)$. Note that at the front tip of the region [i.e., near $(x, y) = (0, 0.65)$ in the case of Fig. 13(a)] the mass density is notably rarefied. This is obviously because, as may be seen in Fig. 11(a), at this point the plasma flow turns its direction to the positive x direction to eject the fluid along this thin region. It can further be observed from Fig. 13(b) that the change of mass density becomes steeper and somewhat oscillatory in the y direction and that the front of the long thin transition region shifts towards the

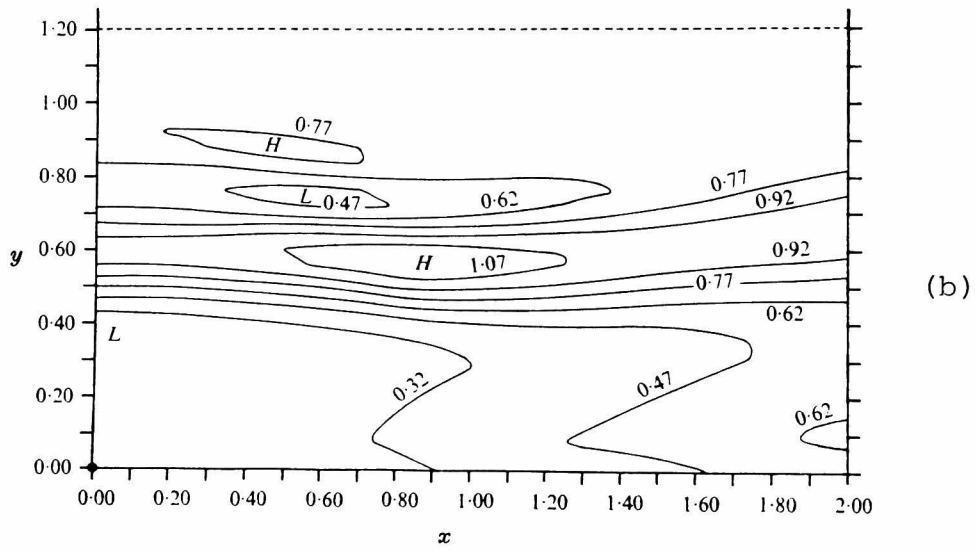
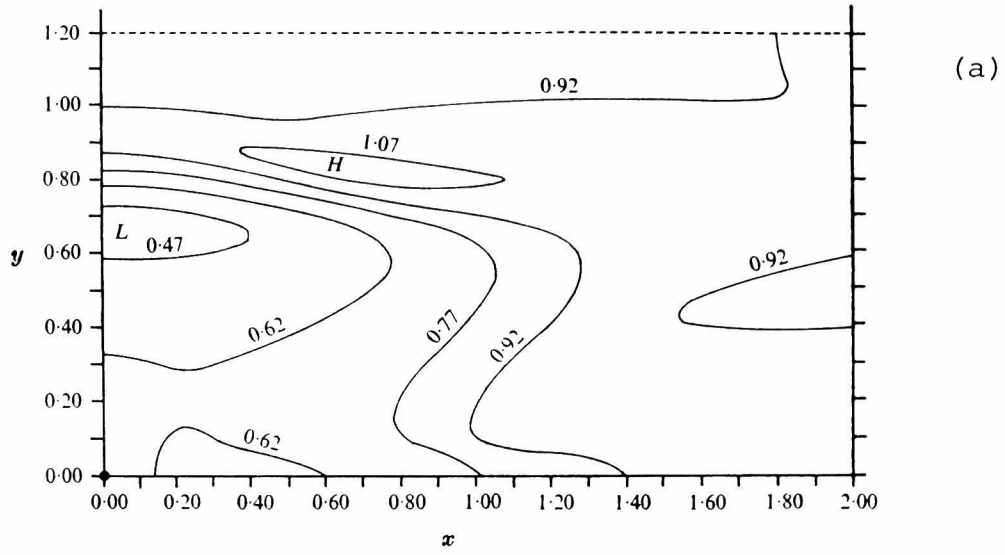


Fig. 13. Contour lines showing the temporal variations of plasma density distribution with contour interval of 0.15. H , high density ; L , low density. (a) $t = 9.0$; (b) $t = 14.4$.

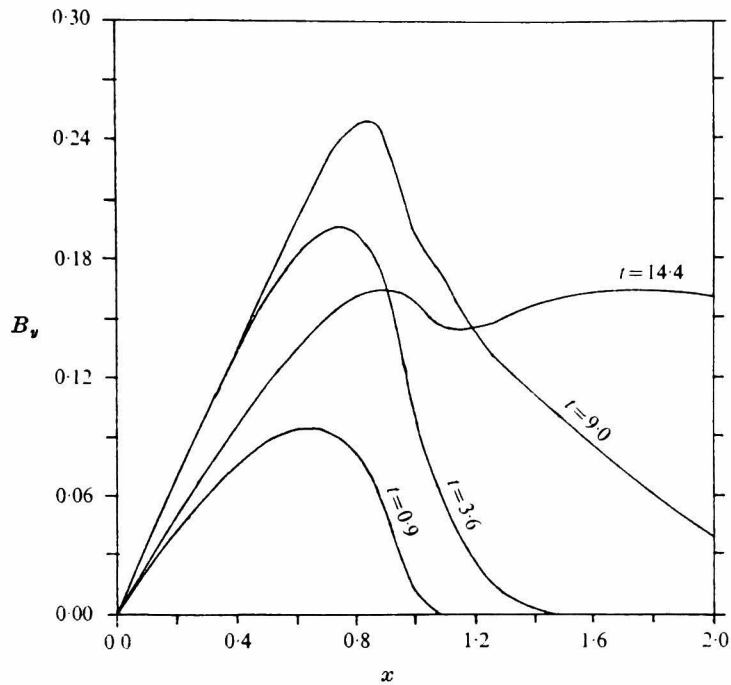


Fig. 14. Profiles of B_x for different times along the x-axis.

field reversal region in accordance with the rapidly growing inflow.

4.3. Further remarks

We now examine more quantitatively the important features of the evolutionary process from other angles.

Figs. 14 and 15 show respectively the variation with x of the normal magnetic field component B_y and the outflow velocity u_x at different times. The reconnected field lines are initially accumulated within the region of enhanced resistivity, since, as already mentioned, the reconnection is diffusively

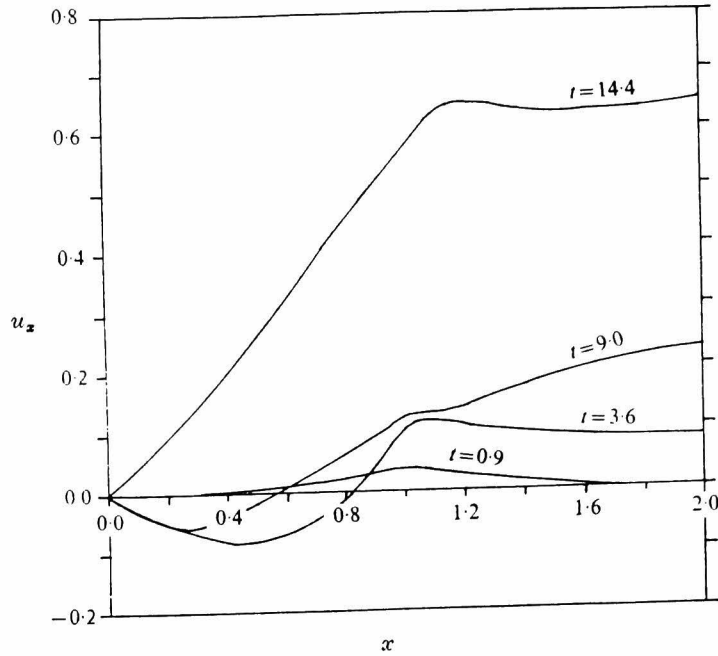


Fig. 15. Profiles of u_x for different times along the x-axis.

initiated before the outflow velocity grows. Note that the current density tends to decrease where B_y increases and increases where B_y decreases. Hence such an accumulation of the reconnected field lines obviously tends to check the field diffusion near the neutral point and push the plasma by the $\underline{J} \times \underline{B}$ force. This will result in the excitation of fast-mode MHD waves due to B_y that carry the plasma away from the neutral point. These tendencies are more and more apparent with the passage of time.

Figs. 16 and 17 show respectively the variation with y of the inflow velocity u_y and the magnetic field component B_x at different times. In the initial time range, B_x decreases near the neutral point owing to the diffusion of

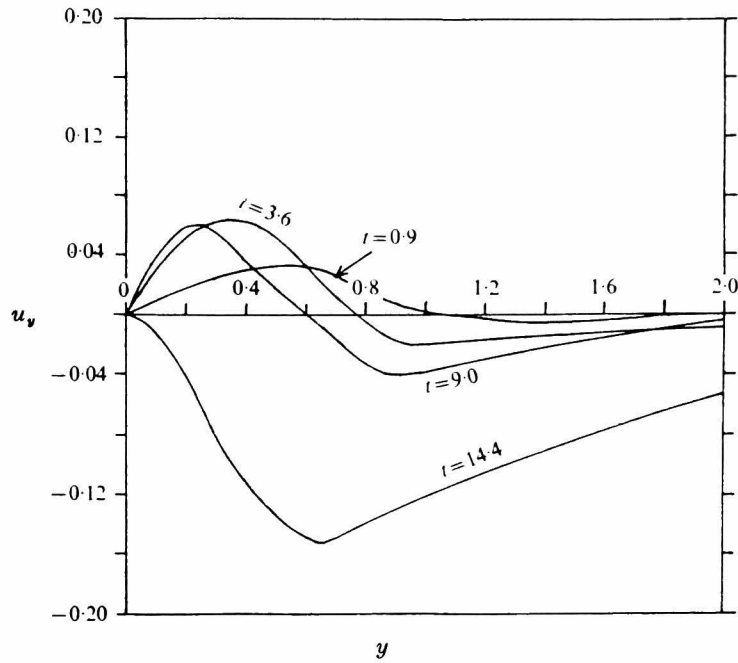


Fig. 16. Profiles of u_y for different times along the y -axis.

field lines. The inflow velocity, however, grows in accordance with the growing outflow mentioned previously, and B_x in turn increases near the neutral point owing to the convection of field lines. Such a convection of field lines evidently reinforces the current density near the neutral point that has been initially depressed (see Fig. 18) and thus furthers the magnetic field diffusion.

In Fig. 18, we show how the mass density ρ , the gas pressure P and the current density J (multiplied by -1 in the figure) vary with time at the magnetic neutral point. This figure clearly indicates the following process in the immediate vicinity of the X -line. The mass density decreases

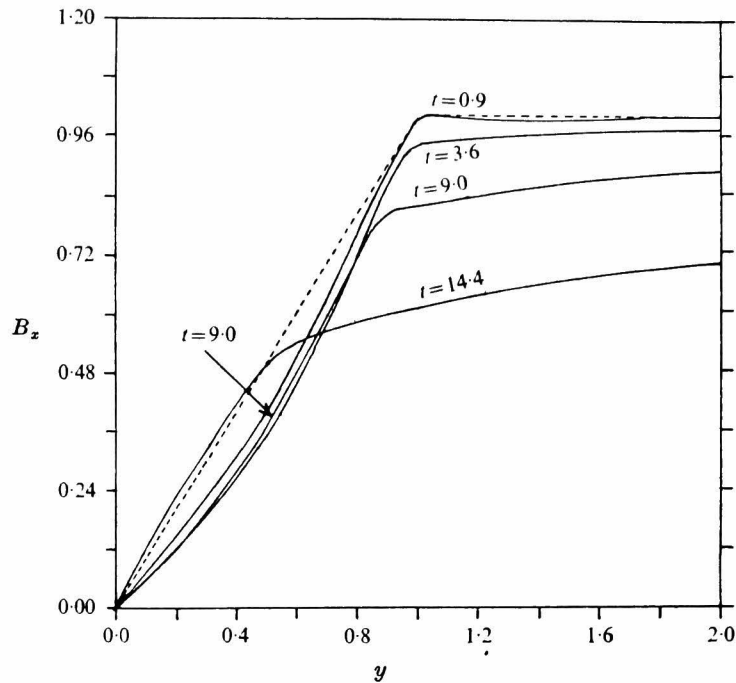


Fig. 17. Profiles of B_x for different times along the y -axis. The dotted line shows the initial profile.

because of the fluid escape from the vicinity of the neutral point. The gas pressure initially increases due to Ohmic dissipation near the neutral point and then decreases because of the fluid expansion there. This decrease of gas pressure near the neutral point can then trigger the plasma flow towards the field reversal region. The current density initially decreases owing to the diffusion of magnetic field lines by the local enhancement of resistivity and then increases owing to the convection and accretion of field lines by the growing inflow velocity.

The hydromagnetic nonlinear effects promote the growth of field-line reconnection, which, as will be shown in the

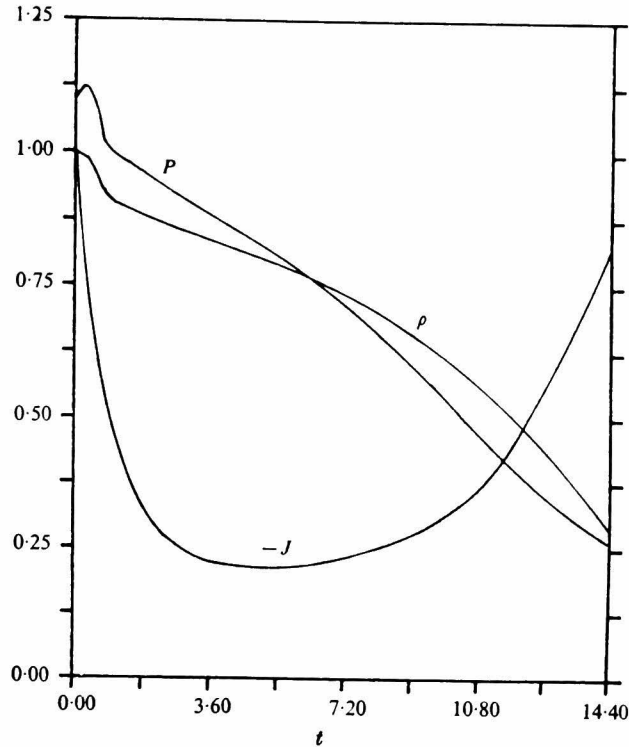


Fig. 18. Temporal variations of current density, mass density and gas pressure at the magnetic neutral point.

next section, involves a remarkable release of magnetic energy. In particular, the interdependence between the diffusion of field lines near the neutral point and the convection of field lines in the surrounding region seems significant in the above evolutionary process. Hence, it may be worthwhile to see more quantitatively the distinction between the diffusion region and the convection region. For this purpose, we may simply examine the values of $D \equiv \left| \frac{\underline{u} \times \underline{B}}{R_m^{-1} \eta \underline{J}} \right|$ at some points and consider that $D \ll 1$ holds in the diffusion region and that $D \gg 1$ holds in the convection region. The calculated results at time $t = 14.4$ are, for example, as follows. Along the y axis, $D \simeq 1/16$ at $(x, y) = (0, 0.2)$ and $\simeq 46$ at $(0, 1.0)$; and along the x axis, $D \simeq 1/3$ at $(x, y) =$

(0.4, 0) and $\simeq 49$ at (1.0, 0). Also, the boundary of the diffusion region given by $D = 10$ is indicated in Fig. 10. We thus see that, as the plasma flow grows, the diffusion region virtually "shrinks" to a smaller region in the neighbourhood of the neutral point, an interesting effect due to the interactions between the flow and the field.

§5. Magnetic Energy Conversion

Another significant aspect of the reconnection problem, in addition to the question of field-line topology, is the magnetic energy conversion. In the analyses of steady plasma flows, the magnetic field-line reconnection rate, which is proportional to the energy conversion rate, is measured by the magnitude of the inflow velocity of plasma at distances far from the field reversal region on the basis of the Poynting flux. In the present time-dependent process, however, the magnetic energy content in the region of numerical solution will vary with time because of the temporal variations of the field configuration as well as the Poynting fluxes across the boundaries. Hence, we will quantitatively examine the temporal behavior of each form of energy and directly see the process of energy conversion using the energy conservation law described by the sixth component of (3.2).

The Poynting vector theorem in our dimensionless form

becomes

$$\frac{\partial}{\partial t} \underline{\underline{B}}^2 + 2 \nabla \cdot (\underline{\underline{E}} \times \underline{\underline{B}}) + 2 \underline{\underline{E}} \cdot \underline{\underline{J}} = 0 .$$

Here the electric energy is neglected. Note that $\underline{\underline{F}} \cdot \underline{\underline{J}}$ indicates the exchange of energy between the magnetic field and the plasma and that $\underline{\underline{E}} \times \underline{\underline{B}}$ indicates the magnetic energy flow. Remembering the electric field $\underline{\underline{E}}$ given by (3.4), we can readily see that the second term on the left-hand side of the above equation is none other than the third terms of F and G , on the right-hand side of (3.2'). As expected, $\underline{\underline{E}} \cdot \underline{\underline{J}}$ does not appear explicitly in the energy equation, since the change of magnetic energy due to this quantity should be compensated by that of other forms of energy. It may be noted that the first, the second and the third terms of E_T , F and G , on the right-hand side of (3.2'), correspond to the convection of the thermal energy E_p , the kinetic energy E_K and the magnetic energy E_M , respectively.

Let S denote the whole region of numerical solution (see Fig. 8). Integrating the energy equation over this region, we obtain

$$\frac{\partial}{\partial t} \int_S E_T \, dS = - \int_{\Gamma_4} F \, dy - \int_{\Gamma_3} G \, dx. \quad (3.9)$$

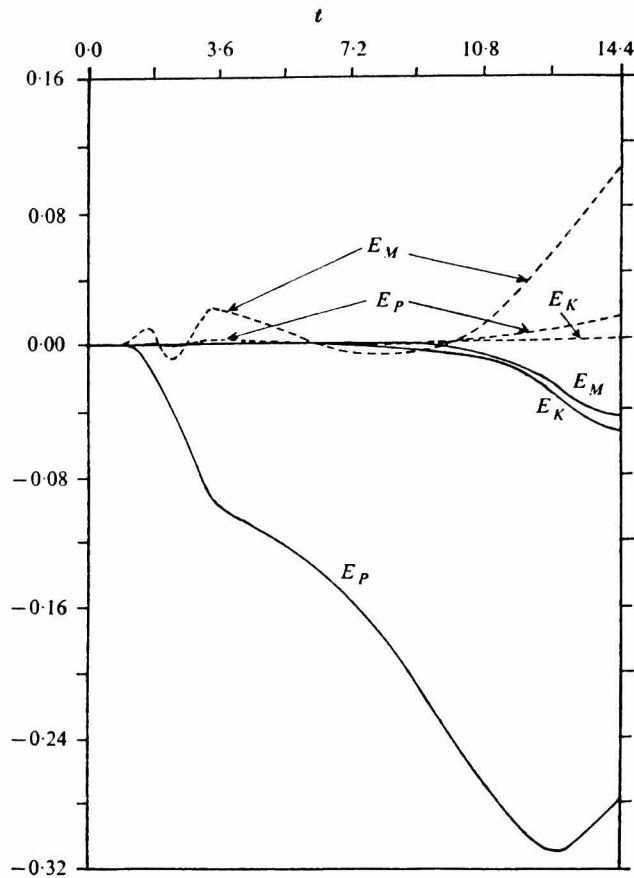


Fig. 19. Temporal variations of flows of thermal energy (E_P) magnetic energy (E_M) and kinetic energy (E_K) across boundaries Γ_3 (-----) and Γ_4 (——).

Here we have used the fact that there is no energy flow across Γ_1 and Γ_2 because of the axisymmetry. The first term on the right-hand side of (3.9) gives the temporal energy flow into the region across boundary Γ_4 . The results of numerical integration of this term with respect to y at different times are shown in Fig. 19 separately for each form of energy, i.e. thermal (plasma) energy E_P , magnetic energy E_M and kinetic (flow) energy E_K . Note that the negative value indicates the energy flow out of the region. From this figure, we see that each form of energy, especially the thermal

energy, flows out of the region in accordance with the growth of plasma outflow at Γ_4 (see Fig. 15). The second term on the right-hand side of (3.9) gives the energy flow across boundary Γ_3 . Its temporal variations are shown also in Fig. 19 separately for each form of energy. We can see from this figure that the magnetic energy rapidly flows into the region across boundary Γ_3 after the plasma inflow grows (see Fig. 16). Note here that, since the β -ratio is small near this boundary, the inflow of thermal energy is much smaller. We may consider that the energy inflow across boundary Γ_3 is virtually uniform, since, as seen from Fig. 11, the plasma flows in almost uniformly at distances far from the field reversal region.

Further integration of (3.9) with respect to t gives

$$E_{ST}(t) - E_{ST}(0) = - \int_0^t \left(\int_{\Gamma_4} F dy + \int_{\Gamma_3} G dx \right) dt, \quad (3.10)$$

where

$$E_{ST}(t) = \int_S E_T(t) dS .$$

$E_{ST}(t)$ indicates the energy content at time t in the region, which is shown in Fig. 20 for each form of energy. The thermal energy content initially increases by a small amount due to Ohmic dissipation and then notably decreases because of its rapid escape across boundary Γ_4 . The magnetic energy

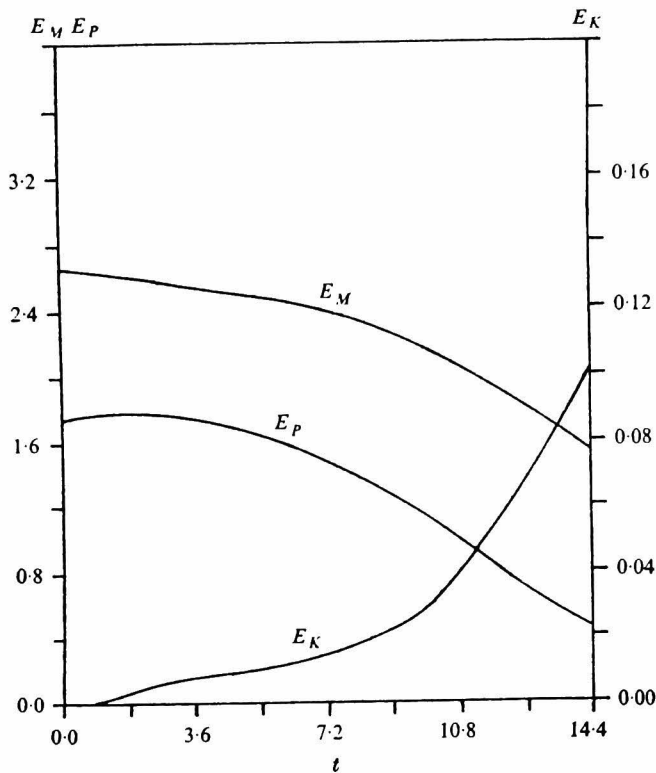


Fig. 20. Temporal variations of magnetic energy content (E_M), thermal energy content (E_P) and kinetic energy content (E_K) of the 2.0×2.0 region.

content becomes remarkably reduced in spite of the rapidly increasing flow of this energy into the region. This is obviously because, through the convection and reconnection of field lines, the field configuration is transformed and the field intensity decreases. Remember that the net amount of magnetic energy released in the region during a given interval of time is the amount of decrease of the magnetic energy content plus the total amount of the magnetic energy injected into the region over this time interval. These results show therefore that, in the present evolutionary process, the magnetic energy is quite efficiently released into kinetic and thermal energies through field-line reconnection and that the enhanced energy of the plasma is rapidly ejected along

the length of the field reversal region, i.e. the x axis.

Equation (3.10) states that the total energy content increases by the total amount of energy injected into the region. The numerical errors may be examined on the basis of this fact. We have numerically calculated each term of (3.10) and examined the energy conservation relations by the percentage

$$100 \times \left| \frac{E_{ST}(t) + \int_0^t \left(\int_{\Gamma_4} F dy + \int_{\Gamma_3} G dx \right) dt - E_{ST}(0)}{\int_0^t \left(\int_{\Gamma_4} F dy + \int_{\Gamma_3} G dx \right) dt} \right|.$$

It is then found that the energy conservation was correct to within 2-3 % throughout the present computation.

§6. Concluding Remarks

We now give physical interpretations to the two interesting facets of the evolutionary process observed in the numerical experiment: first, the mechanism by which the MHD flow, initially quiescent, is induced and, second, the generation and propagation of MHD waves near the neutral point.

The peculiar two-layered flow toward the positive x direction observed near $(x, y) = (0.3, 0.7)$ and $(1.0, 0.0)$

of Fig. 11(a) could occur as follows. In the diffusive stage ($t \lesssim 1$) there is a local pressure rise (and, hence, a temperature rise) at the neutral point due to the Joule dissipation (see Fig. 18) which allows the fluid to expand away from the neutral point. This, together with the $\underline{J} \times \underline{B}$ force (in the form of $J B_y$, with B_y produced by reconnection), drives the fluid to the right at $x \gtrsim 1.0$ on the x axis. See the confluence from above and below at about $(x, y) = (0.0, 0.7)$ that gives rise to the rightward motion of the other flow. The flow pointing downward to $(x, y) = (0.0, 0.7)$ seems to be due to the $\underline{J} \times \underline{B}$ force (a downward force) where \underline{J} is the current enhanced by the erosion of magnetic field. Note that Fig. 17 in fact indicate this erosion due to magnetic field diffusion or in other words the local increase of magnetic field gradient. The flow pointing upward to $(x, y) = (0.0, 0.7)$ can be driven not only by the already mentioned expansion force due to the Joule dissipation at time $t \lesssim 1$ but also by the local decrease of magnetic field gradient near the neutral point (see Fig. 17).

In the present evolutionary process MHD waves must have played crucial roles. For instance, the fast wave propagating along the magnetic field must have been excited by the field-line kink due to the locally enhanced resistivity, to form the extended X-type field configuration, and the fast mode expansion wave propagating upward must have been excited by the erosion of magnetic field due to the enhanced resis-

tivity to allow for the persistent inflow of plasmas. Also, the rapidly growing inflow observed in Fig. 11(b) may suggest the appearance of a magnetic merging mechanism such as the slow mode compression wave that propagates upward from the field reversal region, and is also convected toward it by the plasma inflow (see, for instance, Vasyliunas 1975). The slow wave, if any, would form a standing shock structure in the steady state, although it is difficult, at least at the present stage, to confirm unambiguously its existence from the compressional wavy structures seen in Figs. 13(a) and (b). This will be discussed in the next chapter.

In summary, the present numerical experiment has revealed many interesting and important features of reconnection processes. The compressible MHD fluid model, simple as it is, is a useful tool to study the realistic aspects not accessible to analytical methods. All the results, in contrast to the analytical results of the steady state process, show that the evolutionary process of field-line reconnection can be strongly influenced by the local conditions near a magnetic neutral point.

QUASI-STEADY PROCESS*

§1. Introduction

In the previous fast-reconnection models, most attention has been focused on the convection region where the field lines are frozen into the plasma. Surrounded by this convection region, there is the diffusion region where the field lines slip through the plasma. In recent years the importance of matching the variables between these two regions has been stressed (Priest and Cowley 1975), and more sophisticated treatments have been given (Priest 1973; Roberts and Priest 1975); but there is as yet no completely satisfactory method of matching (Vasyliunas 1975). There remain many interesting problems about the details of the self-consistent configuration of fast reconnection in compressible plasmas, and, more essentially, how the reconnection process can eventually be established and maintained in the system. The purpose of this chapter is to study these problems quantitatively by

* See Tsuda and Ugai (1977)

means of numerical experiment.

It has already been shown in the foregoing chapter that, if a sudden local increase in the electrical resistivity occurs in a current sheet, then the reconnection process simultaneously takes place. This results in the formation of an X-type magnetic field configuration involving the global plasma flow. In this chapter it is shown that, as time passes, the evolution is checked and a quasi-steady configuration is finally established. To cover this time range, however, some modification of the numerical scheme is mandatory as will be described in §2. The present reconnection process provides a large-scale mechanism of releasing magnetic energy into plasma energy without any external cause taken into account and, therefore, may be regarded as a gross instability in which the current-sheet system is involved by itself. (See the emerging flux model of the solar flare phenomenon (Heyvaerts, Priest and Rust 1977).)

The spatial domain of interest is usually divided into the diffusion region and the convection region; the latter may further be divided into the field reversal region where the field and flow properties notably change in both direction and magnitude and the external region where they change only slightly (cf. Fig. 24(a)). In the diffusion region, the magnetic field lines slip through the plasma and bend towards the magnetic neutral point owing to the locally enhanced resistivity (see chapter 3), which results in an increase of

magnetic tension in the system; in the field reversal region, the plasma is accelerated outwards by the magnetic tension and the outflow velocity grows to relax the magnetic stress; in the external region, the magnetized plasma is sucked into the inner region and is accelerated to compensate for the plasma ejection from the system. The quasi-steady reconnection process should proceed in a self-consistent way such that the effects in each region counterbalance and accommodate themselves to those in the other regions. Here the term "quasi-steady" is used in the sense that the overall structures of field and flow patterns have ceased changing with time, except for minor fluctuations, and become more or less stabilized.

In this chapter we shall study the numerical solution of the quasi-steady reconnection and quantitatively discuss the field and flow configurations in connection with the analytical results for steady reconnection. Above all, it will be remarked that the MHD properties across the boundary of the field reversal region can be characterized by a slow mode compression wave, and those in the external region by a fast mode expansion wave, so that the present quasi-steady configuration that has been set up from an antiparallel magnetic field will be found to be similar to that proposed by Petschek (1964) (cf. Vasyliunas 1975).

§2. Numerical Experiment

The numerical experiment will now be briefly described. All the basic equations, notations and numerical techniques are the same as in chapter 3 except that a viscosity term must be added to the two-step Lax-Wendroff scheme in the way shown below to carry out numerical computation over a time range beyond that of chapter 3. Readers are referred to §3 of chapter 3 for details other than this modification.

For smooth flows, the two-step Lax-Wendroff method, adopted in the computation of chapter 3, gives excellent results; however, for some problems, numerical instabilities show up in regions of rapid change and quickly swamp the entire solution, unless a viscosity term is used (Richtmyer and Morton 1967). In the present problem we find that the computational scheme of chapter 3 suddenly meets a numerical instability at about time $t=16.5$, when, as shown later, the plasma flow has grown so remarkably and rapidly changes across the field reversal region. Let us describe below the remedy for such an instability by introducing a viscosity term; for details the readers are referred to Richtmyer and Morton (1967).

As already shown, Eq.(3.1) can be transformed to the conservation form

$$\partial \underline{U} / \partial t + \partial \tilde{F}(\underline{U}) / \partial x + \partial \tilde{G}(\underline{U}) / \partial y = 0$$

in the present two-dimensional case (see Eq.(3.2) of chapter 3). The Lax-Wendroff scheme consists of two procedures: first, the auxiliary variables are provided at time $t = (2m + 1) \Delta t$ (Δt denotes the time step); second, the physical variables are computed at $t = (2m + 2) \Delta t$. The viscosity term adopted here takes the form

$$\frac{\Delta t}{2\Delta} [\Delta_{0x} (Q_x \Delta_{0x} \underline{U}) + \Delta_{0y} (Q_y \Delta_{0y} \underline{U})],$$

where, for any $f(x, y)$, $2 \Delta_{0x} f(x, y) = f(x + \Delta, y) - f(x - \Delta, y)$, and similarly for Δ_{0y} ($\Delta (= \Delta x = \Delta y)$ is the mesh size). Here Q_x and Q_y are given by

$$(Q_x)_{j+1, l} = \mathcal{K} \left| (u_x)_{j+2, l} - (u_x)_{j, l} \right|,$$

$$(Q_y)_{j, l+1} = \mathcal{K} \left| (u_y)_{j, l+2} - (u_y)_{j, l} \right|,$$

where \mathcal{K} is the viscosity coefficient. This viscosity term, with \underline{U} interpreted as \underline{U}^n ($n = 2m$), is simply added to the right-hand side of the equation at the second step when the physical variables are computed.

With this modified numerical scheme, we find that the calculations are indeed stable for sufficiently large \mathcal{K} . Note that the viscosity term is chosen in such a way that it gives the dissipative effect desired for numerical stability

when the spatial changes of \underline{U} are very large, but it is negligible when they are small; in the present case, we find by a number of computations that for smaller κ the flow properties change more steeply across the field reversal region but involve rather more oscillations (when and where changes in flow properties are small, these results are of course almost the same). It should perhaps be pointed out that the dissipation does not represent any loss of energy or other conserved quantities (Richtmyer and Morton 1967); indeed, throughout the present computation the energy conservation is correct up to a small fraction of about 2 % .

In chapter 3 the computed results were shown and discussed up to time $t = 14.4$ as meaningful in light of precision considerations. Actually the numerical experiment had been pursued with the previous numerical scheme (before modification) till time $t = 16.5$ when the numerical instability was seen to blow up suddenly. With the above modified numerical scheme, therefore, the computation is continued in this paper from time $t = 14.4$ onwards to obtain a quasi-steady solution.

The magnitude of the viscosity coefficient is $\kappa = 7.0$, and all the other parameters are, of course, the same as in chapter 3; namely, $\Delta t = 0.0045$, $\gamma = 2.0$, $\beta_0 = 0.1$, R_m ($= \mu_0 L V_A / \eta_0$, the magnetic Reynolds number) = 1000 and, for the locally enhanced resistivity η given by (3.5), $S = 100$ and $k = 1.0$.

§3. General Remarks

The steady process of magnetic field-line reconnection has been studied by several authors. The diffusion region, the field reversal region and the external region are indicated in Fig. 24(a), where the division is made on the basis of our numerical results, described later. Historically, most of efforts, directed to the fast-reconnection problem, have been focused on the analysis of characteristic MHD properties of each region, and also on the way of matching distinct regions self-consistently to find the possible reconnection rate.

Sweet (1958) and Parker (1963) first considered that, when two oppositely directed magnetic fields are pressed together, the plasma is squeezed out by the plasma-pressure gradient between the neutral point and the boundary at a large distance from it. If the system is in a steady state, then the magnetic field must continually be carried in by the plasma inflow with velocity u_{in} at the same rate as that at which the field lines diffuse away owing to finite resistivity in the diffusion region; in our dimensionless form, this means

$$u_{in} = R_m^{-1} \bar{\eta} / l^* , \quad (4.1)$$

where l^* is the half-width of the diffusion region and where $\bar{\eta}$ is the resistivity η averaged over the diffusion region.

It should be noted that this condition must hold in any steady-state reconnection process.

The importance of an MHD slow mode compression wave was first recognized by Petschek (1964) concerning the fast-reconnection problem. He realized that changes in MHD properties across the field reversal region can be accomplished by such a wave (which would be a shock in a steady state) bounding the field reversal region, and after computing the field and flow configuration by a perturbation expansion for small reconnection rates, then found the allowable maximum rate of reconnection, sufficiently large for solar flares. Fig. 21 illustrates the changes in flow properties across a switch-off shock (shown by a dotted line), which is the strongest possible slow shock. Since we require it for the interpretation of numerical results later, let us give below a quantitative description of the shock structure. For a detailed discussion, see Kantrowitz and Petschek (1966). Consider that, as shown in Fig. 21, the shock propagates in the positive y direction only and exists steadily in a coordinate system moving with the shock velocity, and denote the flow properties ahead of and behind the shock by the subscripts 1 and 2, respectively. The jump conditions across the shock, determined by the conservation of the fluxes of MHD quantities, can give all the conditions behind the shock if those ahead of it are known. For doing this, making use of (3.1) (only the terms related to $\partial/\partial y$ remain in this

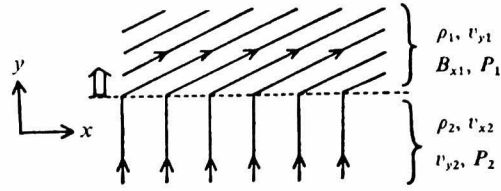


Fig. 21. Change of magnetic field lines (—) across a switch-off shock (-----). Ahead of the shock, v_{x1} is supposed to vanish. \uparrow shows the direction of propagation of the shock.

case), the conditions of the switch-off shock (in which B_{x2} vanishes) are readily determined as follows:

$$v_{y1} = -b_y, \quad v_{x2} = b_x, \quad (4.2)$$

where $b_y = B_y / (\mu_0 \rho_1)^{1/2}$ (B_y remains constant across the shock) and

$$b_x = B_{x1} / (\mu_0 \rho_1)^{1/2},$$

and if ahead of the shock the conditions

$$(B_y/B_{x1})^2 \ll 1 \quad \text{and} \quad P_1 \ll B_{x1}^2 / 2 \mu_0 \quad (4.3)$$

hold, then we obtain after some algebra

$$v_{y2} \simeq -b_y/2, \quad \rho_2 \simeq 2\rho_1, \quad P_2 \simeq B_{x1}^2 / 2 \mu_0. \quad (4.4)$$

In the similarity model, the structure of the field reversal region is similar to that of Petschek's model (namely, the slow shock is the dominant process there), but in the external region there is another discontinuity in contrast to Petschek's model. With respect to this discrepancy between the similarity model and Petschek's, Vasylunas (1975) points out that the physical process occurring within the external region corresponds to a slow mode expansion in the similarity model and, on the other hand, a fast mode expansion in Petschek's model.

In both the similarity model and Petschek's model, most of the argument concerned the convection region; they considered that the resistive effect determines the extent and structure of the diffusion region but has no other significant influence upon the configuration (Vasylunas 1975). However, Priest and Cowley (1975) suggested that the diffusion region does not necessarily adjust its size automatically to accommodate any inflow; rather, it may provide a subtle feedback to the inflow. Above all, as shown by the present numerical experiment, the locally enhanced resistivity can finally bring about the X-type field configuration involving the fast-reconnection process, and this exemplifies the vital importance of the diffusive effect in constructing the required configuration. We may note that the major difference between the present model and the previous analytical models lies in the treatment of the diffusion region.

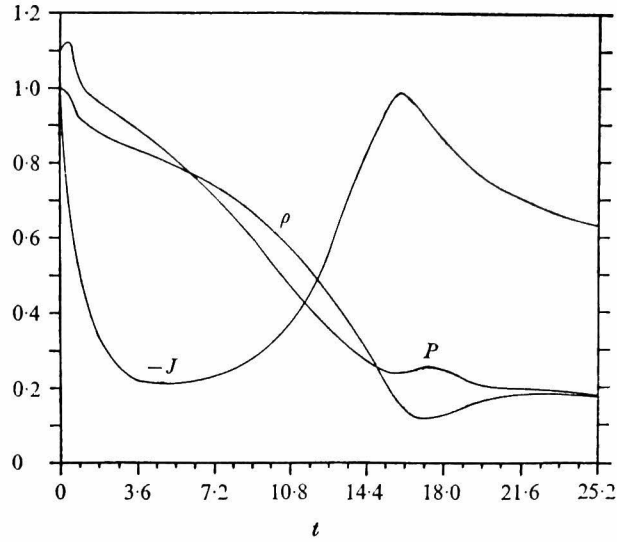


Fig. 22. Temporal variations of current density (J), mass density (ρ) and gas pressure (P) at the magnetic neutral point.

With these in mind, we shall discuss numerical results in §4. Note that we are investigating the effect on a current sheet of a sudden local increase of resistivity. This is quite different from those situations considered by many previous authors, who start with pressing the antiparallel magnetic field lines by external causes. Nevertheless, the reader will see that the quasi-steady configuration that we ultimately reach is quite similar to the one proposed by Petschek.

§4. Quasi-Steady Process of Reconnection

Let us now examine whether the present reconnection process

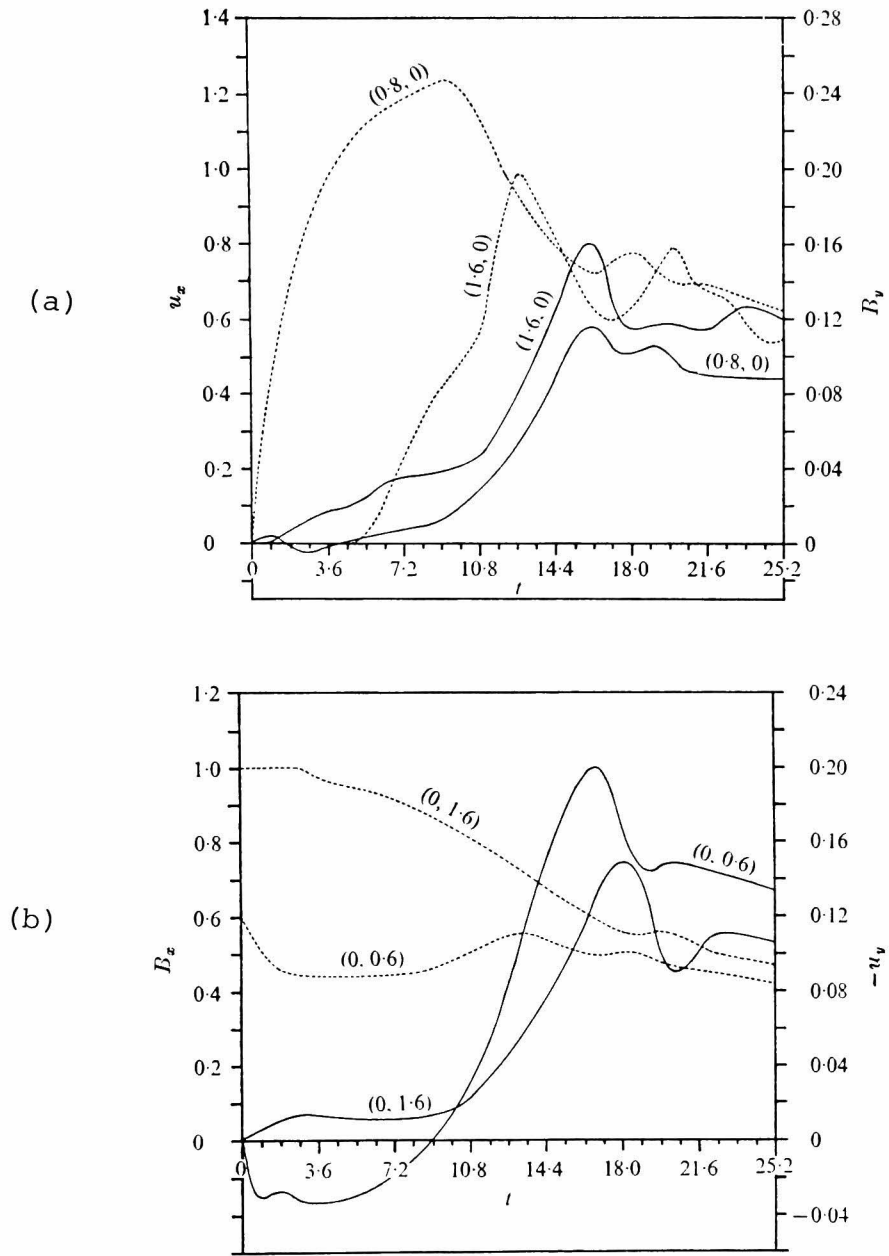


Fig. 23. Temporal variations of (a) B_y (.....) and u_x (—) at two typical points on the x axis, $(x, y) = (0.8, 0)$ and $(1.6, 0)$, and (b) B_x (.....) and u_y (—) (multiplied by -1 in the figure) at two typical points on the y axis, $(x, y) = (0, 0.6)$ and $(0, 1.6)$.

in fact approaches a steady state. Fig. 22 shows the temporal behaviour of the plasma density ρ , the plasma pressure P and the current density J (multiplied by -1 in the figure) right at the magnetic neutral point; also, Fig. 23 shows the temporal behaviour of magnetic field components B_x and B_y and the flow velocity components u_x and u_y at some typical points of space. In chapter 3 the numerical results were shown up to time $t = 14.4$. We can see from these figures that the process of reconnection apparently contains a stage at which the plasma flow grows very rapidly with time, accompanied by notable changes in the other physical quantities; finally, the growth of the plasma flow is quenched (at $t \simeq 16.0$) by some nonlinear effect, and the changes of all the quantities turn out to be reductions.

On the basis of the quasi-steady configuration that has thus resulted, we investigate below the characteristic MHD properties in the diffusion, field reversal, and external regions, respectively, and also their mutual dependence; in Fig. 24(a) these regions are marked on the magnetic field configuration at time $t = 18.0$, when the evolution of reconnection has just been checked and the system tends to be steady. Findings are that, thereafter, the typical dimension and structure of each region does not vary much, although, as shown below, the field reversal region is somewhat depressed towards the x axis by the impact of the plasma inflow that has grown so large. Also, Figs. 24 (b), (c), (d), and (e) show the flow pattern, the current density

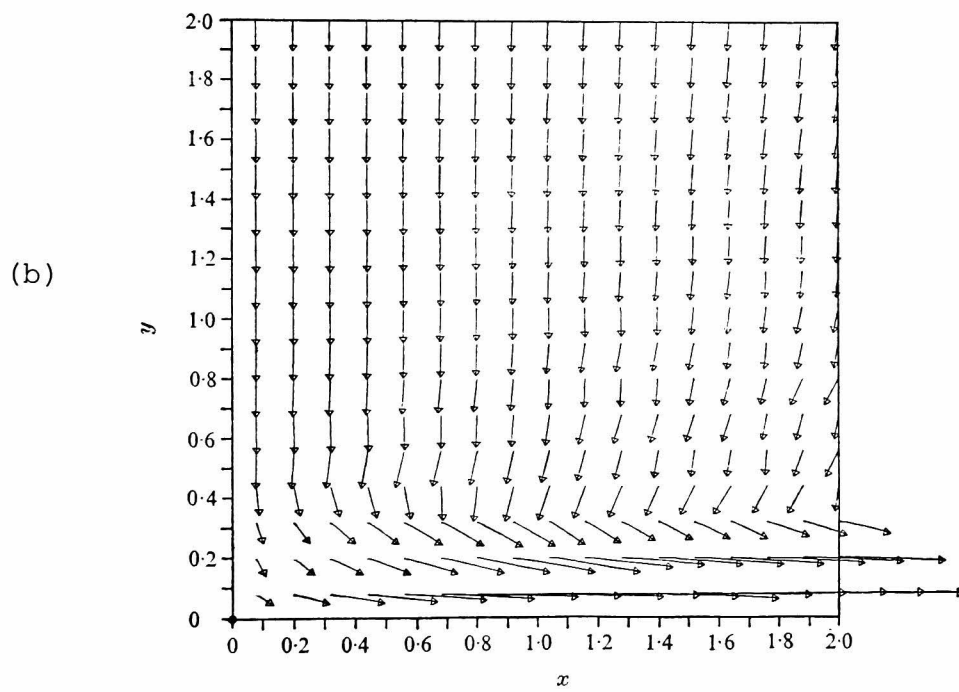
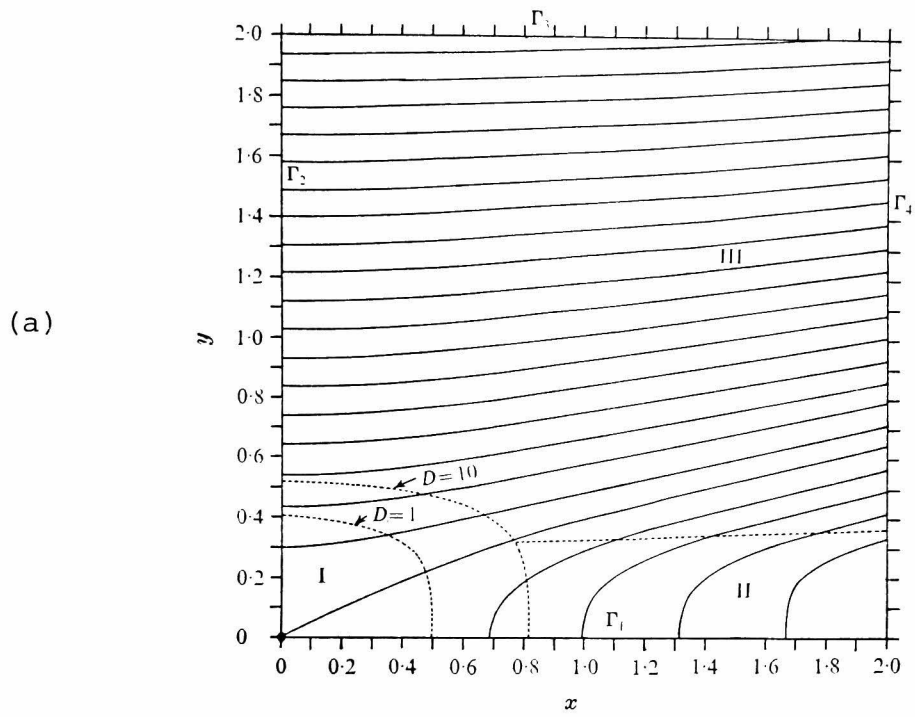


Fig. 24(a), (b). For legend see page 81.

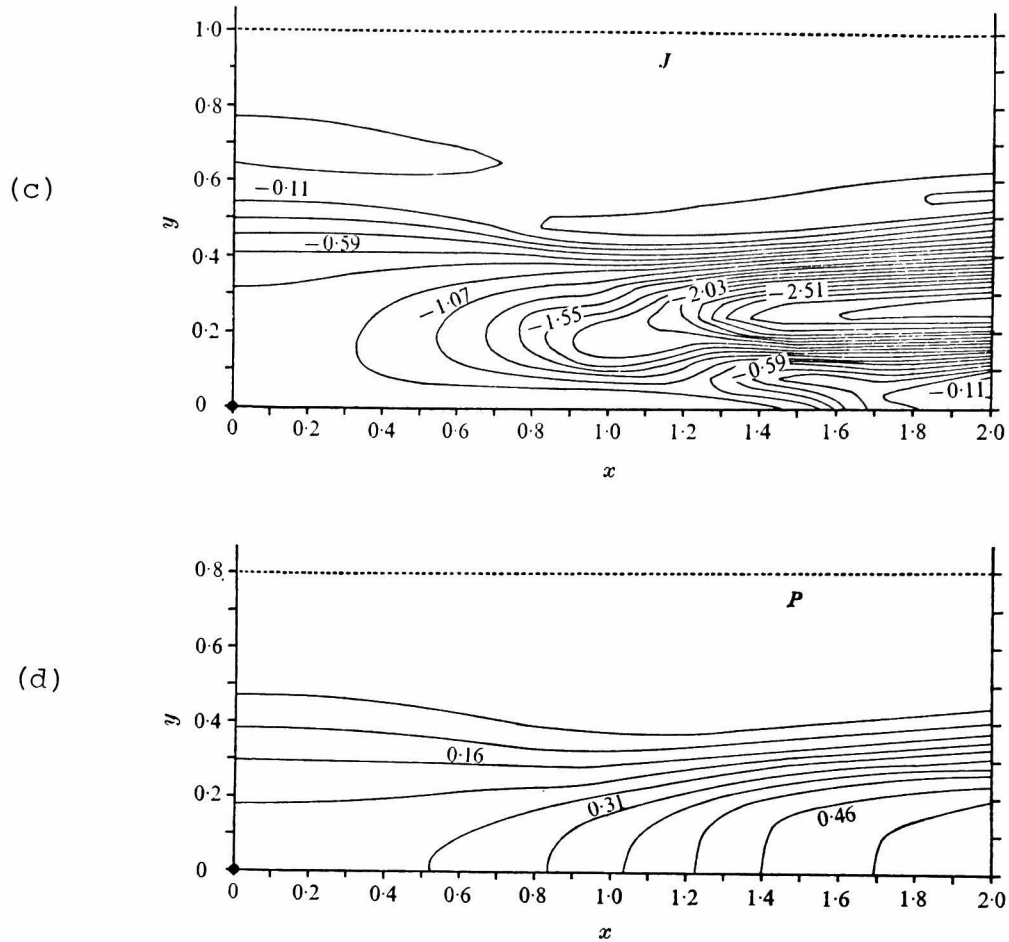


Fig. 24(c), (d). For legend see page 81.

distribution, the gas pressure distribution and the mass density distribution, respectively, at time $t = 18.0$. To see the smoothing effect of the artificial viscosity \mathcal{K} , note that in Fig. 24(c) the spacing between the two groups of dense contour lines that intersect \mathcal{T}_4 gives the approximate width of discontinuity. If we use viscosity coefficient $\mathcal{K} = 3$, then this width is reduced by about one fourth. The computation

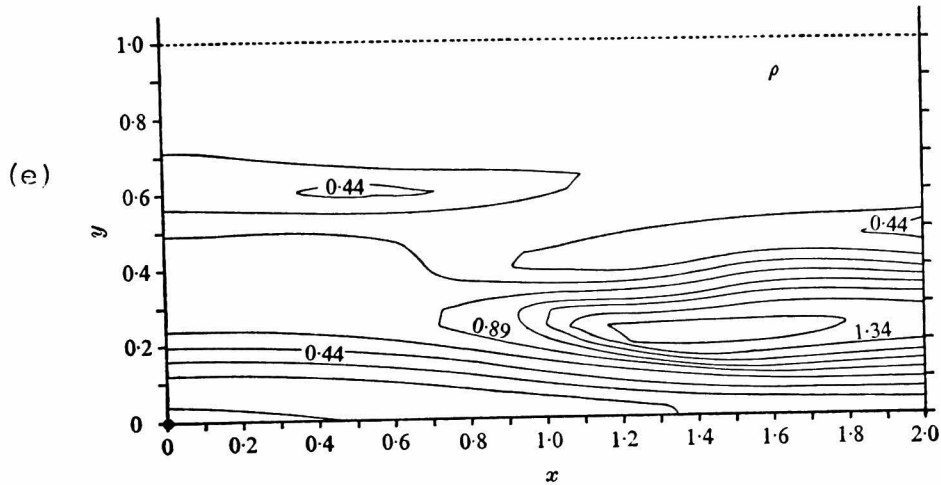


Fig. 24. Field and flow configuration at time $t = 18.0$. The dot at the origin is the position of both the magnetic neutral point and the stagnation point of the plasma. (a) The magnetic field configuration; the boundaries are labelled by Γ_i ($i=1,2,3,4$) and the whole region is divided into: I, the diffusion region (bounded by contour $D (= |\underline{u} \times \underline{B} / R_m^{-1} \eta \underline{J}|) = 1$ and 10); II, the field reversal region (where escape flow velocity is markedly high); and III, the external region. (b) The flow pattern. The magnitude of the velocity at the rear end of each arrow is measured by the distance from there to the center of the associated triangle. Length of 0.07 on the scale of the co-ordinate axes corresponds to 0.1 in the magnitude of normalized velocity. (c) Contour lines of current density distribution with contour interval of 0.16 . (d) Contour lines of gas pressure distribution with contour interval of 0.05 . (e) Contour lines of mass density distribution with contour interval of 0.15 .

with $\mathcal{K} = 1$ meets numerical instability and therefore does not make any sense.

4.1. The diffusion region

Concerning the convection region, the field and flow configurations required for fast reconnection have been investigated by previous authors; but the detailed structure of the diffusion region actually formed in the course of reconnection, is still not well understood (e.g. Cowley 1975). We will discuss the crucial role of the diffusion region in the development of the present reconnection process.

The ultimate cause of the present reconnection process is the locally enhanced resistivity, which is assumed to be sustained in the form given by (3.5). The direct effect of this can most readily be seen in the diffusive stage discussed in 4.1 of chapter 3: the field lines bend towards, and re-connect at, the magnetic neutral point. This implies that the horizontal magnetic field component B_x is eroded, whereas the vertical field component B_y is enhanced. This process concludes with the formation of an X-type field configuration near the neutral point, and is obviously accompanied by a decrease in the current density near there. There is also a decrease in the magnetic field diffusion, since its rate is proportional to the current density. So long as the diffusion region is concerned, the reconnection will soon be checked.

Note, however, that the most interesting aspect of the reconnection arises from the nonlinear hydromagnetic interactions in the outer region and this contributes to increasing the current density near the neutral point. That is, while the field component B_y is carried away by the plasma outflow from the diffusion region towards the field reversal region, the field component B_x is carried in by the plasma inflow to the diffusion region from the external region.

The temporal behaviour of the electric current density at the magnetic neutral point, shown in Fig. 22, may thus indicate which effect, the diffusion or the convection of magnetic field lines, is predominant: when the field diffusion dominates over the field convection in the outer region, then the current density will decrease at the magnetic neutral point, and vice versa. Fig. 22 thus shows the following process: in the initial time range the current density rapidly decreases since the diffusive effect is dominant then; but, as the plasma flow grows (see Fig. 23), the current density increases because of the increasing convection of the field lines and arrives at a peak value at about time $t = 16.0$, when the evolutionary process is checked; then it begins to decrease again but more and more slowly than before.

For reconnection to proceed efficiently, the X-type field configuration must be established over a large region, which is found to be the case in our model (see Fig. 24(a)). This must be because the field component B_y , produced through

field-line reconnection in the diffusion region, is continuously carried away to the outer region where $B_y = 0$ initially. One may interpret this as follows: fast mode waves propagating along the field lines into the external region (similar to Alfvén waves in the general case where the z component also exists) can continually be excited by the bending of field lines in the diffusion region, which will necessarily cause the field lines to decline in the external region where there exists a strong magnetic field; in the field reversal region, where the magnetic field is weak, the field component B_y can be transported by a sufficiently large outflow of plasma.

In those reconnection models studied to date, it is usually argued on the diffusion region that the pressure gradient accelerates the plasma whereby the ejection is performed along the field reversal region. In our model, however, the resulting pressure distribution does not act in such a way, but instead the magnetic tension, produced through field-line reconnection, accelerates the plasma outflow. Indeed, we see from Fig. 24(d) that the pressure gradient rather decelerates the plasma outflow in the immediate vicinity of the x axis spanning the field reversal region. Notice that in our case the plasma is subject to a remarkable expansion near the magnetic neutral point during the evolutionary process (Fig. 22) and that the decrease in the plasma density as well as the plasma pressure is largest at the neutral point (see also Fig. 24(e)). This discrepancy may have arisen from the difference of our

model from the analytical models: in our model, as described later, the ambient field-lines are sucked into the inner region as a result of the plasma ejection out of the inner region rather than pressed inwards by external causes.

4.2. The field reversal region

The plasma energy acquired in the reconnection process is ejected away through the field reversal region. This region is essentially composed of high- β plasma (i.e. the magnetic energy is smaller than the plasma energy); and in this region, as defined before, the magnitude of both the field component B_y and the outflow velocity u_x are sufficiently large and the field lines are frozen to the plasma.

Note that by the Lorentz force, not by the pressure gradient, the plasma is accelerated outwards. In Fig. 23(a) the temporal variations of B_y and u_x are shown at two points along the x axis, namely, at the point $(x, y) = (0.8, 0)$ located just outside the diffusion region, and at the point $(1.6, 0)$ located within the field reversal region. We observe that, as the reconnection suddenly takes place in the initial time range, $B_y(0.8, 0)$ rapidly increases, giving rise to the Lorentz force ($\mathbf{J} \times \mathbf{B}_y$) to accelerate the plasma outwards; and with the growth of u_x , $B_y(1.6, 0)$ also starts increasing due to the convection of field lines, which in turn reinforces the Lorentz force in the field reversal region (

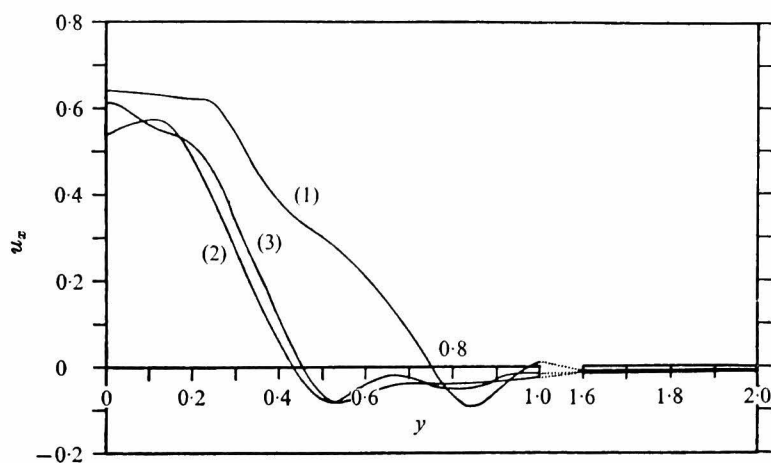


Fig. 25. Profiles of u_x at different times along the line $x = 2.0$ (boundary Γ_4). (1) $t = 14.4$, (2) $t = 18.0$, (3) $t = 22.5$.

thus, this time interval corresponds to the growth stage of the reconnection process); but, as the plasma outflow becomes very large, B_y is found to decrease since the field lines are convected away faster than they are produced in the diffusion region, and, as the rates of the convection and the diffusion of magnetic field lines get closer to each other, then these quantities tend to be constant. In short, this procedure may be restated as follows: the field-line reconnection occurring in the diffusion region produces the magnetic tension in the system which acts on the field reversal region to accelerate the plasma outwards; the outflow velocity grows so as to relax the magnetic stress energy stored in the system, which provides the continual process of reconnection.

Consider now Petschek's suggestion that the flow properties across the field reversal region can be those of slow mode MHD

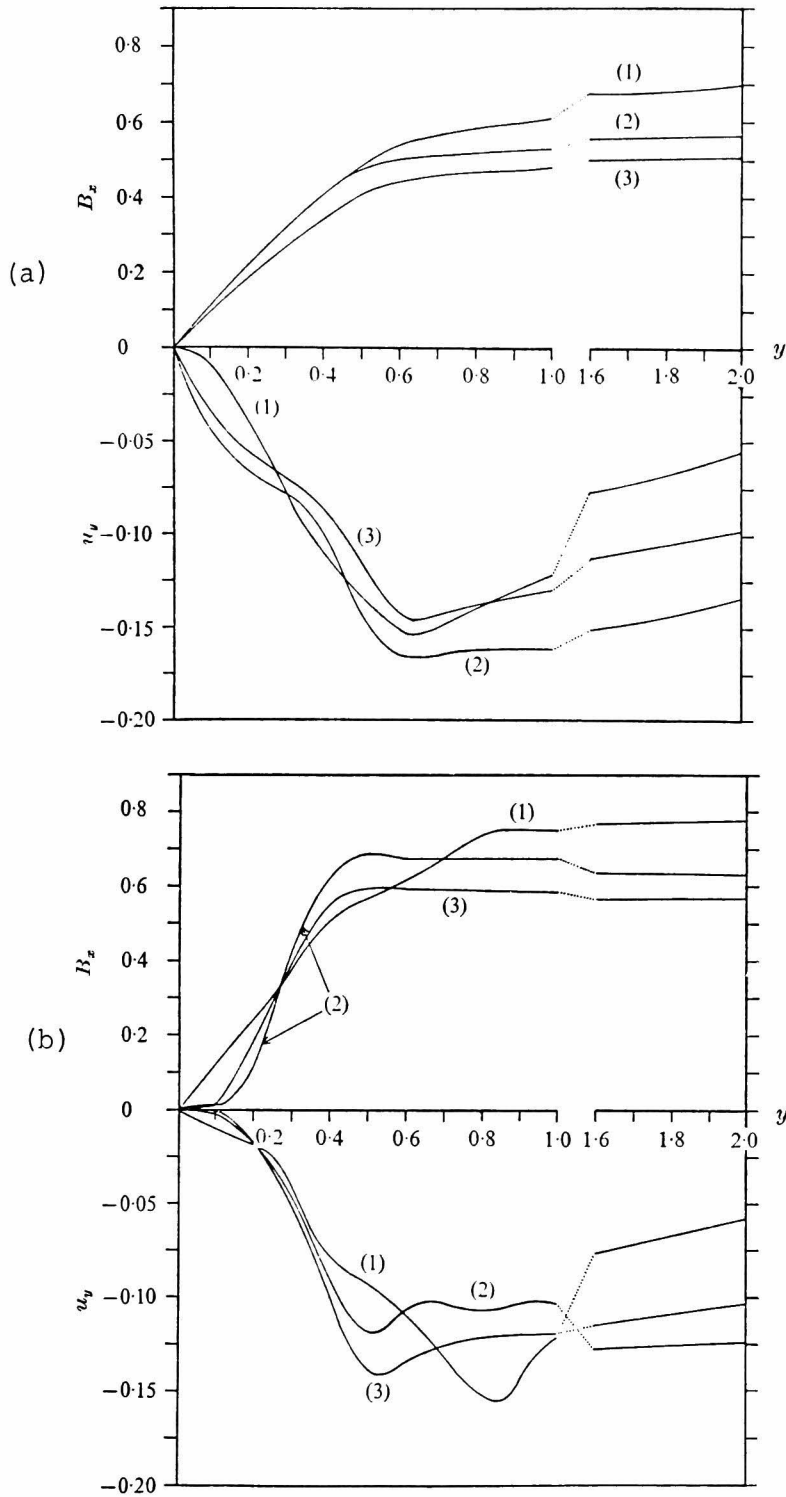


Fig. 26. Profiles of B_x and u_y at different times along the lines (a) $x = 0$, which crosses the diffusion region, and (b) $x = 2.0$, which crosses the field reversal region. (1) $t = 14.4$, (2) $t = 18.0$, (3) $t = 22.5$.

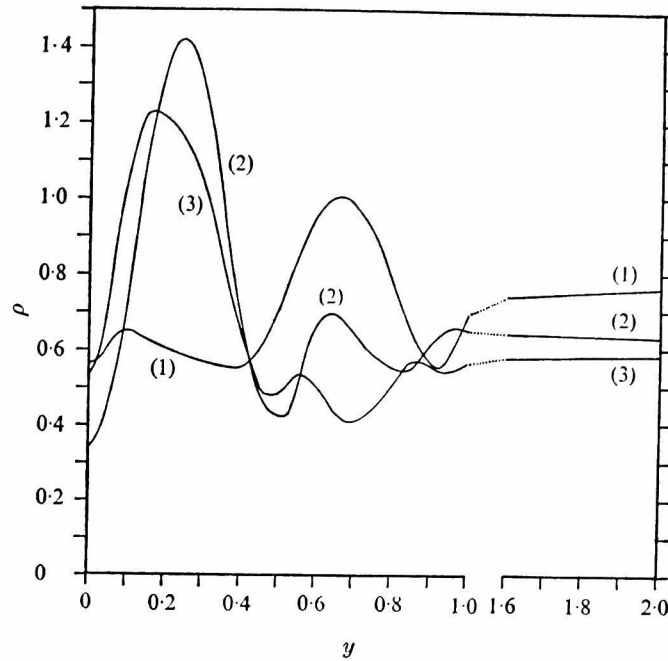


Fig. 27. Profiles of ρ at different times along the line $x = 2.0$ (boundary Γ_4). (1) $t = 14.4$, (2) $t = 18.0$, (3) $t = 22.5$.

compression wave. In Figs.26(a) and (b) the horizontal field component B_x and the inflow velocity u_y are shown at different times along the two lines $x = 0$ and $x = 2.0$ (boundary Γ_4 ; see Fig.24(a)). Also, in Figs. 25, 27 and 28 the outflow velocity u_x , plasma density ρ , and plasma pressure P are shown similarly along the line $x = 2.0$. From these figures, it follows that flow properties along the line $x = 2.0$, which traverses the field reversal region, change very markedly towards the boundary of the field reversal region; and we may note that these changes possess the same properties as those that a slow wave requires. However, the wave has a width of about 0.25 due to the effects of artificial

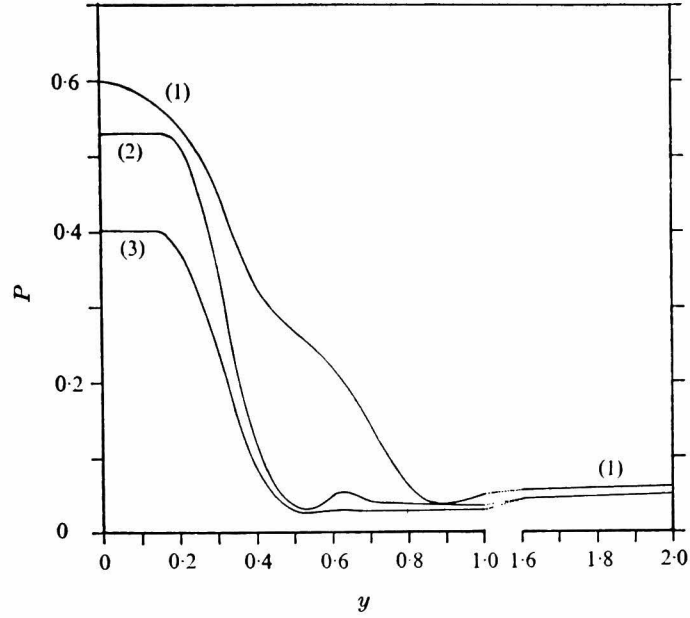


Fig. 28. Profiles of P at different times along the line $x = 2.0$ (boundary \overline{T}_4). (1) $t = 14.4$, (2) $t = 18.0$, (3) $t = 22.5$.

numerical diffusion.

To compare these numerical results with the flow properties of the idealized switch-off shock described in §3, let us make use of the MHD quantities along the line $x = 2.0$ at time $t = 18.0$; then we observe that the quantities above (or, in shock-wave terminology, ahead of) the field reversal region (denoted by subscript 1) are given by

$$\rho_1 \approx 0.6, \quad B_{x1} \approx 0.67, \quad P_1 \approx 0.04, \quad u_{x1} \approx 0,$$

where some oscillations have been smoothed. The magnitude of B_y changes considerably in the y direction. This is differ-

ent from the type of shock now at issue, where B_y should be constant everywhere. Therefore, for B_y , we tentatively take its mean value across the boundary of the field reversal region, then

$$B_y \simeq 0.15 .$$

If the switch-off shock, shown in Fig. 21, is supposed to be present along the field reversal region, then the quantities behind the shock can be obtained as described in §3 ; substituting the above quantities for those ahead of the shock, we see that the conditions given by (4.3) in fact hold approximately and then the switch-off shock solutions given by (4.2) and (4.4) become in the dimensionless form:

$$\begin{aligned} v_{y1} (= -b_y) &\simeq -0.19 , & v_{x2} (= b_{x2}) &\simeq 0.87 , \\ v_{y2} &\simeq -0.095 , & \rho_2 &\simeq 1.2 , & P_2 &\simeq 0.45 . \end{aligned} \tag{4.5}$$

Hence, we see that essentially the present numerical results agree well with the requirements given for the switch-off shock, only with some quantitative difference. This difference may have come from the discrepancy of the basic situations between the present reconnection process and the above idealized switch-off shock: namely, in our case, the system is neither strictly steady in the sense $\partial/\partial t = 0$ nor one-dimensional;

furthermore, u_y must always vanish on the x axis by the symmetry condition imposed on our system (in terms of the shock, v_{y2} must be zero), and, as already mentioned, B_y changes considerably in the y direction, as also does the propagation speed of the slow wave accordingly.

There is in fact the nonlinear slow wave standing along the boundary of the field reversal region, although numerical diffusion due to artificial viscosity might have somewhat obscured the slow shock. Fig. 24(c) apparently indicates a remarkable increase in the current density across the boundary of the field reversal region inside which B_x vanishes because of the slow wave. Note also that the plasma density ρ is notably rarefied immediately near the x axis (see Fig. 24(e)), which implies that the plasma temperature, proportional to P/ρ , is much enhanced there. Therefore an interesting result in the present reconnection process is that the plasma experiences an efficient heating when crossing the field reversal region from above and/or when passing through the diffusion region.

In analytical studies for the steady reconnection, the magnitude of the outflow velocity is usually given by the Alfvén speed just outside the diffusion region (Vasyliunas 1975). To examine this, take, for instance, the Alfvén speed V_{AD} at point $(x, y) = (0, 0.6)$ and time $t = 22.5$. We can then obtain $V_{AD} = B_x / \rho^{1/2} \simeq 0.59$, considering $B_x(0, 0.6) \simeq 0.45$ (cf. Fig. 23(b)) and $\rho(0, 0.6) \simeq 0.58$ at this time.

In the present quasi-steady reconnection, the outflow velocity, shown in Fig. 23(a), thus agrees with V_{AD} , as it should do.

4.3. The external region

In our model, the magnetic energy initially stored in the external region (including the regions external to the domain of computation) is spent for the reconnection process to proceed persistently. This region is essentially composed of low- β plasma (the magnetic energy is larger than the plasma energy), and the spatial changes of physical quantities are small as compared with the other regions.

With regard to the temporal variations of inflow velocity u_y shown in Fig. 23(b), let us discuss how the plasma inflow, whereby the field lines are carried in, arises from the process occurring in the inner region. In Figs. 29(a) and (b), the variations of the sum $P + B_x^2$ in the direction parallel to the y axis are shown at times $t = 14.4$ and 22.5 , respectively. This quantity, $P + B_x^2$, may approximately represent the total pressure, since B_y^2 is much smaller than B_x^2 . At time $t = 14.4$, when the plasma flow is rapidly growing (Fig. 23), we can observe the total pressure is notably reduced in the inner region, especially in the middle of the system, since the high-energy plasma has been ejected away from the inner region. Hence, the magnetized plasma in the external region can be more and more accelerated inwards. The rapidly growing

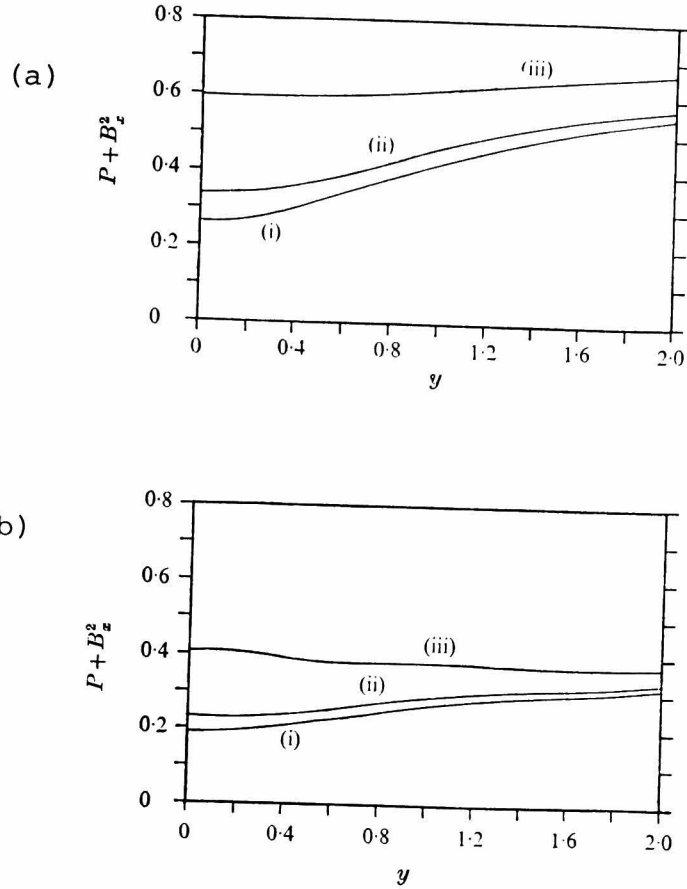


Fig. 29. Profiles of $P + B_x^2$ along different lines in the y direction at times (a) $t = 14.4$ and (b) $t = 22.5$. (i) $x = 0$, (ii) $x = 0.8$, (iii) $x = 2.0$.

plasma inflow thus causes a significant increase in the plasma energy in the inner region, hence a decrease in the magnetic energy in the external region. The accelerated inflow initially depresses the field reversal region, but the inflow is then subdued at a certain level. We thus observe from Fig. 23(b) that the inflow velocity u_y decreases at about $t = 16.5$ at the point $(x, y) = (0, 0.6)$ and, with some delay, at the point $(0, 1.6)$, because the upward propagation of information

from below always requires some time. We further see from Fig. 29(b) that, at $t = 22.5$, the spatial variations of the total pressure become rather smooth, so that the system tends to become steady.

Hence, in the external region the magnetized plasma is persistently "sucked" into the inner region, where in the diffusion region field-line reconnection proceeds and where in the field reversal region the plasma is ejected away. Such a process in the external region can obviously be accomplished by a fast mode expansion (see Kantrowitz and Petschek 1966). The propagation of fast mode expansion waves always results in a decrease of the magnetic-field intensity as well as a decrease in the plasma. In fact, Fig. 23(b) shows that the field component B_x , at the point $(x, y) = (0, 1.6)$ within the external region, decreases with time, while Figs. 27 and 28 indicate that the plasma density ρ and the plasma pressure P decrease in the external region from their initial values $\rho_0 = 1$ and $P_0 (= \beta_0) = 0.1$, respectively.

The fast mode expansion waves, which cannot stand in the subsonic flow, successively propagate through the external region, modifying the entire configuration. Therefore, at distances far from the neutral point where the fast waves have just arrived, there must be a significant modification of the configuration as was seen in the evolutionary phase of reconnection (see chapter 3). If, however, as in the present model, the domain under consideration is restricted to the

vicinity of the neutral point, where the changes of physical quantities become small with time as we have seen in this chapter, the reconnection process can be considered to be in a quasi-steady state. This state should be compared with those analytical models for steady reconnection that have been studied by several authors.

The fast mode expansion, occurring in the external region, can proceed by the previously mentioned sucking mechanism of the diffusion region; on the other hand, the resulting plasma inflow in turn expedites the reconnection because of the convection of magnetic field lines into the diffusion region. Any steady process of reconnection requires that the above two effects be well matched to each other and therefore that, as shown in §3, the inflow velocity u_{in} be given by (4.1). Applying this equation to our present case, we may roughly take $l^* \simeq 0.5$ (in view of the ambiguity in defining the diffusion region, l^* may be taken for the scale length of magnetic field variation; see Fig. 26(a)), $R_m = 1000$, and $\overline{\eta} = 80$ (cf. (3.5)); then we obtain $u_{in} \simeq 0.16$. One sees from Fig. 23(b) that, as the system approaches the quasi-steady state, the inflow velocity u_y at the point $(0, 0.6)$, just outside the diffusion region, is nearly the same as this steady-state inflow velocity, u_{in} . This implies that in our quasi-steady configuration of the diffusion region the rate at which the field lines are carried in by the plasma inflow is well adapted to the rate at which they diffuse away owing to finite resistivity.

§5. Concluding remarks

We have investigated by numerical experiment the effect on a current sheet of a sudden local increase in electrical resistivity. It has been found that a quasi-steady configuration of field-line reconnection can ultimately be established from an initially antiparallel magnetic field. By examining this configuration in detail, we discussed the outstanding MHD characteristics manifested in the diffusion, field reversal and external regions. Namely, in the diffusion region, the field lines bend towards, and reconnect at, the magnetic neutral point due to the locally enhanced resistivity; hence, the horizontal field component B_x is eroded, and simultaneously the vertical field component B_y is enhanced in this region. In the field reversal region, the slow mode compression is the dominant process; the resulting plasma outflow carries away both the enhanced plasma energy and the field component B_y . In the external region, the fast mode expansion is the key process; the resulting plasma inflow transports the field component B_x into the inner region from the surrounding. Hence, the quasi-steady configuration presented in this chapter is similar to that proposed by Petschek (1964).

Recall that any steady configuration requires a precise matching of variables among the above three regions. For instance, the field component B_y must continually be produced in accordance with the ejection of it by the plasma outflow

in order to sustain the configuration (especially, in order for the slow wave to be persistently standing along the field reversal region); in our case this can be accomplished by none other than the bending of the field lines towards the neutral point. To see how the matching is done among the above three regions, let us examine the dimensionless electric field E ($= -(u_x B_y - u_y B_x) + R_m^{-1} \eta J$) about the diffusion region. Table 2 shows the temporal variations of E at three typical points of space, namely at $(x, y) = (0, 0)$ (the magnetic neutral point), $(0, 0.6)$ (on the boundary between the diffusion and the external regions), and $(0.8, 0)$ (on the boundary between the diffusion and the field reversal regions). The geometrical dimension of the diffusion region here considered is based on that shown in Fig. 24(a). The respective values of E at the above three points may be considered to be the reconnection rate of magnetic field lines at the neutral point, the rate of field line injection into the diffusion region, and the rate of field line ejection from the diffusion region. This statement holds after the plasma flow has grown sufficiently large. From the table the temporal development of the reconnection process is seen from another angle: the electric field, which is initially much larger in the immediate vicinity of the neutral point than in the surrounding because of the sudden local increase in resistivity (note that $E(0, 0) = -0.1$ at time $t = 0$), becomes soon reduced owing to the rapid magnetic-field diffusion; then, in the evolutionary stage

	t					
	1.8	9.0	12.6	16.2	19.8	23.4
$E(0, 0)$	-0.033	-0.027	-0.055	-0.092	-0.076	-0.067
$E(0, 0.6)$	-0.023	-0.033	-0.069	-0.096	-0.072	-0.065
$E(0.8, 0)$	-0.013	-0.028	-0.063	-0.089	-0.078	-0.068

Table 2. Temporal variations of electric field E , given by $-\underline{u} \times \underline{B} + R_m^{-1} \nabla \cdot \underline{J}$, at three typical points: $(x, y) = (0, 0)$, $(0, 0.6)$ and $(0.8, 0)$.

with growing plasma flow, the electric field increases everywhere till the evolution is checked; and, after the quasi-steady configuration is established (i.e. $t \simeq 16.5$), the electric field on the whole tends to decrease again, and its spatial uniformity prevails with time as expected. Note that, in a steady state ($\partial/\partial t = 0$), $E = \text{constant}$ everywhere.

We have presented in this chapter, within the framework of MHD approximation, the numerical solution that exemplifies the quasi-steady reconnection process involved in an "isolated" current-sheet system. In other words, in this system the energy was supplied in the form of an initially given current sheet, which thereafter was free to decay with a time scale much longer than that of the reconnection process. The triggering mechanism of the evolutionary process resided in a local area that was to be identified with the neutral point. In actual systems, however, some external conditions would also be important in maintaining the process of reconnection, so that there remains the problem of how the external region,

together with the diffusion and field reversal regions presumably, will adapt themselves to some specific boundary conditions. This problem will be examined in the following chapter.

CONTROLLING FACTORS OF FAST RECONNECTION*

§1. Introduction

In this chapter, the numerical computations will shed light on the effect of special boundary conditions; namely, it is assumed here that there is persistent injection of magnetic fluxes across the inflow boundary at a constant rate, this injection being forced by some external agency. Three cases of boundary values are examined, such that the rates of magnetic flux injection are higher than, comparable with, and smaller than, the intrinsic reconnection rate up to which the process of reconnection spontaneously evolves by a local resistivity enhancement in the absence of such externally given boundary conditions (see §3 of this chapter). It is shown that in each case the system ultimately arrives at a stationary state involving some oscillations with time so long as the effective resistivity is enhanced locally near the neutral point. In addition, we also examine the case in which the condition of local resistivity enhancement is suddenly removed in an X-type field configuration, where the

* See Ugai and Tsuda (1979 a)

evolutionary process of reconnection has been going on, with resistivity kept uniform in space. We then find that the global X-type field configuration can no longer be sustained; with time the angle between the two X-lines of magnetic field becomes much reduced near the neutral point, the magnetic field thus regaining the initial antiparallel configuration.

From the present numerical results, the following will be remarked. In so far as the local resistivity enhancement is maintained near the neutral point, the reconnection process adapts itself to any of the imposed boundary conditions; thus the amount of the magnetic field lines that reconnect per unit time in each of the resulting stationary configurations is determined by the respective influx of field lines at the boundary. Note that in the ordinary theoretical treatments the reconnection rate is defined to be the inflow speed at large distance from the neutral point scaled by the local Alfvén speed. With this in mind, we examine the local Mach numbers at a point on the inflow boundary in individual stationary configurations and find that they are similar in magnitude. This suggests that the reconnection rate in the theoretical sense can hardly be influenced by the boundary values; in the theoretical studies, on the contrary, it has so far been predicted that the reconnection rate, defined as such, is determined by the boundary conditions.

§2. Numerical Experiment

The procedure of the present numerical experiment is different from the previous ones of chapters 3 and 4 in the treatment of initial-boundary conditions, but in the other respects remains the same.

The initial state of physical quantities with which the present computations begin is the one where the reconnection process has grown from an initially antiparallel field configuration because of the local resistivity increase; the details of such an evolutionary process of reconnection are shown in chapter 3. For this purpose the state of physical variables at time $t = 14.4$, previously obtained as a result of numerical calculation, is considered. See, for instance, Fig. 10 of chapter 3 for the corresponding field configuration. In what follows all the numerical computations start with this configuration on which the special boundary condition, described below, is imposed.

The boundaries are labelled by Γ_i ($i=1,2,3,4$) as shown in Fig. 31(a). Let us suppose a situation where some external agency forces magnetic field lines at a large distance to approach the neutral point. In order to have such a situation in our computer experiment, it is assumed that there is persistent magnetic flux injection at a constant rate as dictated by the external agency. This condition may equivalently be

given by having $u_y B_x = \text{constant}$ along the boundary Γ_3 since the field should almost be frozen into the fluid near there. In practice, inflow velocity u_y at that boundary is calculated every time step so that $u_y B_x$ is kept constant there. On those boundaries other than Γ_3 , all the conditions are the same as before; namely, on Γ_1 and Γ_2 , the symmetry conditions are given, and Γ_4 is the free boundary across which the plasma can freely flow in or out according to the states of the inner region (see 3.2 of chapter 3). Similarly the boundary Γ_3 is a free boundary for physical quantities other than u_y .

Throughout the present computations the domain for computation is reduced in the y direction to the one of size 2.0×1.2 (cf. Fig. 31 of this chapter), while the size of the previous ones was 2.0×2.0 (cf. Fig. 8 of chapter 3). Such a reduction of the domain size for computation can considerably reduce the computation time. This truncation is justifiable, because as already seen in chapters 3 and 4 the spatial changes of physical quantities are very small at distances from the neutral point. All the physical and numerical parameters are of course kept the same as in chapter 3; namely, $\gamma = 2.0$, R_m (the magnetic Reynolds number) = 1000, Δx (= Δy , the mesh size) = 0.04, Δt (time step) = 0.0045, and so forth.

§ 3. Some Remarks on the Present Model

In general the rate of energy exchange per unit volume between the magnetic field and the plasma can be given by $\underline{E} \cdot \underline{J}$ (in the present model the electric energy is neglected). There is a sheet of electric current concentrated between two oppositely directed magnetic fields. If there exists over the whole region a large-scale electric field in the same direction as the current, a concentrated release of magnetic energy will therefore be realized. Any fast-reconnection process must involve such a strong large-scale electric field. A question may then arise as to how and under what conditions such a large-scale electric field can eventually result: this is a fundamental problem in studying the controlling factor and the mechanism of fast reconnection. From this viewpoint, let us reconsider the present numerical model below.

The recent critical review by Vasyliunas (1975) summarized the general features of the previously proposed hydromagnetic models with the following conclusion about the problem now at issue: the configuration is determined by the boundary conditions; resistive effects, on the other hand, determine the extent and the structure of the diffusion region but have no other significant influence on the configuration. Obviously, the previous authors have expected that an electric field, generated at a large distance by some external agency, can enter

and ultimately permeate the whole region, especially the region in the immediate vicinity of the neutral point; and this region will be identified with the diffusion region, its size being controlled by the magnitude of the electric field.

However, it may be remembered that in the previous analytical treatments two significant problems still remain unsolved because of mathematical difficulties. One is that of matching; namely, there is as yet no completely satisfactory method of matching between the diffusion region and the convection region in the steady configuration of fast reconnection (Vasyliunas 1975). The other, which is more fundamental, is that of the temporal dynamics of reconnection. Although the theoretical models have indeed succeeded in describing some of the configurations in the convection region that are required for the growth of fast reconnection, they obviously failed in making clear whether or not these configurations could in fact be maintained in actual systems without any special local condition near the neutral point. In fact, if one leaves aside this problem, which necessarily involves the time-dependent process of reconnection, then one may not attain perfect understanding of the major factors that control the fast reconnection.

It may be noted that the quasi-steady reconnecting situation, argued in chapter 4, describes quite a different situation from the one considered in the above conventional theoretical models. We remind the reader that the quasi-steady configura-

tion can eventually be established and maintained because of the locally enhanced resistivity without any specially imposed boundary condition. The resulting large-scale electric field in the initial time range is the so-called induction electric field due to $\partial \underline{B} / \partial t$, the temporal variations of magnetic field configuration. Ultimately together with the flux transport it grows and overspreads outwards from near the neutral point with increasing time because of the hydromagnetic wave effects. Such a reconnecting situation can obviously provide a mechanism whereby the energy critically stored in the magnetic field is suddenly released by an occurrence of anomalous resistivity. This mechanism may hence be responsible for large dissipative events such as solar flares. See, for instance, the emerging flux model of the solar flare phenomenon by Heyvaerts, Priest and Rust (1977).

The purpose of the present numerical model is to study the effect of persistent injection of magnetic fluxes as already mentioned. Let that value $u_y B_x$ which is kept constant on the boundary Γ_3 be denoted by E_b . Note that E_b is the approximate value of the electric field at the boundary, since near the boundary the term $u_y B_x$ is found much larger in magnitude than the other terms in the Ohm's law throughout the computation. Hence the present model, in contrast to our previous ones, is designed to examine another significant reconnecting situation such that an externally generated electric field permeates the reconnection region in

the vicinity of the neutral point. With this computer model, we wish to clarify the controversial points in the fast-reconnection theories, mentioned above, by investigating the temporal dynamical processes of reconnection. In the following, it will be shown and discussed how the configuration is influenced by different boundary values E_b 's and by the local resistivity increase near the neutral point.

§4. Results

The reconnection process, such as the one modelled in this chapter, describes a decay process of the current-sheet system ; in particular, this decay takes place much more rapidly in the presence of the locally enhanced resistivity at the neutral point than in its absence. We may hence consider as the intrinsic reconnection rate (which is denoted by E_0) the maximum value of the electric field at the neutral point up to which the induction electric field grows because of the strong hydromagnetic effects in the evolutionary process of reconnection. From Fig. 22 of chapter 4, we can readily observe that the current density J right at the neutral point grows up to about -1 (at time $t \simeq 16$) through the evolutionary process. Hence, we obtain $F_0 \simeq -0.1$ by considering that the electric field at the neutral point is given by $R_m^{-1}SJ$ with parameter values $R_m = 1000$ and $S = 100$. In what follows

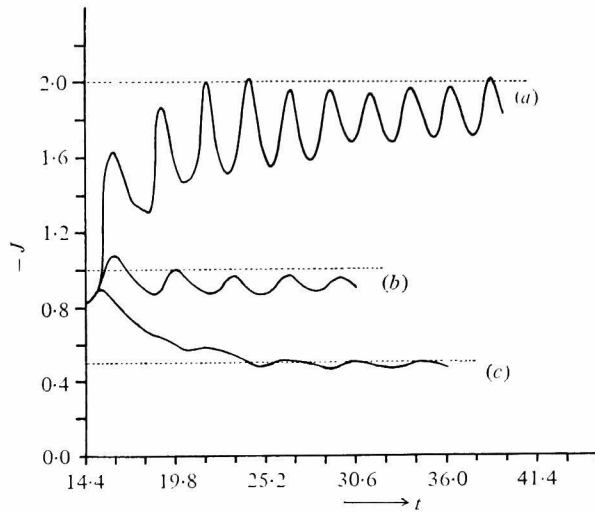


Fig. 30. Temporal variations of current density (multiplied by -1 in the figure) right at the neutral point (namely, at $(x, y) = (0, 0)$) for the three cases corresponding to the boundary values (a) $E_b = -0.2$, (b) $E_b = -0.1$ and (c) $E_b = -0.05$.

we first examine three choices of E_b of the order E_0 , supposing the same form of the local resistivity increase as before, with $S = 100$ and $k = 1.0$ in (3.5); and next, we consider a case where the condition of the local increase in resistivity is removed, in order to assess the effect of this important condition on the global configuration.

In order to have an overall picture of the solution, it may be instructive to observe the time-sequential variations of the current density at the neutral point. This is shown in Fig. 30 for each of the three boundary values, i.e. $E_b = -0.2$, $E_b = -0.1$ and $E_b = -0.05$. In the figure two major features are conspicuous. First, we find that in each case the current density becomes ultimately stationary after a

certain time interval. Here, the term "stationary" is used in the sense that the mean value with respect to time is almost constant. Second, it is observed that there appears an oscillation with time corresponding to each of the imposed boundary values. The resulting periods and amplitudes are distinct for the respective oscillations; namely, with larger E_b the period becomes shorter and the amplitude larger. It should also be noted that in each of these stationary configurations the other physical quantities at any spatial point oscillate in the same manner as the current density.

Such an appearance of oscillations may be interpreted as follows. Note that in an ordinary oscillatory system there must be forces that counteract each other. In the present numerical model, there are in fact two such factors. As already seen in chapters 3 and 4, the localized enhancement of resistivity can always cause a significant expansion in the plasma over the whole region through field-line reconnection. On the other hand, the forced injection of magnetic fluxes may obviously tend to compress the plasma into the inner region in accordance with the magnitude of E_b . These two forces act on the system through fast-mode MHD waves (expansion and compression) to counterbalance each other alternately, which should result in an oscillation in the system. In addition, for the larger value of E_b the above two competing forces must obviously be stronger. Note that the magnetic-field diffusion should then proceed more rapidly near the

	ρ	B_x	u_y	$\frac{V_A}{(= B_x \cdot \rho^{-1/2})}$	u_y/V_A
$E_b = -0.2 (t = 36.0)$	1.55	1.06	-0.197	0.851	-0.231
$E_b = -0.1 (t = 27.0)$	0.811	0.602	-0.168	0.669	-0.251
$E_b = -0.05 (t = 30.6)$	0.510	0.388	-0.134	0.543	-0.247

Table 3. Characteristic physical quantities at $(x, y) = (0.0, 1.2)$, a point on the boundary Γ_3 , in each of the respective stationary configurations corresponding to the boundary values $E_b = -0.2, -0.1$ and -0.05 .

neutral point since there is a larger current flow as seen from Fig. 30 ; therefore the resulting expansion effect becomes stronger. Also, the local Alfvén speed at distances from the neutral point becomes faster with larger E_b as can be observed from table 3 , where characteristic quantities at the spatial point $(x, y) = (0.0, 1.2)$ on the boundary Γ_3 are shown in each of the stationary configurations. Upward transmission for the expansion and downward transmission for the compression may thus be faster for larger values of E_b . We therefore expect that for larger values of E_b the amplitude of the oscillations is larger and their period is shorter; this is in fact consistent with the results shown in Fig. 30 and table 3. Table 3 gives the relative magnitude of V_A^{-1} (which is proportional to the Alfvén travel time) for $E_b = -0.2, -0.1$ and -0.05 . The ratio of V_A^{-1} between these three cases coincides with that of periods of oscillations observed in Fig. 30 . This is consistent with the preceding interpretation.

Now let us consider how the overall configuration is

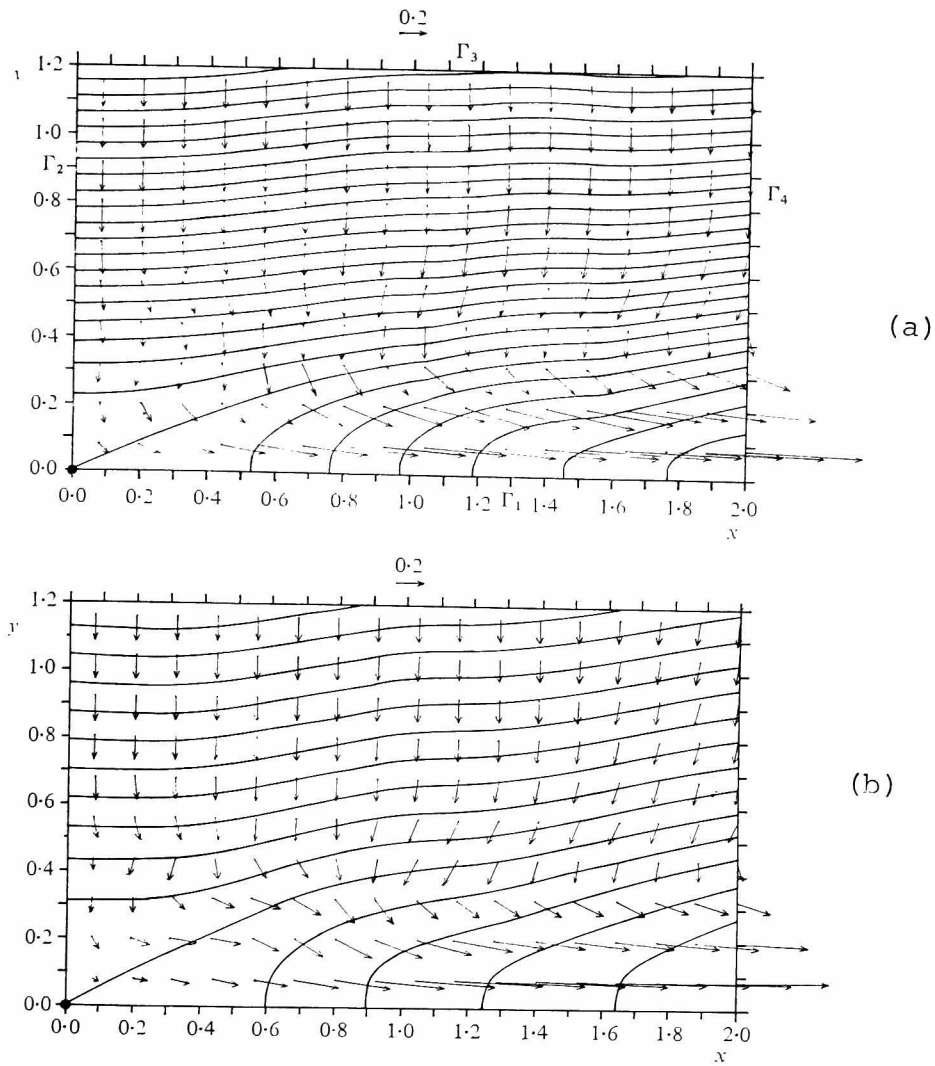


Fig. 31. For legend see page 112.

influenced by the different boundary values. Figs. 31(a), (b) and (c) show the resulting stationary field configurations, in which the corresponding flow patterns are also shown, for the cases $E_b = -0.2, -0.1$ and -0.05 , respectively, at times when the current densities at the neutral point have nearly the top values during the respective oscillations (cf.

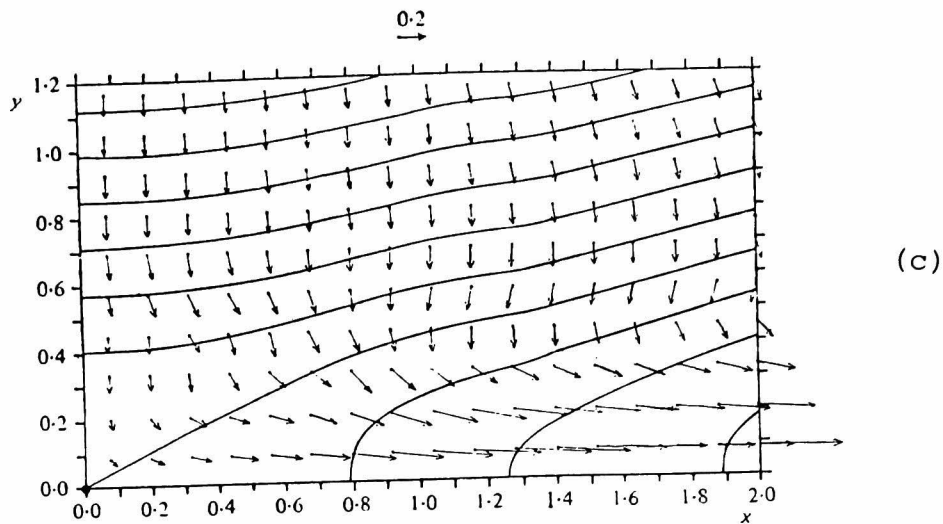


Fig. 31. Field and flow configurations in the stationary states that correspond to the boundary values (a) $E_b = -0.2$ (at time $t = 36.0$), (b) $E_b = -0.1$ (at $t = 27.0$) and (c) $E_b = -0.05$ (at $t = 30.6$). In (a) of the figure the boundaries are labelled by Γ_i ($i=1,2,3,4$). In each of the figures, the dot at the origin is the position of the magnetic neutral point, and at the top the scale of velocity is indicated.

Fig. 30). It may be observed that each configuration has wavy structures in both the x and y directions and is more complicated than the quasi-steady configuration shown in chapter 4. By comparing these configurations, we can readily see that for larger values of E_b more magnetic field lines are piled up in the external region; on the other hand, the plasma flow speeds are not so different from each other, so that the same is true of the sizes of their diffusion regions. See also Figs. 32 and 33, where the field component B_x and the inflow velocity u_y are respectively shown along the y axis in each of the stationary configurations. From the figures,

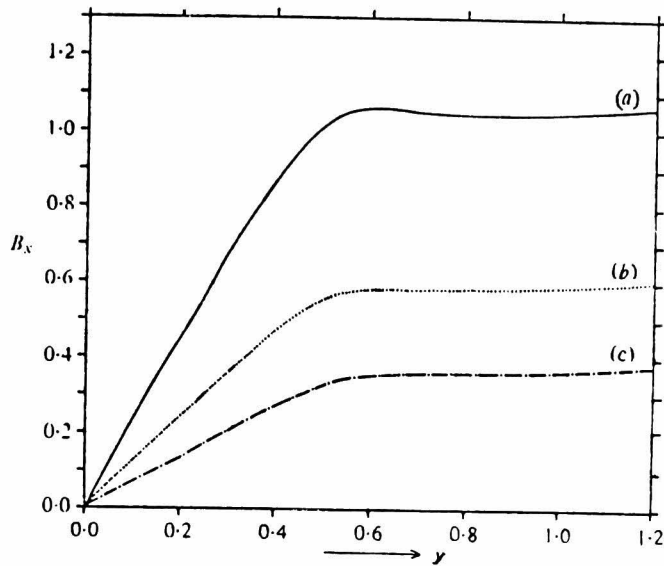


Fig. 32. Profiles of B_x along the y axis in the stationary configurations corresponding to the boundary values (a) $E_b = -0.2$ (at time $t = 36.0$), (b) $E_b = -0.1$ (at $t = 27.0$) and (c) $E_b = -0.05$ (at $t = 30.6$).

it is more clearly observed that the relative structures of the spatial variations of these quantities are not much influenced by the different boundary values; but their absolute magnitudes, especially of the magnetic field, are largely influenced by them.

We can see from the above numerical results that the amount of the magnetic field lines that are reconnecting per unit time in each of the stationary configurations can indeed be controlled by the imposed boundary values, E_b : this is primarily because the field strength in the external region is largely controlled by them. However, it should be recalled that the theoretical study of the reconnection rate has been based on

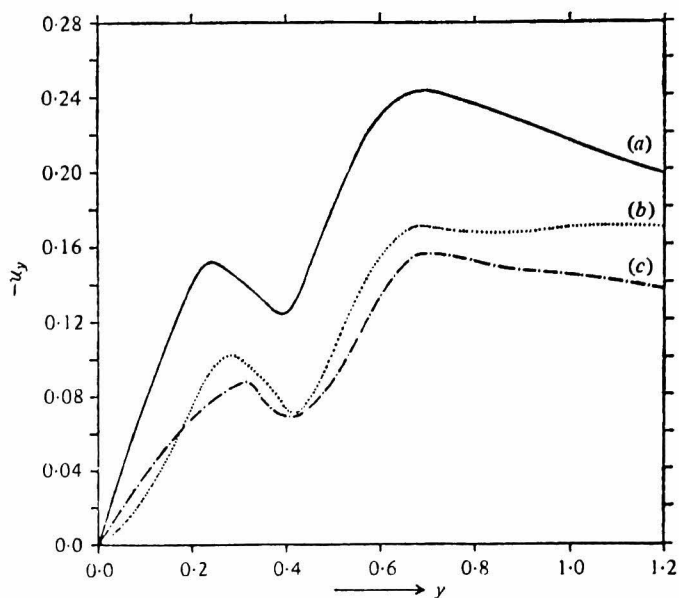


Fig. 33. Profiles of u_y (multiplied by -1 in the figure) along the y axis in the stationary configurations corresponding to the boundary values (a) $E_b = -0.2$ (at time $t = 36.0$), (b) $F_b = -0.1$ (at $t = 27.0$) and (c) $E_b = -0.05$ (at $t = 30.6$).

a mathematical model in which the plasma and field conditions at large distances from the neutral point are assumed to be the same for any of the configurations under consideration; thus, in the ordinary theoretical treatments the reconnection rate is given by the inflow speed at distances far from the neutral point measured in terms of the local Alfvén speed (Vasyliunas 1975). It may therefore be instructive in the present case to calculate the local Mach number $u_y / (B_x \beta^{-1/2})$ on the boundary Γ_3 at $x = 0$ (namely, at the spatial point $(x, y) = (0.0, 1.2)$). This is shown in table 3 for each of

the above stationary configurations. From the table we can see that the local Mach number at a distance from the neutral point is scarcely influenced by the difference between the boundary values of E_b . As already mentioned in §3, in the theoretical arguments based on the analytical results, it has so far been predicted that the reconnection rate (measured by the local Mach number at large distances from the neutral point) in the steady configuration is determined by the boundary conditions; this statement does not agree with the present numerical result. Our numerical experiment may rather suggest that the reconnection rate (in the theoretical sense) would be determined not by the boundary conditions, but, perhaps, by the local conditions in the vicinity of the neutral point.

Next, let us exemplify briefly the process of magnetic energy conversion in the present stationary configuration. In Fig. 34 the temporal variations of the energy flow rates across the boundaries Γ_3 and Γ_4 (see Fig. 31(a)) are shown only for the case $E_b = -0.2$ for each form of energy (magnetic, dynamic (bulk flow), and thermal (plasma) energies are denoted by E_M , E_D and E_P , respectively). The energy flow rates shown in the figure are given by integrating the respective energy flux densities (normalized by $v_A B_0^2 / 2 \mu_0$) over the boundary Γ_3 or Γ_4 : for details, see §5 of chapter 3, where the mathematical treatments are the same except for the difference in the size of the computational region. As expected, each form of energy flows into the region across Γ_3 , on the

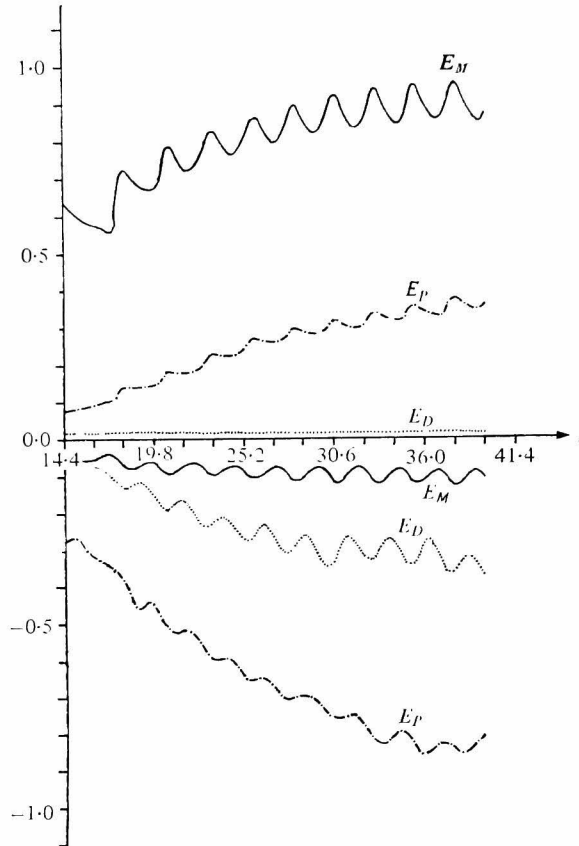


Fig. 34. Temporal variations of flow rates of magnetic energy (F_M), dynamic (flow) energy (F_D) and thermal (plasma) energy (F_P) across the boundaries Γ_3 (shown above the horizontal axis), and Γ_4 (shown below), in the case $E_D = -0.2$.

other hand, across Γ_4 it is ejected away because of the reconnection process proceeding in the region (note that the negative value indicates the flow out of the region). It may be interesting to examine how much each form of energy is enhanced in the region through the stationary reconnection process. For this purpose, let us consider the quantity

$$\left[\left| \text{rate of ejection (across } \Gamma_4) - \text{rate of injection (across } \Gamma_3) \right| \right]$$

for each form of energy, which may be averaged over times in the neighbourhood of $t \simeq 36.0$: this quantity may well be regarded as the mean value that each form of energy gains per unit time in the restricted region now at issue while the plasma is passing through the region. These quantities can readily be estimated from Fig. 34 as follows: the gain of $E_M \simeq -0.8$, that of $E_D \simeq 0.3$ and that of $E_P \simeq 0.5$ (the negative gain of the magnetic energy, in fact, indicates the loss of the energy). We can hence see that the reconnection process proceeding in that stationary configuration presents quite an effective mechanism for releasing the magnetic energy into the plasma energy; also, in this case now at issue the rate of the enhancement of thermal energy E_P is observed to be about twice as big as that of dynamical energy E_D .

For the above results so far shown, the local resistivity enhancement has been assumed to be sustained in the form given by (3.5) as in the previous chapters. Finally, we are now interested in how the dynamical process of reconnection is influenced by the removal of the effect of such a local resistivity enhancement. For this purpose, putting $S = 1$ in (3.5), and $R_m = 20$ in order to avoid numerical limitation, with the resistivity remaining now uniform in space and raised by a factor of 50 (note that previously $R_m = 1000$), and adopting the boundary value $E_b = -0.1$, we start the computation with the configuration at time $t = 14.4$ just as in the previous computations in this chapter. In Fig. 35 the result-

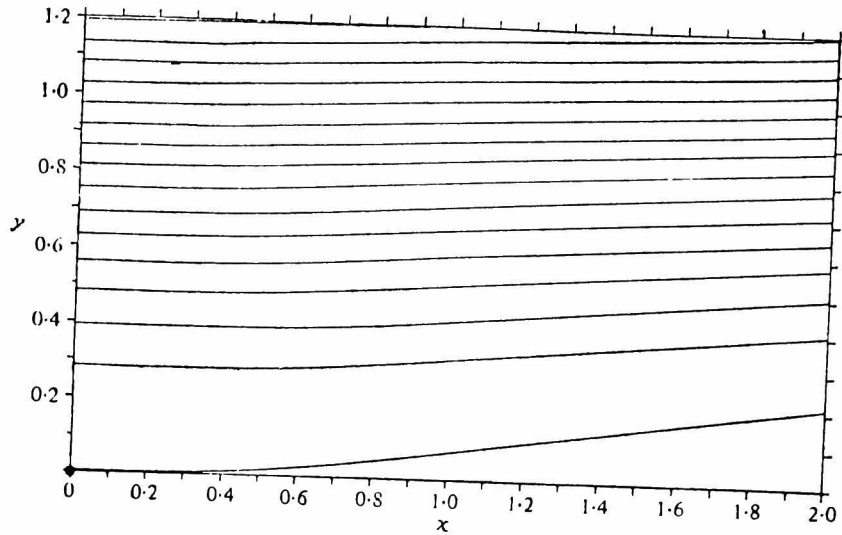


Fig. 35. Field line configuraion at time $t = 27.0$ where there has been no local increase in resistivity since $t = 14.4$, with resistivity spatially distributed uniformly and raised by a factor of 50 (i.e. $R_m = 20$); the boundary value $E_b = -0.1$ is assumed.

ing field configuration is shown at time $t = 27.0$. As illustrated in the figure, we have found that the large-scale X-type field configuration (which was indeed present at $t = 14.4$; see Fig.10 of chapter 3) can no longer be retained: the field line configuration becomes merely more and more flattened with increasing time. The field lines and the plasma are simply more and more piled up in the region, which results in diminishing the plasma global flow: this can readily be seen from Fig. 36 where the temporal behaviour of the inflow velocity u_y at $x = 0.0$, $y = 0.6$ and the outflow velocity

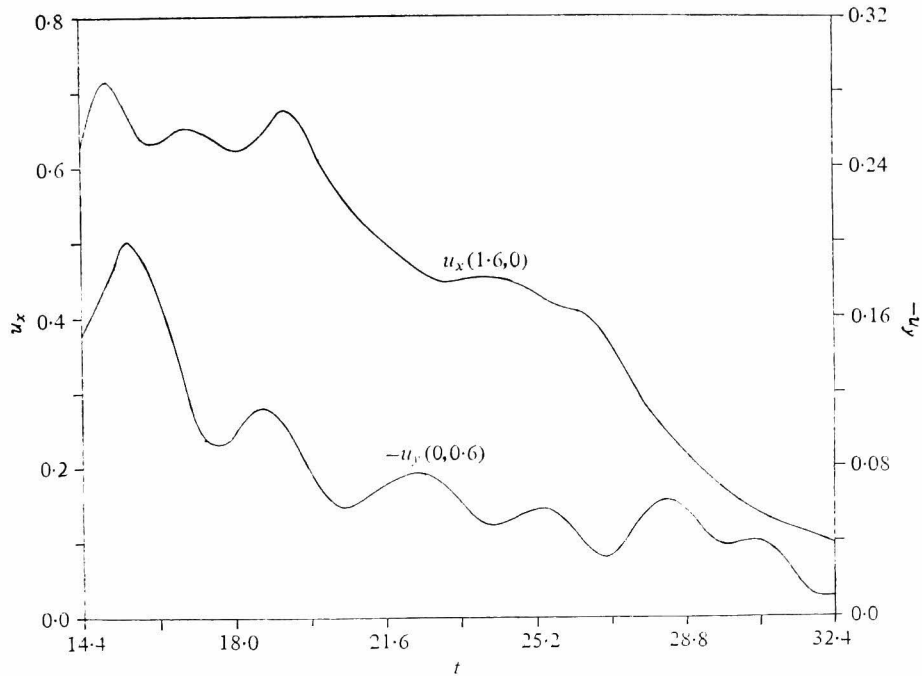


Fig. 36. Temporal variations of u_x at $(x, y) = (1.6, 0.0)$ and u_y at $(0.0, 0.6)$ where there has been no local increase in resistivity since $t = 14.4$; the boundary value $E_b = -0.1$ is assumed.

u_x at $x = 1.6$, $y = 0.0$ are shown. It seems quite natural that in such a flat field configuration the plasma, which is persistently being injected across Γ_3 , is accumulated in the region since it can no longer be efficiently ejected away owing to the magnetic body force in the form $J \times B_y$ (note that in the large-scale X-type field configuration the resulting magnetic tension effectively accelerates the plasma away from the region to retain the quasi-steady process of fast reconnection; see chapter 4).

Such a flattening of the magnetic field line configuration may have the following explanation. In the first place, we recall that the major effect of the local resistivity enhancement

lines in bending the field lines towards the magnetic neutral point in the diffusion region. As a result, MHD wave effects can lead to the consecutive ejection of the locally bent field lines from near the neutral point. This promotes the evolution and also the maintenance of the large-scale X-type field configuration in the whole region. For the details of this argument, readers are referred to chapters 3 and 4. In the absence of local resistivity enhancement, however, the X-type field line configuration becomes more and more flattened with increasing time from the vicinity of the neutral point, since there is then no continuous bending of the field lines that are convected with the inflow of plasma and are successively approaching the neutral point; the outward transmission of field-line bend can never occur. It may be noted that this dynamical process is similar to that of Stevenson (1972). He considers an initially hyperbolic magnetic field line configuration where there is a persistent injection of constant momentum flux (not magnetic flux, different from our model) from top and bottom. He finds that, as the system evolves, the configuration becomes flatter and that magnetic and fluid pressures continue to increase everywhere with no indication of approaching asymptotic values, just as seen here. It seems quite apparent that these two models, Stevenson's and ours, describe no true reconnection process; if there is any reconnection it is the small amount expected from the finite resistivity. Hence, a local increase in effective resistivity

near the neutral point should be required for the growth of fast reconnection; otherwise, the large-scale X-type field configuration could not be sustained.

§5. Concluding Remarks

In chapters 3 and 4, we examined the effect of a local resistivity increase on the current sheet system under no special boundary conditions. In this chapter, we have shown how the configuration of fast reconnection is controlled by a persistent injection of magnetic flux into the reconnection region. This injection is assumed to be forced by some external agency. We have also studied how the global configuration is affected by the disappearance of the local resistivity increase. The following significant consequences, derived from the present numerical models, should be noted.

(i) Distinct imposed boundary values give correspondingly distinct stationary configurations that are established in the presence of a local resistivity increase near the neutral point. The resulting stationary configurations involve the individual oscillations with time. The amount of the magnetic field lines that are reconnecting per unit time in each of the stationary configurations is determined in accordance with the corresponding boundary value: this seems consistent with the observations in the dayside magnetosphere. On the other

hand, the reconnection rate, which is given by the inflow speed measured in terms of the local Alfvén speed at a distance from the neutral point, can hardly be influenced by the different boundary values; on the other hand, in the theoretical arguments for the analytical models, it has been said that the reconnection rate, defined in the above sense, is determined by externally imposed boundary conditions. Our numerical results may suggest that the reconnection rate would probably be controlled by the local conditions near the neutral point rather than the boundary conditions.

(ii) But for the local enhancement of the effective resistivity near the neutral point considered in the present computation, the large-scale X-type field configuration can no longer exist; with increasing time the field configuration becomes simply more and more flattened, the field lines and the plasma being more and more accumulated in the region. Note that the large-scale X-type field configuration is required for the growth of fast reconnection since without such a field line configuration the plasma could not effectively be ejected away by the Lorentz ($\mathbf{J} \times \mathbf{B}$) force (Petschek 1964). The numerical result thus suggests that a local increase in effective resistivity in the neighborhood of a neutral point may be needed for the growth of fast reconnection in actual systems.

The results obtained from the somewhat idealized computational models illustrate the fundamental effect of a local increase in effective resistivity in the vicinity of the neutral

point upon the occurrence and growth of fast reconnection. The increase in effective resistivity may well result from, for instance, anomalous and/or inertial effects in the local region near the magnetic neutral point; however, this problem should in essence require that the complex microscopic behaviour of plasmas be studied, which is outside the scope of the present hydromagnetic approach.

DEPENDENCE OF FAST RECONNECTION ON *
THE MAGNITUDE OF RESISTIVITY

§1. Introduction

The present chapter will further examine how the fundamental configuration of fast reconnection is controlled by various resistivity enhancements, imposed locally in the vicinity of the magnetic neutral point. We shall argue that the present numerical results are essentially consistent with the previous theories of fast reconnection, once the problem is reconsidered from another point of view.

In the present numerical procedure all the conditions are the same as in chapters 3 and 4, and for several different resistivity enhancements, which are assumed to have been suddenly triggered locally in the vicinity of the magnetic neutral point, the corresponding solutions are sought. It is shown that according to the initially indented local resistivity increases the respective quasi-steady Petschek-type

* See Ugai and Tsuda (1979 b)

configurations are eventually set up without any special external agency in a similar manner to that shown in chapters 3 and 4. In order to estimate the efficiency of the resulting fast reconnection, we may introduce the intrinsic reconnection rate for each case, which is defined as the maximum value of the electric field at the neutral point up to which the induction electric field grows because of the strong hydro-magnetic effects involved in the system. It is found that the intrinsic reconnection rate thus defined has a weak dependence on the resistivity in the diffusion region. Note that this implication is essential in studying the fast reconnection problem as argued by previous authors (Petschek 1964, for instance). Such a weak dependence of the efficiency of the fast reconnection process on the resistivity in fact results from the fact that the fundamental structure of the established quasi-steady configuration is directly controlled by the initially imposed localized enhancement of resistivity; namely, for the smaller value of locally enhanced resistivity the size of the diffusion region becomes smaller and hence the current density more enhanced in the diffusion region. It should be remarked that how the diffusion region size is eventually determined in real plasmas is one of the most significant keys to any realistic mechanism of fast reconnection.

We may now clarify how the present numerical results are related to the previous theoretical work in both qualitative and quantitative aspects. As argued in chapter 5, there is

an apparent discrepancy between the numerical models and the analytical models concerning the basic question of which specific conditions (either far from, or near to, the neutral point) are essential in determining the fundamental structure of the Petschek-type configuration. Nevertheless, it should be noted that most of the analytical results could still be applicable to any steady configuration of fast reconnection regardless of how it originated. This is apparent if one takes it into account that the analytical studies have not considered the temporal evolution of fast reconnection but rather have only found various steady-state external flow configurations which yield fast reconnection. We shall see later in this chapter that this conceptual difference has the following consequence: in the analytical treatments any reconnection rate is possible up to an upper limit that is determined by the given resistivity in the diffusion region, since it is postulated there that the diffusion region size is freely adjusted to any given external flow, whereas in the present numerical experiment the reconnection rate should be uniquely determined by the resistivity, locally enhanced in the diffusion region. We shall then point out that each of the quasi-steady configurations, obtained by the numerical experiments, is equivalent to none other than the Petschek-type configuration that corresponds to the allowable maximum reconnection rate for the relevant magnetic Reynolds number based on the resistivity in the diffusion region. This conclusion is of actual importance in

applications of the mechanism of fast reconnection, since it is now well known that the maximum reconnection rate of the Petschek-type configuration is sufficiently large to be applied to large dissipative events in cosmic plasmas.

In the present experiment, all the numerical methods are the same as those of chapters 3 and 4. For the basic equations and the normalization procedure, see §2 of chapter 3; also, for the numerical scheme see 3.3 of chapter 3 and 2.3 of chapter 4. The initial and boundary conditions are described in 3.2 of chapter 3. In the following computations, the value of k is fixed at 1, and taking various values of S (see Eqn. (3.5) of chapter 3) we seek the corresponding solutions. The other parameters have the following values: the domain for computation is of size 2.0×2.0 and the mesh size $\Delta x (= \Delta y) = 0.04$ (see Fig.8 of chapter 3), the time step Δt is appropriately chosen so as to satisfy the numerical stability condition (cf. 3.3 of chapter 3). In addition, it is again assumed that the specific heat ratio $\gamma = 2.0$ and the initial ratio of the gas pressure to the magnetic pressure outside the current sheet $\beta_0 = 0.1$; also, $R_m (= \mu_0^{LV} A_0 / \eta_0$, the magnetic Reynolds number) = 1000.

§2. Results

In order to have an overall picture of the development

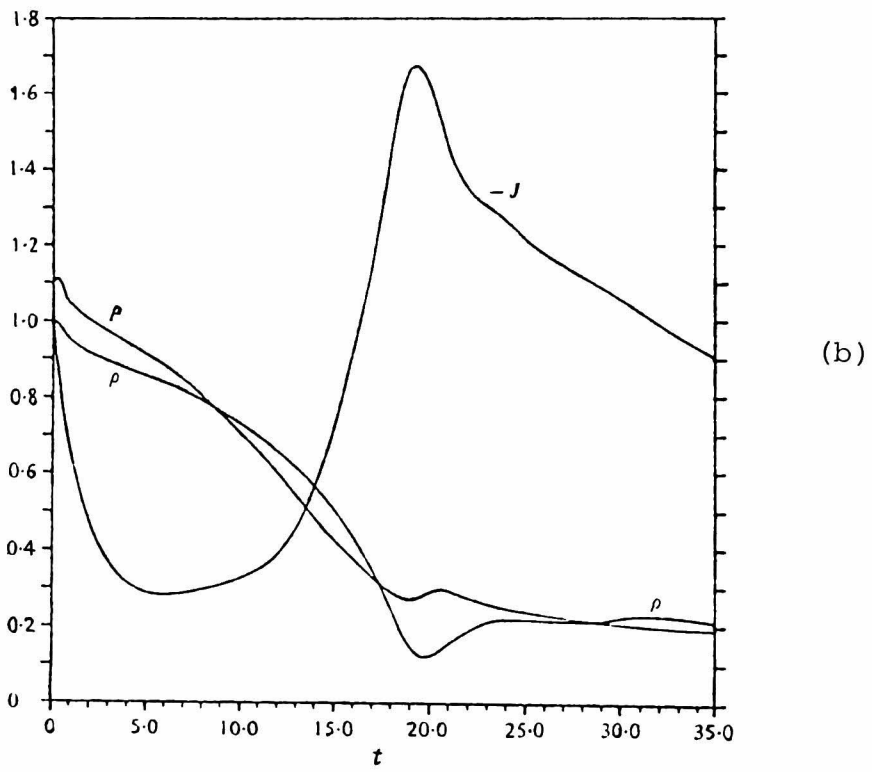
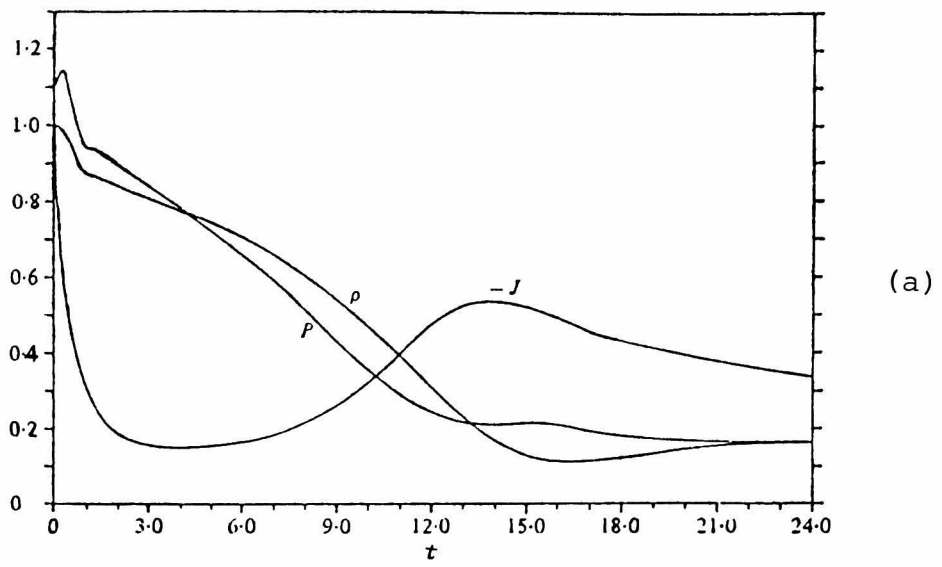


Fig. 37 (a), (b). For legend see page 129.

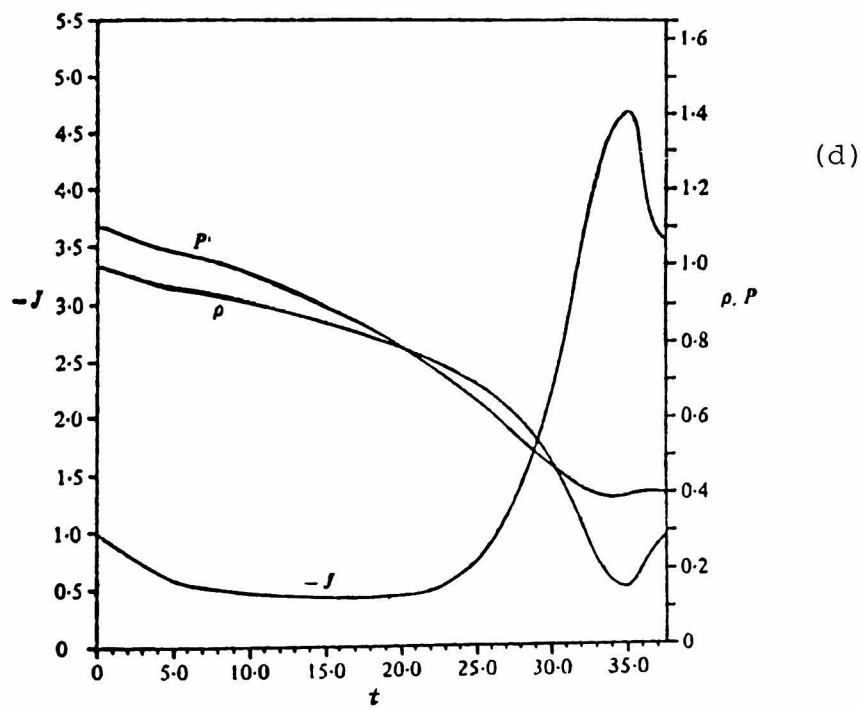
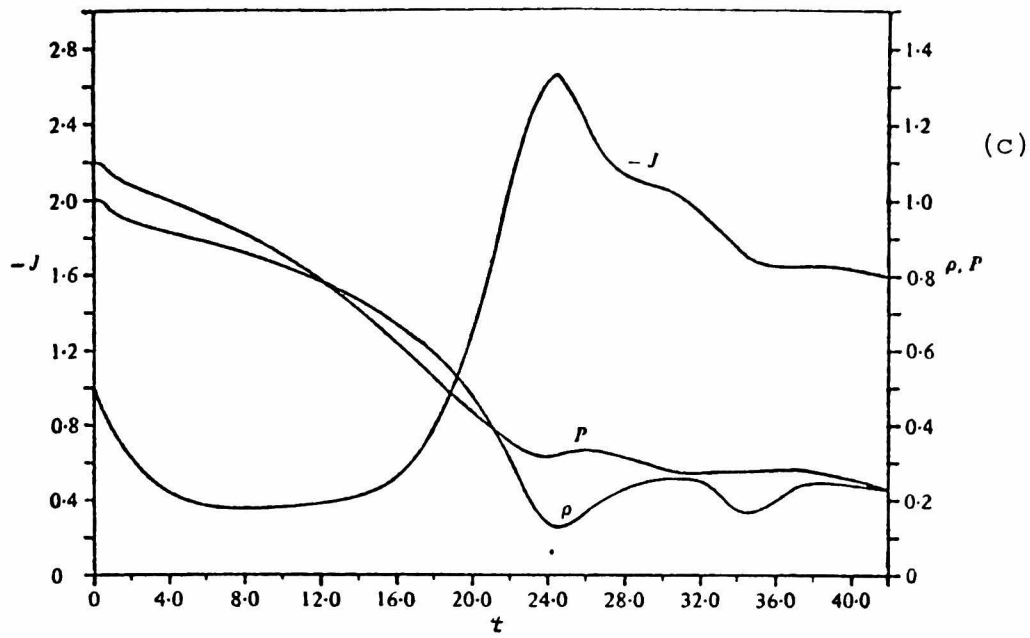


Fig. 37. Temporal variations of current density (J), mass density (ρ) and gas pressure (P) right at the magnetic neutral point, corresponding to the local resistivity enhancements (a) $S = 200$, (b) $S = 50$, (c) $S = 25$ and (d) $S = 10$.

of fast reconnection, in Fig. 37 are shown, as before, the temporal evolution of the mass density ρ , the plasma pressure P and the current density J (multiplied by -1 in the figure) right at the magnetic neutral point for each of the distinct local resistivity enhancements (characterized by S), From the figure, we can readily see that qualitatively the evolution of each reconnection process is quite similar to that already shown in chapters 3 and 4. In the quantitative aspect, however, some distinct features should be remarked. First, we may see that for a smaller value of S the corresponding time needed for establishment of the configuration of fast reconnection becomes longer (notice that immediately after the current density attains its peak value the quasi-steady configuration of fast reconnection is established; see chapter 4). It may be noted that magnetic tension is produced in the system through the initial diffusive effect due to locally enhanced resistivity (diffusive stage; see chapter 3), which in turn causes the global plasma flow. For a weaker enhancement of resistivity, the smaller the initial diffusive effect, so that the growth of plasma flow of course requires more time. This is consistent with the implication of Fig. 37 since it is the resulting global flow that plays a crucial role in constructing the overall configuration. We next notice from the figure that the peak value of the current density during the evolutionary process is larger for smaller values of S . In this connection, it should be noted that

the resulting plasma flow in turn reinforces the diffusive effect by enhancing the current density in the diffusion region until the diffusive effect becomes comparable with the hydromagnetic effect, when the quasi-steady configuration is set up (for details see chapter 4). This result, obtained numerically, originates in the very complicated nonlinear interactions between the hydromagnetic effect outside the diffusion region and the diffusive effect inside it. This result obviously indicates that, as will soon be seen more directly, the diffusion region becomes smaller in a configuration corresponding to smaller resistivity in the diffusion region, which has a most important consequence in the problem of fast reconnection.

We find that for the variously imposed values of S the corresponding configurations strongly support Petschek's mechanism in the same manner as shown in chapter 4. Let us exemplify the quasi-steady configurations for two extreme cases of $S = 25$ and $S = 200$ (in the case of $S = 10$ the size of the diffusion region is so much reduced that the corresponding quasi-steady configuration seems to be somewhat obscured, especially in the inner region, because of the coarse grid taken in the present numerical scheme). In Fig. 38 the field and flow configuration and in Fig. 39 the current density distribution are shown for each of these cases. The fundamental difference between these quasi-steady configurations is quite apparent from these figures. In the configuration correspond-

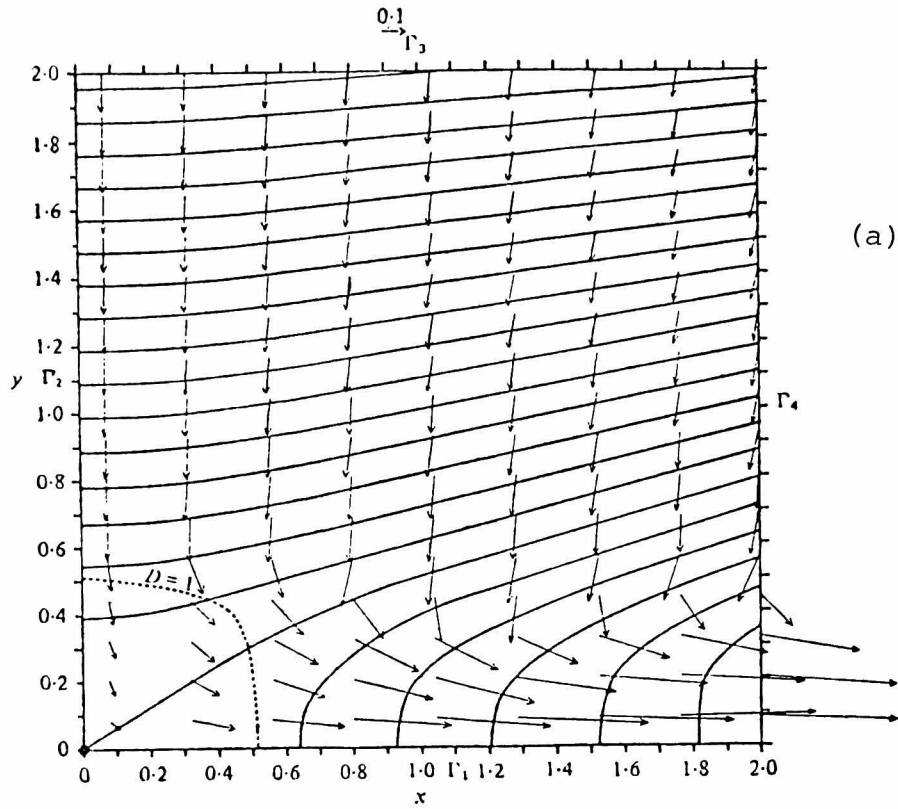


Fig. 38(a). For legend see page 133.

ing to $S = 25$, the diffusion region is more contracted to the vicinity of the neutral point. Hence the slow shock, which stands in the external flow region and is attached to the diffusion region, is more depressed as seen in Fig. 39 (note that the current density is notably enhanced where the shock stands).

For the purpose of seeing more directly how the corresponding sizes of the diffusion regions in the established quasi-steady configurations differ from one case to another, it seems relevant to examine the spatial variations of the magnetic field

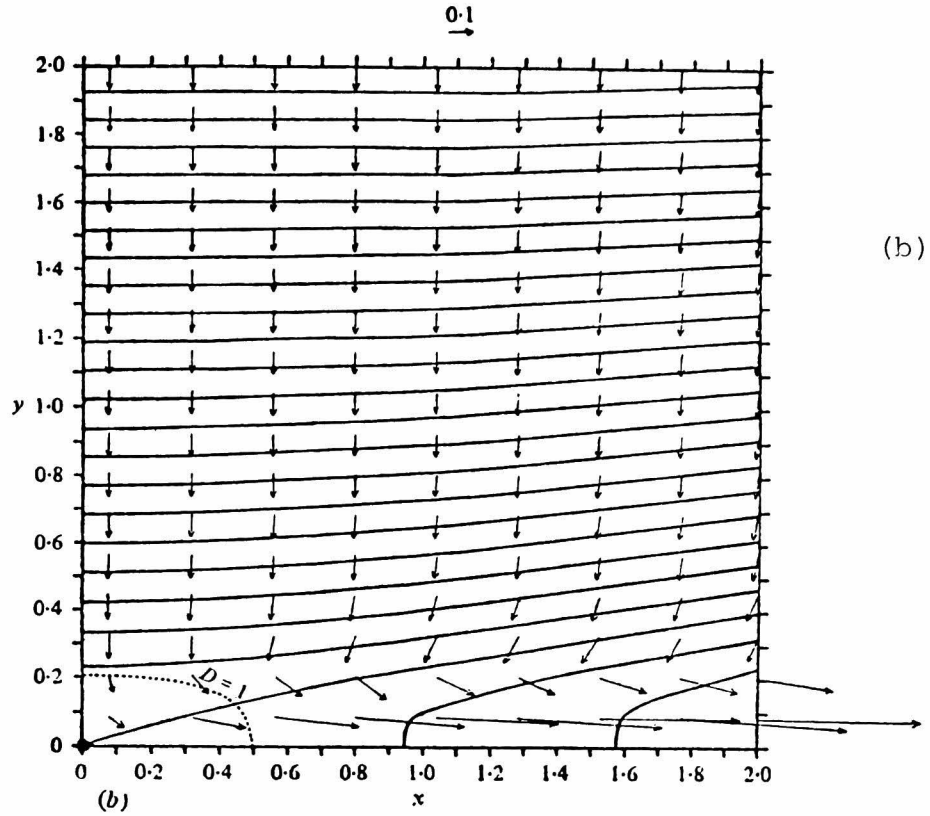


Fig. 38. Field and flow configurations in the quasi-steady states corresponding to the local resistivity enhancements (a) $S = 200$ (at time $t = 17.4$) and (b) $S = 25$ (at $t = 27.0$). In (a) of the figure the boundaries are labelled by Γ_i ($i=1,2,3,4$). In each of the figures, ----- indicates the boundary of the diffusion region given by $D (\equiv | \underline{u} \times \underline{B} / (R_m^{-1} \eta \underline{J}) |) = 1$, and at the top the scale of velocity is indicated. The dot at the origin is the position of the magnetic neutral point.

component B_x along the y axis for each configuration, which is shown in Fig. 40. It is apparent from the figure that the size of the diffusion region, where the magnetic field shows a large variation, becomes smaller corresponding to smaller values of S . It should especially be remarked that the

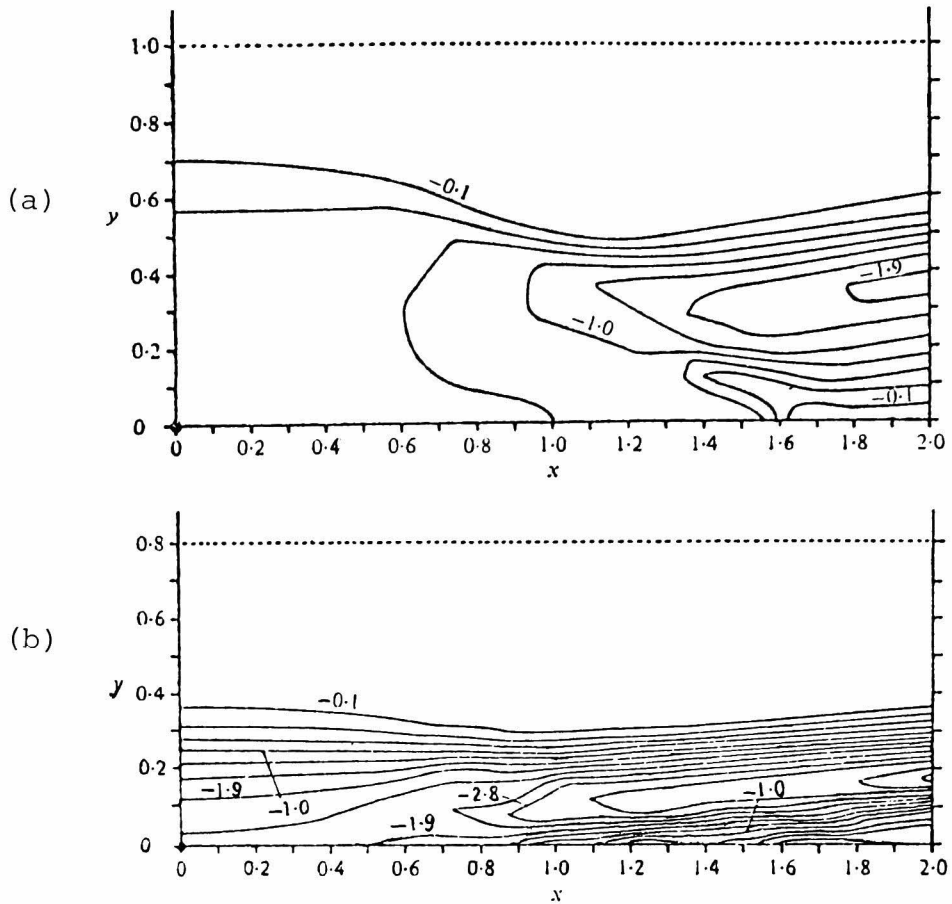


Fig. 39. Contour lines of current density distributions in the quasi-steady states with contour interval of 0.3, corresponding to the local resistivity enhancements (a) $S = 200$ (at time $t = 17.4$) and (b) $S = 25$ (at $t = 27.0$).

fundamental structure of the final configuration is largely controlled by the magnitude of the enhanced resistivity, which suddenly appeared at the initial time locally in the vicinity of the neutral point.

As argued in chapter 4, the process of the development of fast reconnection should be viewed as a gross instability, inherent to the current sheet system itself. We may now consider quantitatively how the magnitude of such a gross instability

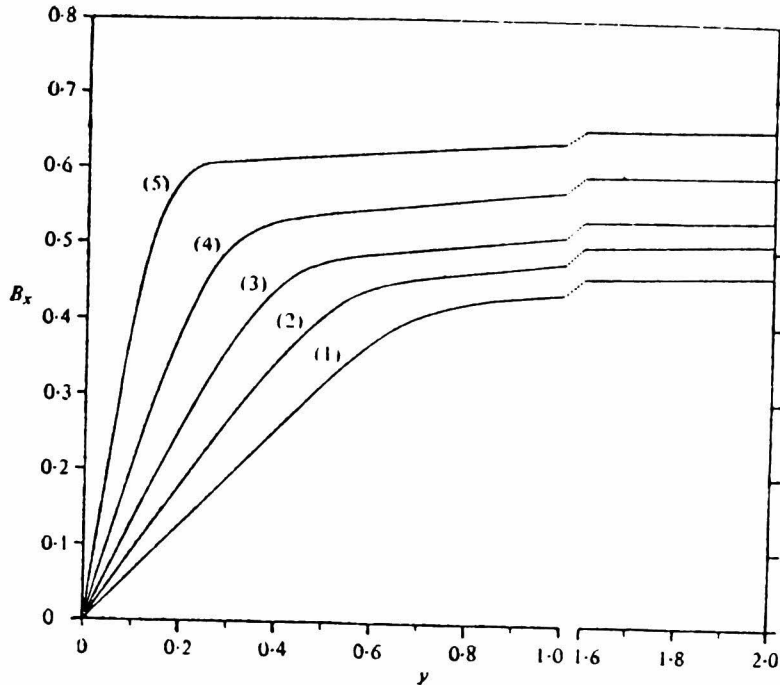


Fig. 40. Profiles of B_x along the y axis in the quasi-steady configurations corresponding to the different resistivity enhancements. (1) $S = 200$ (at time $t = 21.0$), (2) $S = 100$ (at $t = 22.5$), (3) $S = 50$ (at $t = 26.4$), (4) $S = 25$ (at $t = 30.0$) and (5) $S = 10$ (at $t = 36.0$).

depends on the locally enhanced resistivity. For this purpose let us introduce an intrinsic reconnection rate (denoted by E_0) for each of the temporal dynamical processes of reconnection as already defined in §1 of this chapter (remember that E_0 thus defined is the same as in chapter 5). We may well measure the magnitude of the reconnection process simply by E_0 . By observing that the electric field is given by $R_m^{-1}SJ$ at the neutral point, E_0 can readily be obtained from Fig. 37. In Fig. 41 is shown the dependence of the intrinsic reconnection rate E_0 on the local resistivity enhancement characterized by S . In this figure we take into account that when $S = 1$ (i.e. there is no resistivity increase), E_0 must nearly equal

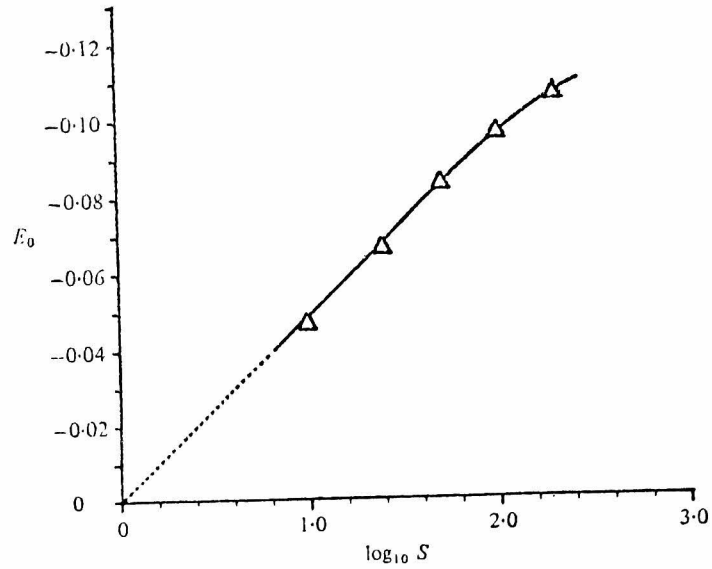


Fig. 41. Dependence of the intrinsic reconnection rate E_0 on the local resistivity enhancement, characterized by S . E_0 is defined as $R_m^{-1} S J_{\max}(0, 0)$, where $R_m (= \mu_0 L V_{A0} / \eta_0)$, the magnetic Reynolds number) is taken as 1000 and $J_{\max}(0, 0)$ is the maximum value of the current density at the magnetic neutral point during each of the evolutionary processes of fast reconnection.

zero since there is no gross instability (although some resistive instabilities would take place). Note that the abscissa shows S on a logarithmic scale. We can thus see that E_0 has a weak dependence on S . It should be noted that such a weak dependence of the magnitude of the fast reconnection rate on the local resistivity near the neutral point has directly resulted from the fact that the diffusion region becomes smaller as the magnitude of the local resistivity enhancement becomes smaller. A similar consequence has been

suggested in the previous theoretical studies under a certain assumption in calculating the reconnection rate. With respect to this, more systematic arguments will be given in the following section.

§3. Discussion

One of the most fundamental problems concerning the fast reconnection process is to seek the possible maximum reconnection rate. In the Sweet-Parker model, magnetic energy is released only because of magnetic field diffusion due to finite resistivity. The reconnection rate, hence, is strongly dependent on the resistivity and is found to be too small to be applied to solar flares, since in cosmic plasmas the magnetic Reynolds number is usually extremely large. In Petschek's model the diffusion region is restricted to a small region in the vicinity of the magnetic neutral point, so that the reconnection rate depends weakly on the resistivity and the allowable maximum rate is sufficiently large for solar flare phenomena. With this in mind, one may note that one of the keys to the basic mechanism of fast reconnection lies in how the diffusion region can eventually be reduced to a small region near the neutral point through the temporal dynamical process involved in the system. Therefore in studying the fast reconnection problem we should take into consideration the physical

grounds on which the diffusion region is constructed. Note, however, that in previous analytical treatments, which mostly gave steady-state configurations, the detailed structure of the diffusion region which should be matched to the external flow has not as yet been shown in a convincing manner. In obtaining the definite reconnection rate, it was postulated that the size of the diffusion region adapts to any imposed external flow; thus the external conditions at large distances from the neutral point largely determine the overall configuration of fast reconnection.

There may arise a question whether or not the basic postulate prescribed in the analytical treatments in fact holds in the real physical world. Of course, any convincing answer to this question requires the careful study of distinct characteristics involved in the temporal dynamics of fast reconnection. Parker (1973) pointed out that Petschek's configuration required some extra mechanism that can produce an apex in the field lines as they approach the neutral point. As a matter of fact, it seems quite difficult to envisage a situation where some external agency far from the neutral point can cause any bend of the lines of force that appear in the external region, because they could readily be smoothed by the resulting Alfvén-wave transmission. Also, our numerical experiment, shown in chapter 5, directly examines the effects of persistent injection of magnetic fluxes, forced by some external agency, upon the process of fast reconnection. As

pointed out there, the numerical results did not support such an analytical postulate; that is, the external agency cannot have any significant effect upon the fundamental structure of the Petschek-type configuration. It seems therefore questionable in real plasmas that the diffusion region adapts itself to any given external flow by varying its size.

On the other hand, all the present numerical results have shown that local resistivity enhancement is essential to establishing and, further, to sustaining, the overall configuration of fast reconnection. (Note that locally enhanced resistivity in fact produce an apex in the lines of force as required by Parker (1973); for details see chapter 3.) In this case, the fundamental structure of the established configuration is determined accordingly by initially imposed local resistivity enhancement, which also determines the corresponding reconnection rate. Obviously, this situation is inconsistent with the basic consideration that results from the analytical studies. However, as already pointed out, the analytically obtained mathematical solutions are relevant only to established steady configurations with no regard to their evolutionary development. For this reason, it is not surprising that the quasi-steady configurations, obtained by the present numerical experiment, are in good agreement with the theoretically derived Petschek-type configuration (see also chapter 4).

We may now quantitatively examine the relation between

the present numerical results and the previous theoretical works. Note that in usual analytical treatments the effect due to finite resistivity is taken into account only in the diffusion region. Hence, to compare with the analytical studies, the magnetic Reynolds number R_{me} is defined, by the effective resistivity in the diffusion region, as

$$R_{me} = (L_e/L)S^{-1}R_m . \quad (6.1)$$

Here, L_e is the characteristic scale length of the whole region to be considered, L the half-width of the initial current sheet as before and $R_m (\equiv \mathcal{M}_0 LV_A / \eta_0)$ the previously defined magnetic Reynolds number; also, the mean value of resistivity in the diffusion region is taken to be $S \eta_0$ for simplicity. In the analytical treatments the reconnection rate can be parametrized by the values of R_{me} .

As mentioned in §3 of chapter 2, the analytical studies presented the mathematical solutions on the steady Petschek-type configurations in incompressible fluids and calculated the relations between the Alfvén Mach number M_e at the distance L_e and the same quantity M_i just outside the diffusion region on the y axes. See, for instance, Fig. 6, which is based on the result by Priest and Soward (1976), in which the relation between M_i and M_e is shown using R_{me} , as a parameter. According to Vasyliunas' statement, the reconnection rate M_e may lie anywhere on the corresponding

curve and has the allowable maximum value when M_i reaches unity. Note that this conclusion is a direct outcome of the basic postulate prescribed in their models. However, one may notice that there is some ambiguity in this analytical result. Consider the case of $M_i = 1$, which corresponds to the maximum value of M_e according to the above result. But, it is obvious from the consideration of the diffusion region by these authors that when $M_i = 1$ the inflow and outflow speeds just outside the diffusion region are equal to each other. Therefore, the inflow- and outflow-side dimensions of the diffusion region must also be the same because of the mass conservation of incompressible fluid. Obviously, this indicates that there exists no net current flow in the diffusion region as can be seen by taking the curl of \underline{B} . This in turn implies that no effective reconnection can take place in the diffusion region. This apparent paradox seems to have resulted from a lack of detailed examination of the precise structure of the diffusion region especially in the case when M_i is not much less than unity. It should therefore be remarked that not every reconnection rate up to the upper limit could necessarily be realized in the real physical world.

In the present numerical experiments, on the other hand, the reconnection rate is uniquely determined by any given R_{me} as already pointed out. Table 4 shows characteristic quantities on the y axis just outside the diffusion region in each of the quasi-steady configurations that correspond to the local

	t	y_i	ρ	B_x	u_y	V_{Ai} ($= B_x \cdot \rho^{-1/2}$)	M_i ($\equiv u_y/V_{Ai} $)
$S = 200$	21.0	0.76	0.521	0.421	-0.170	0.583	0.292
$S = 100$	22.5	0.68	0.550	0.454	-0.144	0.612	0.235
$S = 50$	26.4	0.52	0.568	0.486	-0.119	0.645	0.184
$S = 25$	30.0	0.40	0.626	0.530	-0.0977	0.670	0.146
$S = 10$	36.0	0.32	0.730	0.607	-0.0862	0.710	0.121

Table 4. Characteristic physical quantities at $(x, y) = (0, y_i)$ on the y axis, just outside the diffusion region, and at time t , in each of the quasi-steady configurations corresponding to the local resistivity enhancements $S = 200, 100, 50, 25$ and 10 .

resistivity enhancement, S . In the table, the numerically obtained local Alfvén Mach number (denoted by M_i in accordance with the analytical treatments) is defined as $|u_y/V_{Ai}|$ which is calculated for each quasi-steady configuration. We find that the temporal variation of M_i is sufficiently small during each of the quasi-steady processes. Suppose that the present numerical solutions could be extended to some larger region of characteristic scale length L_e , although the region for the numerical solutions has been restricted to a rather small region near the diffusion region because of numerical limitations. Note that the analytical solutions are given for the external flow of characteristic length L_e . The present numerical results may thus be applied to the theoretically

developed Petschek's models, though the analytical models are usually highly idealized.

In spite of some differences in basic mathematical treatment between our numerical and the analytical models (such as fluid compressibility, etc.), let us directly apply the numerical results shown in table 4 to Fig. 6 (see chapter 2). We may first note in Eqn. (6.1) that $R_m = 1000$ in the present numerical computations and that L_e/L is usually much larger than unity. Table 4 gives the numerical value of M_i for a given value of S , which also determines the value of R_{me} (see Eqn. (6.1)). Given a pair of values of M_i and R_{me} , the relevant value of M_e is found in Fig. 6. Each value of M_e thus found corresponds to the maximum (or plateau) value of M_e . It is therefore concluded that quasi-steady configurations that have evolved from the indentation of local resistivity increase are none other than the Petschek-type configuration with the allowable maximum reconnection rate. This conclusion seems to be of fundamental importance in actual systems, since Petschek's mechanism is the only workable model for fast reconnection (Priest and Soward 1976).

§4. Summary

We first recall that attention has been directed primarily towards discovering the basic physical mechanism by means of

which the magnetically stored energy can be released as rapidly as large dissipative events such as solar flares and magnetospheric substorms. The first to set up such a mechanism was Petschek (1964) who recognized the importance of MHD slow shock for this problem. Since Petschek's suggestion, most analytical studies have concentrated on more sophisticated mathematical solutions for the external flow region by incorporating his basic idea. It is now established that the Petschek-type configuration that corresponds to the allowable maximum reconnection rate is most applicable to these flare phenomena. Unfortunately, however, the analytical school has failed to elucidate the temporal dynamics of Petschek's mechanism. In order to calculate the reconnection rate, it is simply postulated in the analytical treatments that the diffusion region size can be freely adjusted according to any given external flow. It should be recognized that this fundamental postulate is not based on a firm mathematical foundation but rather is an ad hoc prescription. The validity of such a postulation is in fact highly questionable, so that the analytical calculation of the upper limit also seems obscure.

We have argued that in most major respects the present numerical results are entirely consistent with theoretical studies on the fast reconnection problem. Specifically, we have shown: (i) the quasi-steady configurations, established according to variously imposed localized enhancements of resistivity, exactly describe Petschek's mechanism; (ii) the re-

connection rate, which is uniquely determined for each of the quasi-steady configurations, corresponds to the allowable maximum reconnection rate of Petschek-type configuration for the relevant magnetic Reynolds number; (iii) the reconnection efficiency is weakly dependent on the resistivity in the diffusion region just as required for the fast reconnection problem. Note that such a weak dependence on the resistivity has resulted from the fact that the size of the finally constructed diffusion region is in each case determined by the initially imposed local resistivity enhancement through the hydromagnetic effects during the evolutionary process. Nonlinear hydro-magnetic effects in fact do play a crucial role in constructing the overall configuration; however, it should be emphasized that the ultimate cause is the localized enhancement of resistivity. The occurrence of anomalous resistivity in the vicinity of the neutral point was observed in agreement with our numerical results by the reconnection experiments (see, for instance, Bratenahl and Baum 1976); also, Amano and Tsuda (1978) recently suggested that current-induced instabilities can easily occur both in the geomagnetic tail and in the solar atmosphere.

All our numerical investigations have shown that, in contrast with the analytical predictions, the local conditions near the neutral point are important in accomplishing fast reconnection. In view of the ambiguity of the basic postulate in the analytical treatments, we suggest that in the real

physical world the fast reconnection process should be regarded as a sort of gross instability, inherent to the current sheet system itself, which can be triggered by some local onset of anomalous resistivity.

SUMMARY AND DISCUSSION

§1. Summary of the Computer Experiments

A series of our computer experiments have studied the two-dimensional temporal dynamics of field-line reconnection, which is a problem of high topical interest in fast reconnection mechanism. In fact, nothing other than the eventual solutions could convincingly clarify the actual mechanism of fast reconnection in the real physical world (Parker 1973). Now let us summarize below the major points that we have argued in a series of chapters 3 - 6.

Chapters 3 and 4 demonstrated in a typical case a nonlinear development of the Petschek mode from the current sheet. By the onset of anomalous resistivity in the local region to be identified with a magnetic neutral point the quasi-steady Petschek mode can eventually be established on the nonlinear saturation level. This process may well be regarded as a decay process, through which the energy stored in the initially antiparallel magnetic field that extends to infinity is brought in across the boundaries and rapidly released, owing

to a gross instability inherent in the current sheet system since there is no special boundary condition in the model.

Chapter 5, on the other hand, examined the effects of persistent externally forced injection of magnetic fluxes. It showed that, corresponding to fixed rates of magnetic flux injection, specified on the inflow boundary, there are stationary configurations in each of which such an external influence is ultimately matched to the inner reconnection process. It was pointed out there that the external agency has little significant influence upon the fundamental structure of the spatial changes of variables; also, the Petschek-type configuration is no longer sustained if the local resistivity increase near the magnetic neutral point disappears.

Chapter 6 further examined the dependence of the Petschek-mode development on the resistivity magnitude in the immediate vicinity of the neutral point. It was shown that the reconnection efficiency, which is determined for each of the Petschek modes, established according to variously imposed localized enhancements of resistivity, has a weak (logarithmic) dependence on the resistivity in the diffusion region. This conclusion in fact assures that even in highly conducting plasmas large-scale conversion of the magnetic potential energy stored in the current sheet system into plasma energies can effectively be realized; the initially antiparallel magnetic field configuration can rapidly be translated topologically into the large-scale X-type field configuration due to magnetic

field reconnection.

§2. Comparison with Fast-Reconnection Theories

Previous analytical treatments concerning the fast-reconnection problem mostly gave steady-state configurations, and the evolutionary process of fast reconnection has not been shown in any convincing manner. There is an apparent conceptual discrepancy between our computer models and analytical models concerning the basic question of how the Petschek mode can eventually be established in actual plasmas. Nevertheless, the computer experiments succeeded in obtaining almost all the important consequences derived from the analytical studies. Now let us summarize below the major controversial points.

(1) Slow-shock formation

One of the most important consequences, suggested by the theoretical studies, is that in order for the fast reconnection to be realized slow shock should stand in the steady configuration. The present computer experiments in fact showed that the slow shock can eventually stand in the quasi-steady configuration.

(2) Controlling factors

This problem necessarily requires that the temporal dynamics of reconnection be studied. The analytical studies merely postulated that the external conditions at large

distances from the neutral point could largely determine the overall configuration of fast reconnection. The computer experiments, on the other hand, showed that the fundamental structure of the Petschek mode is little influenced by external conditions ; rather, it is determined by the resistivity, locally enhanced in the vicinity of the neutral point. Obviously, in the analytical studies, the reconnection process was considered to be, so to say, such a passive mechanism that externally given energy, in the form of large-scale dynamical plasma motion, concentratedly flows out through the thin layer (namely the field reversal region) ; on the other hand, in our computer models, it was regarded as a very active mechanism such that the critically stored magnetic energy is suddenly released as a result of a gross instability inherent to the current sheet system.

(3) Reconnection rate

Theories predicted on the basis of the above postulate that for the Petschek mode any reconnection rate is possible from zero to an allowable maximum rate according to external conditions ; the maximum rate is determined by a given magnetic Reynolds number. On the other hand, our computer experiments showed that the reconnection rate is uniquely determined, independently of external conditions, by a given magnetic Reynolds number ; the resulting configuration corresponds to none other than the Petschek mode with the allowable maximum reconnection rate.

§3. Applications to Phenomena in Actual Plasmas

The present numerical results may be applied to phenomena occurring in the real physical world. In §4 of chapter 1 we showed typical phenomena, associated with magnetic field reconnection, that were observed in laboratory plasmas as well as in space plasmas. We may first refer to the reconnection experiment, called the DIPD, by Baum et al.. As shown in 4.2 of chapter 1, they found that anomalously high electrical resistivity, due to ion-sound waves, is caused locally in the vicinity of the neutral point during the reconnection process. This is entirely consistent with our numerical results (Baum private communication).

In the solar atmosphere, sunspot fields, which are likely to be sheared, are usually very complicated as shown in 4.3.2 of chapter 1. Hence, the present two-dimensional reconnection process could not directly applied to the solar flare phenomenon. But, it should be noted that the major plasma processes involved in a solar flare consist of the impulsive plasma heating due to, perhaps, occurrence of anomalous resistivity and the subsequent large-scale plasma instability. We have in fact seen in this thesis that these properties are quite well provided by the fast-reconnection development.

In the geomagnetic tail, on the other hand, the field geometry is rather simple and can be approximated by an anti-parallel field, so that the present numerical results may

well, in essence, be applied to magnetospheric substorms. In the following, therefore, we shall intend to construct a simplified model for the substorm on the basis of both our computer results and the major observational evidences concerning the substorm which were mentioned in 4.3.3 of chapter 1.

Suppose that the fast reconnection is proceeding in a finite region inside the tail during the explosive phase. The reconnection region, shown in Fig. 1 (see chapter 1), must then have a finite width, $|z| < Z$ say, outside which there is no reconnection disturbance. Fig. 42(a) illustrates a simple version of the three-dimensional process in the (x, z) -plane. Note that the z -axis corresponds to an X-type magnetic neutral line in the reconnection region. In the coordinate system, the y -axis is directed northward and the x -axis directed towards the earth. We may consider here only the region corresponding to $x \geq 0$ and $y \geq 0$ in the figure; hence, the electrical quantities E_1 , I_1 and I_0 are all the same as those shown in Fig. 1. Remark that the current density I_1 associated with the B_y field in the reconnection region should flow along both its sides due to $\partial B_y / \partial z$ as shown in the figure. The ionosphere, represented as a variable resistance in the figure, may well be connected to the reconnection region by the field lines that pass through the reconnection region. Fig. 42(b) hence shows the reconnection process working as a dynamo in the tail and the associated current system that could link the tail to the ionosphere.

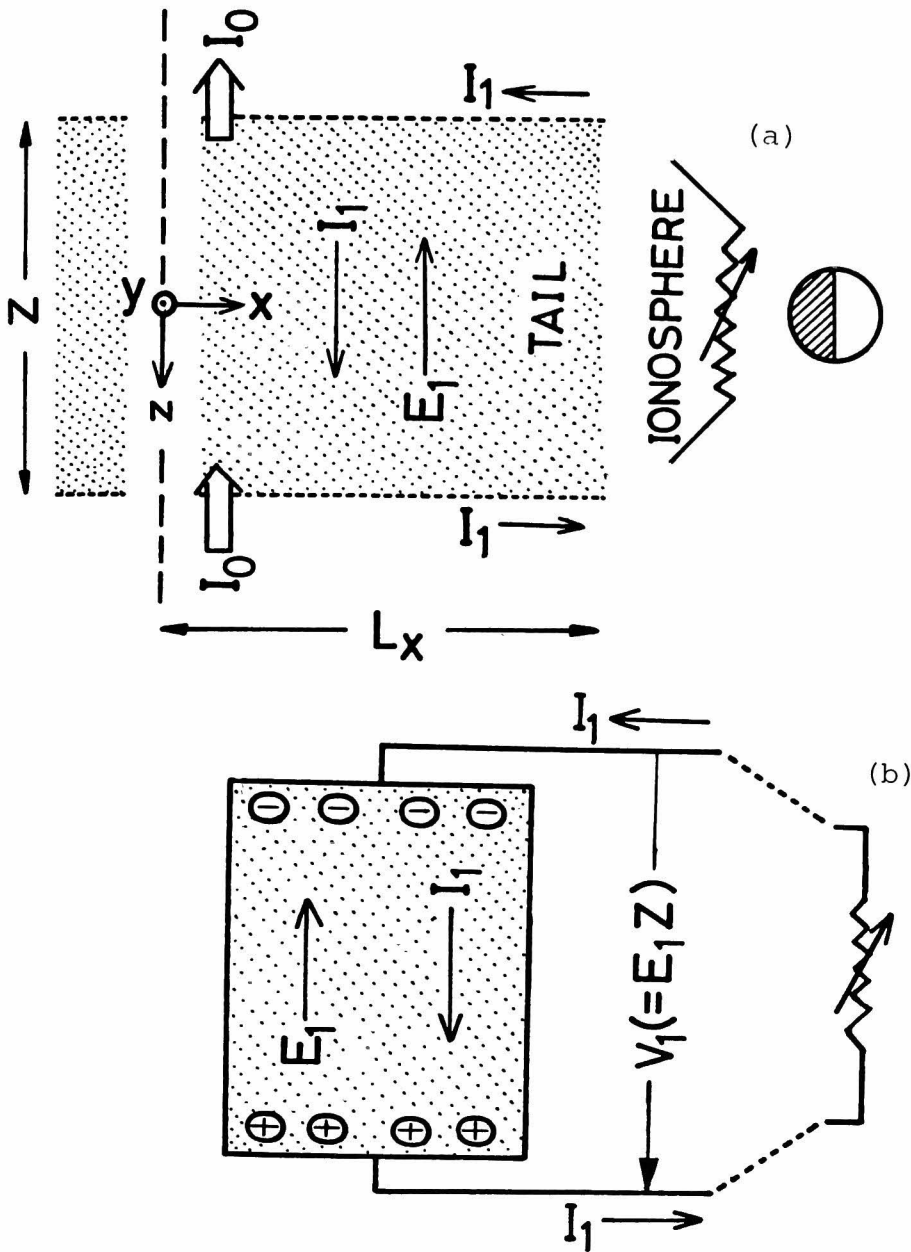


Fig. 42. (a) Electrical quantities shown in the (x, z) -plane: current I_0 is one that initially forms a current sheet; the electric field E_1 and current I_1 result from the reconnection. The reconnection region (shaded area) is of a finite width Z in the tail; the ionosphere is represented as a variable resistance. (b) Generator associated with the reconnection in the tail and current system that will link the tail to the ionosphere.

Fig. 42(b) shows that a westward electrojet may well be caused in the polar ionosphere. The behavior of auroral electrojet would be determined by how the electric field develops in the tail. As have been seen, in the fast reconnection process the associated electric field spreads from the inner region towards the external region; also, the width of the reconnection region Z would become larger with time in actual systems. Accordingly the connected region in the ionosphere would become extended in the east-west direction and move poleward, which is consistent with the well-known behavior of auroral electrojet.

In reality such an electrical connection of the ionosphere to the tail will certainly have some influence on the reconnection process in the tail. However, this problem should involve very complicated plasma processes, so that for simplicity we may assume here that the reconnection (especially the associated electric field E_1) would not so much be influenced by the feedback. In Fig. 42(b), therefore, the dynamo is tentatively thought to be a constant voltage source. In order to give quantitative examinations, we may employ the present numerical results, that give typically $B_{y1} \simeq 0.1B_{x0}$ and $V_0 \simeq 0.6V_{A0}$, where $V_{A0} = B_{x0}(\mu_0 MN_0)^{-1/2}$ is the Alfvén speed in the tail; N_0 and M are the number density and the proton mass, respectively. We thus obtain the voltage $V_1 = E_1 Z \simeq 6 \times 10^{-2} B_{x0} V_{A0} Z$. On the other hand, the amount of magnetic field annihilation in the region during the explosive phase, denoted

by W_T , can be calculated by $W_T = W_0 z \tau = V_1 I_0 \tau$ (see Eqn. (1.2)), where τ is the duration of the explosive phase. Considering the typical values in the tail $N_0 \simeq 5 \times 10^5 \text{ m}^{-3}$ and $B_{x0} \simeq 25 \times 10^{-9} \text{ Wb/m}^2$, assuming $\tau \simeq 10^3 \text{ sec}$, $L_x \simeq 10R_E$ and $z \simeq 10R_E$ (R_E is the earth radius), we obtain $V_1 \simeq 7 \times 10^4 \text{ Volt}$ and $W_T \simeq 0.9 \times 10^{21} \text{ erg}$. Here, we should note that the actual amount of magnetic energy release in the whole region of the tail is at least 4 times larger than W_T and hence larger than $4 \times 10^{21} \text{ erg}$. These estimates are in good agreement with the observations shown in table 1 of chapter 1. We hence confirm that the basic process of fast reconnection, derived from our computer experiments, is quite applicable to auroral phenomena.

§4. Conclusion

Let us conclude the present thesis with remarking some important problems concerning magnetic field reconnection that remain still unsolved.

(1) Being initiated by a resistive disturbance, the fast reconnection develops from the current sheet without any special external agency. The fast-reconnection development may hence be viewed as a sort of resistive instability whose nonlinear saturation corresponds to none other than the Petschek mode where large-scale conversion of magnetic energy is

realized. In this respect, one may be reminded of the tearing mode, a well known resistive instability, that also develops from the current sheet due to finite resistivity. In studying the fundamental problem of magnetic reconnection, hence, it may be quite important to elucidate some definite connection between the tearing mode and the Petschek mode.

(2) In actual systems, there are many important situations where magnetic fields are likely to be sheared. Hence, magnetic field reconnection in a sheared field, or more generally three-dimensional reconnection process, should be elucidated in applications to actual plasmas.

(3) It is now obvious that occurrence of anomalous resistivity is essential for the fast-reconnection development. Hence, physical conditions for triggering increase in effective resistivity in the current-sheet geometry should be examined in a variety of actual systems. This problem certainly requires that microscopic plasma behaviors be examined during the temporal dynamics of (macroscopic) field-line reconnection.

Further researches of these problems will lead to a deeper understanding of magnetic field reconnection. We believe that, because of the remarkable electrodynamic energy conversion involved, magnetic field reconnection will certainly become more and more important in applications to various plasma devices as well as to interpretations of various distinct plasma phenomena observed in space.

REFERENCES

- Alidieres, M., R. Aymar, P. Jourdan, F. Koechlin and A. Samain, Plasma Phys. 10, 841, 1968.
- Amano, K. and T. Tsuda, J. Geomag. Geoelec. 30, 27, 1978.
- Anderson, O. A. and W. B. Kunkel, Phys. Fluids, 12, 2099, 1969.
- Arnoldy, R. L., J. Geophys. Res. 76, 5189, 1971.
- Aubry, M. P., C. T. Russell and M. G. Kivelson, J. Geophys. Res. 75, 7018, 1970.
- Aubry, M. P. and R. L. McPherron, J. Geophys. Res. 76, 4381, 1971.
- Axford, W. I., H. E. Petschek and G. L. Siscoe, J. Geophys. Res. 70, 1231, 1965.
- Baum, P. J., A. Bratenahl and R. S. White, Phys. Fluids, 16, 226, 1973 a.
- Baum, P. J. and J. Pollack, J. Appl. Phys. 44, 163, 1973 b.
- Baum, P. J., A. Bratenahl, M. Kao and R. S. White, Phys. Fluids, 16, 1501, 1973 c.
- Baum, P. J., A. Bratenahl and White, R. Stephen, Radio Sci. 8, 917, 1973 d.
- Baum, P. J. and A. Bratenahl, J. Plasma Phys. 11, 93, 1974 a.
- Baum, P. J. and A. Bratenahl, Phys. Fluids, 17, 1232, 1974 b.
- Baum, P. J. and A. Bratenahl, Planet. Space Sci. 23, 813, 1975.
- Baum, P. J. and A. Bratenahl, J. Plasma Phys. 18, 257, 1977.
- Bratenahl, A. and C. M. Yeates, Phys. Fluids, 13, 2696, 1970.

- Bratenahl, A. and P. J. Baum, Solar Phys. 47, 345, 1976.
- Burch, J. L., J. Geophys. Res. 77, 6696, 1972.
- Burch, J. L., Radio Sci. 8, 955, 1973.
- Caan, M. N., R. L. McPherron and C. T. Russell, J. Geophys. Res., 78, 8087, 1973.
- Cheng, C. C. and K. Widing, Astrophys. J. 201, 735, 1975.
- Colgate, S. A. and H. P. Furth, Phys. Fluids, 3, 982, 1960.
- Coppi, B. and A. B. Friedland, Astrophys. J. 169, 379, 1971.
- Cowley, S. W. H., J. Plasma Phys. 14, 475, 1975.
- Dobrott, D., S. C. Prager and J. Taylor, Phys. Fluids, 20, 1850, 1977.
- Dungey, J. W., Phil. Mag. 44, 725, 1953.
- Dungey, J. W., Phys. Rev. Lett. 6, 47, 1961.
- Fairfield, D. H., and L. J. Cahill, Jr., J. Geophys. Res. 71, 155, 1966.
- Fälthammar, C.-G. Rev. Geophys. Space Phys. 15, 457, 1977.
- Forbes, T. G. and T. W. Speiser, J. Plasma Phys. 21, 107, 1979.
- Fukao, S., M. Ugai and T. Tsuda, Rep. Ion. Space Res. Japan, 29, 133, 1975.
- Furth, H. P., J. Killeen and M. N. Rosenbluth, Phys. Fluids, 6, 459, 1963.
- Giovanelli, R. G., Mon. Not. Roy. Astron. Soc. 107, 338, 1947.
- Giovanelli, R. G., Mon. Not. Roy. Astron. Soc. 108, 163, 1948.
- Gold, T. and F. Hoyle, Mon. Not. Roy. Astron. Soc. 120, 89, 1960.
- Gold, T., Space Res. 2, 828, 1961.
- Gold, T., Space Sci. Rev. 1, 100, 1962.
- Gross, M. A. and G. Van Hoven, Phys. Rev. A4, 2347, 1971.

- Hamberger, S. M. and J. Jancarik, Phys. Fluids, 15, 825, 1972.
- Heyvaerts, J., E. R. Priest and D. M., Rust, Astrophys. J. 216, 123, 1977.
- Hoffman, R. A. and J. L. Burch, J. Geophys. Res. 78, 2867, 1973.
- Hones, E. W., Jr., J. R. Asbridge, S. J. Bame and S. Singer, J. Geophys. Res. 78, 109, 1973.
- Hones, E. W., Jr., J. Geophys. Res., 82, 5633, 1977.
- Imshennik, V. S. and S. I. Syrovatskii, Soviet Phys. JETP, 25, 656, 1967.
- Kabler, S. W., A. S. Krieger and G. S. Vaiana, Astrophys. J. Lett. 199, L57, 1975.
- Kantrowitz, A. and H. E. Petschek, Plasma Physics in Theory and Applications (ed. W. B. Kunkel), p. 148, McGraw-Hill, 1966.
- Maezawa, K., Planet. Space Sci., 22, 1443, 1974.
- Maezawa, K., ISAS Research Note, 11, 1975.
- Maezawa, K., J. Geophys. Res., 80, 3543, 1975.
- Mestel, L., and P. A. Strittmatter, Mon. Not. Roy. Astron. Soc., 137, 95, 1967.
- Newcomb, W. A., Ann. Phys., 3, 347, 1958.
- Nishida, A. and N. Nagayama, J. Geophys. Res. 23, 1119, 1973.
- Nishida, A., J. Geomag. Geoelec. 30, 165, 1978.
- Obayashi, T., Space Sci. Rev. 17, 195, 1975.
- Ohyabu, N., and N. Kawashima, J. Phys. Soc. Japan, 33, 496, 1972.
- Ohyabu, N., S. Okamura and N. Kawashima, Phys. Fluids, 17, 2009, 1974.
- Parker, E. N., Astrophys. J. Suppl. 8, 177, 1963.

- Parker, E. N., J. Plasma Phys. 9, 49, 1973.
- Petschek, H. E., NASA SP-50, p. 425, 1964.
- Priest, E. R., Astrophys. J. 181, 227, 1973.
- Priest, E. R., and S. W. H. Cowley, J. Plasma Phys. 14, 271.
- Priest, E. R. and A. M. Soward, Basic Mechanism of Solar Activity (ed. Bumba and Kleczek), p. 353.
Reidel, 1976.
- Richtmyer, R. D. and K. W. Morton, Difference Methods for Initial-Value Problems, 2nd edition, p. 365.
Interscience, 1967.
- Roberts, B. and E. R. Priest, J. Plasma Phys. 14, 417, 1975.
- Rostoker, G. and C.-G. Fälthammar, J. Geophys. Res., 72,
5853, 1967.
- Russell, C. T. and R. L. McPherron, Space Sci. Rev., 15,
205, 1973.
- Sonnerup, B. U. O., J. Plasma Phys. 4, 161, 1970.
- Soward, A. M. and F. R. Priest, Phil. Trans. Roy. Soc. 284,
369, 1977.
- Stern, D. P., Space Sci. Rev. 6, 147, 1966.
- Stevenson, J. C., J. Plasma Phys. 7, 293, 1972.
- Stodiek, W., R. A. Ellis, Jr., and J. G. Gorman, Nuclear Fusion Suppl., Pt. 1, 193, 1962.
- Sturrock, P. A., Nature, 211, 695, 1966.
- Sturrock, P. A. and C. Barnes, Astrophys. J. 176, 31, 1972.
- Sweet, P. A., Nouvo Cimento, 8, 188, 1958.
- Tanaka, K. and Y. Nakagawa, Solar Phys. 33, 187, 1973.
- Terasawa, T. and A. Nishida, Planet. Space Sci., 24, 855, 1976.
- Tsuda, T. and M. Ugai, J. Plasma Phys. 18, 451, 1977.

- Uberoi, M. S., Phys. Fluids, 6, 1379, 1963.
- Uchida, Y., Pub. Astron. Soc. Japan, 21, 128, 1969.
- Ugai, M. and T. Tsuda, J. Plasma Phys. 17, 337, 1977.
- Ugai, M. and T. Tsuda, J. Plasma Phys. 21, 459, 1979 a.
- Ugai, M. and T. Tsuda, J. plasma Phys. 22, 1, 1979 b.
- Van Hoven, G., Solar Phys. 49, 95, 1976.
- Vasyliunas, V. M., Rev. Geophys. Space Phys. 13, 303, 1975.
- Yeh, T. and W. I. Axford, J. Plasma Phys. 4, 207.

